ΝΙΚΟΛΑΟΣ ΤΖΙΡΗΣ

ΣΧΟΛΗ ΜΗΧΑΝΟΛΟΓΩΝ ΜΗΧΑΝΙΚΩΝ

Τεχνο-οικονομική μελέτη παραγωγής ηλεκτρικής ενέργειας με σύστημα ηλιακού πύργου-Κύκλου Rankine στην Ελλάδα

Τομέας: Θερμότητας

Επιβλέπων: Σωτήριος Καρέλλας, Καθηγητής ΕΜΠ

Αθήνα 2021

NIKOLAOS TZIRIS

SCHOOL OF MECHANICAL ENGINEERING

Techno-economic investigation of power production from a solar power tower coupled with a Rankine cycle in Greece

Section: Thermal Engineering

Supervisor: Sotirios Karellas, Professor

Athens 2021

Ευχαριστίες

Σε αυτό το σημείο θα ήθελα να ευχαριστήσω θερμά τον καθηγητή κ.Σωτήριο Καρέλλα που μου έδωσε τη δυνατότητα να εκπονήσω την παρούσα διπλωματική στο εργαστήριο Ατμοκινητήρων και Λεβήτων του ΕΜΠ. Πέρα από τη διπλωματική εργασία, θα ήθελα να τον ευχαριστήσω και για τις πολύτιμες συμβουλές που μου έδωσε κατά τη διάρκεια των σπουδών μου.

Επίσης, θα ήθελα να ευχαριστήσω από καρδιάς τον υποψήφιο διδάκτορα του εργαστηρίου Τρύφωνα Ρουμπεδάκη, ο οποίος παρά το φορτωμένο του πρόγραμμα, βοήθησε σε κάθε στιγμή αντικειμενικής δυσκολίας και υποκειμενικής αδυναμίας έτσι ώστε να φέρω εις πέρας αυτή τη διπλωματική εργασία. Χωρίς τη συμβολή του το αποτέλεσμα δε θα ήταν το ίδιο.

Ακόμα, θα ήθελα να ευχαριστήσω τον Δρ. Άγγελο Δουκέλη του εργαστηρίου Ατμοκινητήρων και Λεβήτων για τις χρήσιμες συμβουλές του γύρω από τα οικονομικά ζητήματα των σταθμών παραγωγής ηλεκτρικής ενέργειας.

Τέλος, θα ήθελα να ευχαριστήσω την οικογένειά μου, τους φίλους μου και ιδιαιτέρως τη Σπυριδούλα για την αμέριστη συμπαράσταση και τη στήριξη που μου παρείχαν καθ' όλη τη διάρκεια των σπουδών μου.

<u>Υπεύθυνη δήλωση</u> για λογοκλοπή και για κλοπή πνευματικής ιδιοκτησίας:

Έχω διαβάσει και κατανοήσει τους κανόνες για τη λογοκλοπή και τον τρόπο σωστής αναφοράς των πηγών που περιέχονται στον οδηγό συγγραφής Διπλωματικών Εργασιών. Δηλώνω ότι, από όσα γνωρίζω, το περιεχόμενο της παρούσας Διπλωματικής Εργασίας είναι προϊόν δικής μου εργασίας και υπάρχουν αναφορές σε όλες τις πηγές που χρησιμοποίησα.

Ονοματεπώνυμο

Νικόλαος Τζιρής

Contents

Σύνοψη

Στις πλέον αναπτυσσόμενες ανανεώσιμες πηγές ενέργειας συγκαταλέγονται και οι ηλιακοί πύργοι, οι οποίοι από τον σταθμό P10 ισχύος 10MW (ο πρώτος εμπορικός σταθμός) έως και σήμερα, όπου παράγονται περισσότερα από 150MW, έχουν κάνει τεράστια άλματα εξέλιξης. Αυτή η εργασία μελετά, με βάση τον σταθμό Gemasolar στην επαρχία της Σεβίλλης, ισχύος 20MWe, κατά πόσο μπορούν να εγκατασταθούν τέτοιου είδους σταθμοί στην Ελλάδα. Η μελέτη αφορά στην εγκατάσταση σταθμών ισχύος 40 MWe στις τέσσερις διαφορετικές κλιματικές ζώνες της Ελλάδας. Προκειμένου να γίνει αυτό αναπτύσσεται ένα μοντέλο που περιλαμβάνει ηλιακό πύργο, σύστημα αποθήκευσης ενέργειας και σταθμού παραγωγής ηλεκτρικής ενέργειας. Ακολούθως, πραγματοποιείται επαλήθευση στον ήδη υπάρχων σταθμό Gemasolar, έτσι ώστε να είναι διακριβωθεί η ακρίβεια του μοντέλου προσομοίωσης. Κατόπιν, δοκιμάζονται 36 διαφορετικά σενάρια για 6 συλλεκτικές επιφάνειες ηλιοστατών και για 6 διαφορετικούς όγκους δοχείων και παρατηρείται η μεταβολή τεχνικών μεγεθών, όπως η συνολική παραγόμενη ισχύς και ο συνολικός βαθμός απόδοσης συστήματος, αλλά και ο εξεργειακός βαθμός απόδοσης.

Ακόμα, για τα 36 διαφορετικά σενάρια που μελετώνται υλοποιείται και οικονομική ανάλυση χρησιμοποιώντας δείκτες, όπως το ειδικό κόστος, το κόστος της ενέργειας, η περίοδος αποπληρωμής αλλά και η καθαρή παρούσα αξία. Τέλος πραγματοποιείται και ανάλυση ευαισθησίας, έτσι ώστε να διαπιστωθεί με κάποια μικρή μεταβολή σε διάφορα μεγέθη σχετιζόμενα με την οικονομικότητα της εφαρμογής αλλά και της τεχνικής απόδοσης του συστήματος κατά πόσο μεταβάλλονται τα τεχνικά και οικονομικά μεγέθη που αναφέρθηκαν πιο πάνω.

Abstract

The most growing renewable energy sources include solar power towers, which from the P10 power station of 10MW (the first commercial station) to the present day, where more than 150MW are produced, have made huge strides in development. This thesis studies, based on the Gemassolar Power Station in the province of Seville of 20MWe, whether such stations can be installed in Greece. The study concerns the installation of 40 MWe power stations in the four different climatic zones of Greece. In order to do this, a model is being developed that includes a solar power tower, an energy storage system and a power station. Subsequently, verification is being carried out at the existing Gemassolar station in order to verify the accuracy of the simulation model. Subsequently, 36 different scenarios are tested for 6 heliostat collector surfaces and 6 different storage tank volumes and the change in technical sizes, such as the total power generated and the total efficiency of the system performance, as well as the exergetic efficiency, are observed.

In addition, for the 36 different scenarios studied, economic analysis is also carried out using indicators such as specific costs, the Levelized cost of energy, payback period and net present value. Finally, a sensitivity analysis is carried out in order to determine with some slight change in various sizes related to the economicity of the application and the technical performance of the system whether the technical and economic indexes mentioned above are changing.

Nomenclature

A	Area	$[m^2]$
A_l	Tank external (lateral) area	$[m^2]$
A_d	Tank cross section area	$[m^2]$
a	Surface area per unit of volume	$[m^{-1}]$
C	Concentration area	[-]
C_p	Specific heat capacity	[J/kg K]
Di	Tank internal diameter	[m]
De	Tank external diameter	[m]
d	Diameter of receiver tube	[m]
DNI	Direct normal irradiation	$[W/m^2]$
E	Internal energy	kWh
Ex	Exergy	W
Fr	View factor	[-]
Gr	Grashof number	[-]
h	Enthalpy	[J/kg]
H	Height of receiver aperture	[m]
L	Height of tank	[m]
$\dot{m}$	Mass flow rate	[kg/s]
N	Number of receiver tubes	[-]
Nu	Nusselt number	[-]
Pr	Prandtl number	[-]
q	Thermal energy per area	$[W/m^2]$
Q	Thermal energy	[W]
Q_{abs}	Receiver absorbed energy	[W]
Q_{design}	Design thermal energy for Rankine cycle	[W]
Re	Reynolds number	[-]
Re_p	Reynolds number of filler particles	[-]
$\dot{S}_{gen}$	Entropy generation	[W/K]
T	Temperature	[K]
U	Overall heat transfer coefficient	$[W/m^2K]$
V	Volume	$[m^3]$
W	Power output or width of receiver aperture	[W] or [m]

Greek Symbols

α	Convective heat transfer coefficient	[W/m^{2}K]
η_{field}	Heliostat field efficiency	[-]
$\eta_{rec,energetic}$	Receiver energetic efficiency	[-]
$\eta_{rec,exergetic}$	Receiver exergetic efficiency	[-]
λ	Thermal Conductivity	[W/mK]
δ	Thickness	[m]
ε	Emissivity	[-]
ρ	Density	[kg/m^3]

Subscripts

abs	Absorbed
amb	Ambient
att	Atmospheric attenuation
block	Blocking
c	cold region
cond	Conduction
cos	The cosine effect
field	Heliostat field
fc	Forced convection
h	Hot region
HTF	Heat transfer fluid
i or in	Inner, inlet or inside
int	Internal
ins	Insulation
l	Liquid phase
melt	Melting point value
ms	Molten solar salt
nc	Natural convection
o	Outer or outlet
out	Outlet
PB	Power Block
rad	Radiation
rec,ap	Receiver aperture
rec,in	Receiver inlet or incident on receiver
rec,out	Receiver outlet
rec,sur	Receiver surface
rec,tube	Receiver tube
ref	Reflection

s	Solid phase
shadow	Shading
spill	Spillage
t	Total storage system
w	Receiver wall

Abbreviations

CST	Concentrated solar thermal
CSP	Concentrated solar power
EU	European Union
NREL	National Renewable Energy Laboratory
SAM	System Advisory Model
SPT	Solar Power Tower
PTC	Parabolic Trough Collectors
TES	Thermal energy storage
DNI	Direct Normal Irradiation
PB	Pay back period or Power Block
NPV	Net Present Value

1. Introduction

1.1 Solar Energy

Solar energy comes from the sun, which is a sphere made up of hot gaseous matter and plasma with a diameter of $1.39 \cdot 10^9$ is equal to 5,760 K. The total energy produced in the form of radiation by the nuclear fusion reactions that take place in its mass, amounts to $3{,}8 \cdot 10^{20}$ MW. This energy is equivalent to 63 MW / m^2 of its surface. This amount of energy is radiated in all directions. However, the Earth, which is at a distance of $1.5 \cdot 10^8$km, receives only a very small percentage of this energy equal to $1.7 \cdot 10^{14}$ KW. However, even with this small percentage, the radiation that falls in space is calculated. 84 minutes is equivalent to global energy demand.

Solar irradiation, after traveling in space, enters the Earth's atmosphere through the ionosphere. From the radiation that enters the atmosphere, a portion of that radiation is absorbed by the clouds and the various elements in the Earth's atmosphere. A significant part is reflected back into space (about 50%) and a part eventually reaches the earth's surface. The Earth's rotation around its axis results in changes in the intensity of solar radiation during the day for a specific location. As a result the presence of atmospheric and climatic phenomena that occur in it, have the effect of weakening the nature of the initial solar radiation.

The combination of optical phenomena such as reflections, absorption, refraction and scattering implies the formation of highly dynamic levels of radiation in any area of the Earth. In addition, due to the clouds in the atmosphere, as well as due to the scattering of sunlight, the total radiation that falls anywhere on Earth is a combination of diffuse and direct radiation.

Direct Normal Irradiance ,DNI is the part of the solar radiation that reaches the Earth directly from the Sun, without scattering in the atmosphere. Knowledge of the values of this radiation, both on an hourly and annual basis, is essential for the study of concentrated solar systems. , as these can only be exploited radiation of this form.

Diffuse normal irradiance is the part of the sun's radiation that reaches the Earth after scattering and change of direction, along the path in the atmosphere. Diffuse radiation is what provides us with daylight and without which the sky would look black.

In northwestern Europe, about 50% of the radiation is diffuse and the rest is direct, on an annual basis. It is worth noting that systems designed to develop high temperatures are based on direct radiation. At the same time, the concentrated solar systems that will be presented later cannot take advantage of the diffused radiation.

All concentrating solar power (CSP) technologies use a mirror configuration to concentrate the sun’s light energy onto a receiver and convert it into heat. The heat can then be used to create steam to drive a turbine to produce electrical power or used as industrial process heat.

Concentrating solar power plants can integrate thermal energy storage systems so that they can be used to generate electricity during cloudy periods or periods after sunset and before dawn. .This ability to store solar energy makes concentrating solar power a flexible source of renewable energy. CSP systems can be also coupled with combined cycle power plants resulting in hybrid power plants which provide high-value, dispatchable power. They can also be integrated into existing thermal-fired power plants that use a power block like CSP; such as coal, natural gas, biofuel or geothermal plants.

CSP plants can also use fossil fuels to supplement solar production during periods of low solar radiation. In that case, a natural gas-fired heater or a gas steam boiler/reheater is used. There are four types of CSP technologies, with the earliest in use being Parabolic Trough Collectors, and the fastest growing being Solar Power Tower. For each one of these, there are multiple design variations and different constructions, depending on whether thermal energy storage is included, and which methods are used to store solar heat [1], (Karellas & Roumpedakis, 2019) [2].

1.1.1 Parabolic Trough Collectors

A parabolic-trough collector (PTC) is a linear-focus solar collector, basically composed of a parabolic-trough-shaped concentrator that reflects direct solar radiation onto a receiver or absorber tube located in the focal line of the parabola. The larger collector aperture area concentrates reflected direct solar radiation onto the smaller outer surface of the receiver tube, heating the fluid that circulates through it. This is the time when the solar radiation is transformed into thermal energy in the form of sensible or latent heat of the fluid. This thermal energy can then be used to drive either industrial processes demanding thermal energy (e.g., food industry, petro-chemical industry, etc.) or Rankine cycle power plants to produce electricity with a steam turbine.

With current technology, Parabolic Trough Collectors (PTC) can deliver useful thermal energy up to 398 °C. The main limitation on the maximum temperature is imposed by the thermal oil currently used as the working fluid, because it quickly loses its properties above 398 °C. However, research in new fluids promises higher temperatures up to 500 °C in the near future (Moya, 2021) [3] .

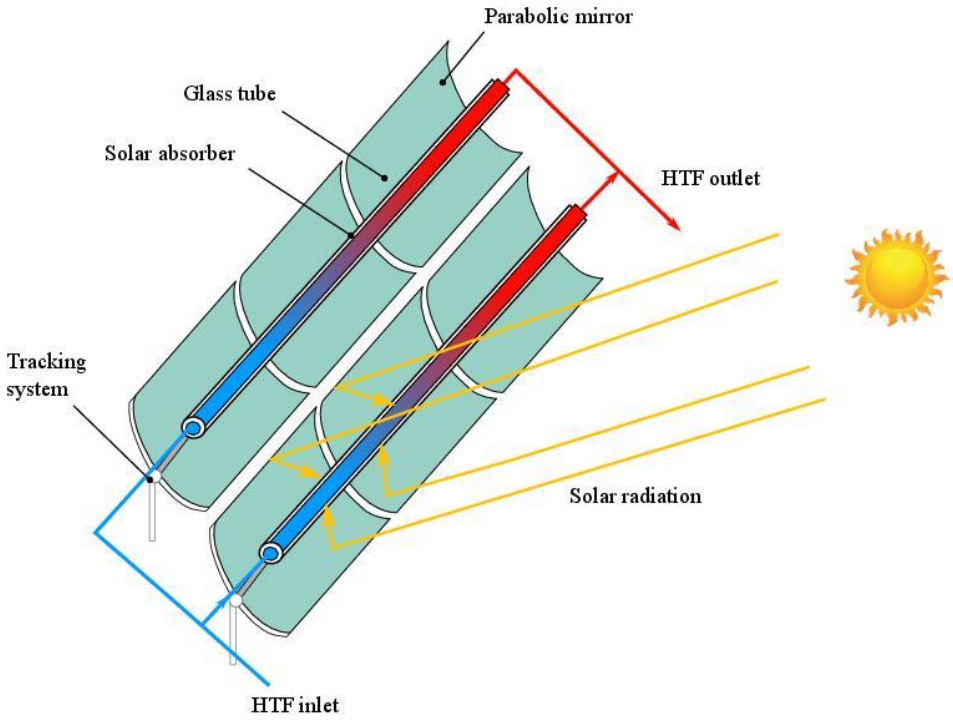

Figure 1-1.Source: Solar Cooling Technologies (Karellas et al. 2018)[4]

1.1.2 Solar Power Tower

A solar power tower plant consists of a tall tower supporting a heat receiver surrounded by heliostats that focus the rays of the Sun onto the receiver. The heliostats are each fitted with a solar tracking system so that they can track the Sun across the sky during the time of the day. Also called point focusing solar concentrators, these plants can achieve concentration ratios of up to 1000. Solar towers often include thermal storage using molten salts, usually nitrates, as heat transfer fluid, which allows them to generate electricity around the clock. Other configurations use direct steam systems. More complex pressurized gas systems have also been proposed using a gas turbine in a hybrid generating system [1].

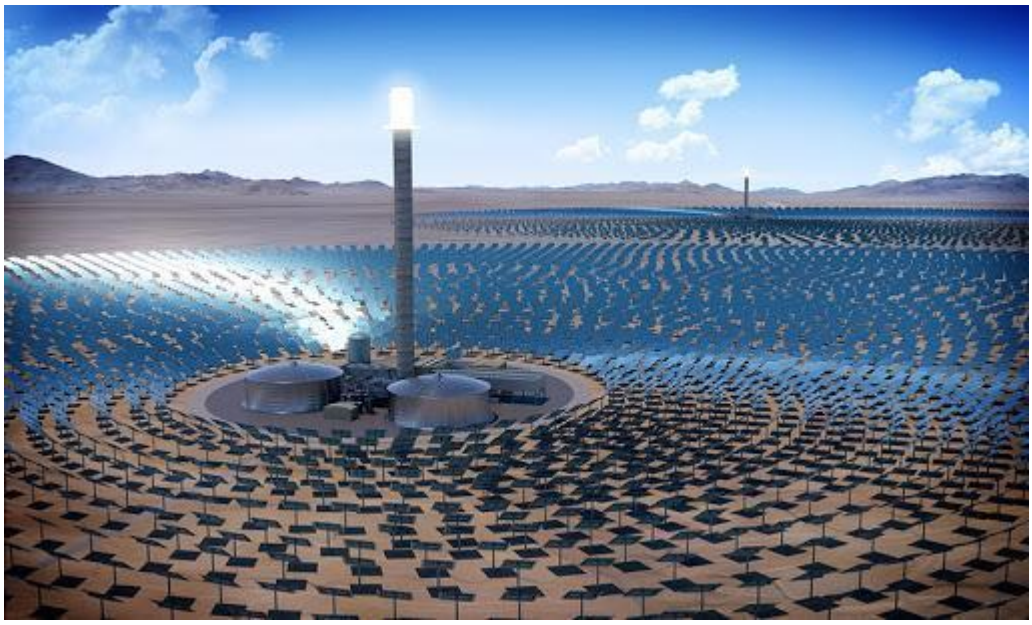

Figure 1-2.Rendering of Copiapo in Chile [5]

1.1.3 Fresnel Reflectors

Linear Fresnel Reflectors are solar concentrating constructions with concentration ratio between 10 and 50. The LFR has its reflectors placed close to the ground. This structure makes the mechanical challenges due to wind load to be low. Furthermore, the land usage is low due to this particular concentrating technology. The LFR receiver is static and located some meters above the ground. Usually, it is mounted on a tower with a typical height of 10-15m (Karellas & Roumpedakis, 2019) [4]. It needs to be mentioned that LFR has a lightweight supporting system which make the collector cost to be relatively low. The receiver of the LFR has usually evacuated tube collector coupled to a secondary concentrator. The secondary concentrator has a parabolic shape which is usually a compound parabolic concentrator (CPC). Another conventional structure is with trapezoidal cavity receivers with many tubes inside. The primary reflector can be flat or curved. The flat reflectors are cheaper but instead introduce higher optical losses. The curved mirrors have a parabolic shape and can increase the overall optical efficiency. The cost is higher in this occasion because curved mirrors are needed. About the working medium water/steam is a usual choice for production of superheated or saturated steam. This steam can be used directly in the turbine of a Rankine Cycle or for an industrial process. Also, thermal oils such as Therminol VP-1are used for several thermal applications up to 400^{o}C.A technical challenge related to this construction is the optimization of reflectors allocation to minimize shading and blocking. Thus a compromise has to be made between increasing mirror's spacing- larger total plant area- and increasing the tower height's which result in higher cost (Bhatia, 2014) [6],[7].

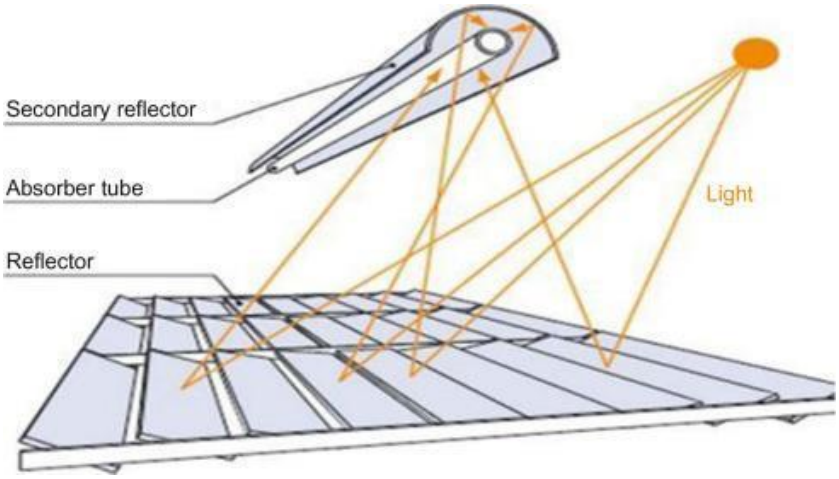

Figure 1-3.Fresnel Reflector (Gouthamraj et al., 2013) [8]

1.1.4 Solar Dish

Energy production plants with systems of solar dishes consist of a number of autonomous "dishes". Each and every one of them has nominal output of some kW and uses mechanism of detection for better sun tracking. Due to the geometry of the concentrator these kinds of systems succeed very high concentration ratios that reach up to 3000, and thus very high temperatures in the absorption system can be accomplished. Solar dishes are characterized by very high efficiency during the conversion of solar power to electricity. An autonomous solar-dish consists of:

- Solar concentrator
- Solar receiver
- Power conversion unit (Stirling machine etc.)

The solar concentrator, or dish, gathers the solar energy coming directly from the sun. The beam of concentrated sunlight, is reflected onto a thermal receiver that collects the solar heat. The dish is mounted on a structure that tracks the sun continuously during the daylight to reflect the highest percentage of sunlight possible onto the thermal receiver.

The power conversion unit includes the thermal receiver and the engine/generator. The thermal receiver is the interface between the dish and the engine/generator. It absorbs the concentrated beams of solar energy, converts the energy to heat, and transfers the heat to the engine/generator. A thermal receiver can be a bank of tubes with a cooling fluid—usually hydrogen or helium—that typically is the heat-transfer medium and also the working fluid for an engine. Alternate thermal receivers are heat pipes, where the boiling and condensing of an intermediate fluid transfers the heat to the engine.

The engine/generator system is the subsystem that takes the heat from the thermal receiver and uses it to produce thermal to electric energy conversion. The most common type of heat engine used in dish/engine systems is the Stirling engine. A Stirling engine uses the heated fluid to move pistons and create mechanical power. The mechanical work, in the form of the rotation of the engine's crankshaft, drives a generator and produces electrical power [9], (Karellas & Roumpedakis, 2019) [4].

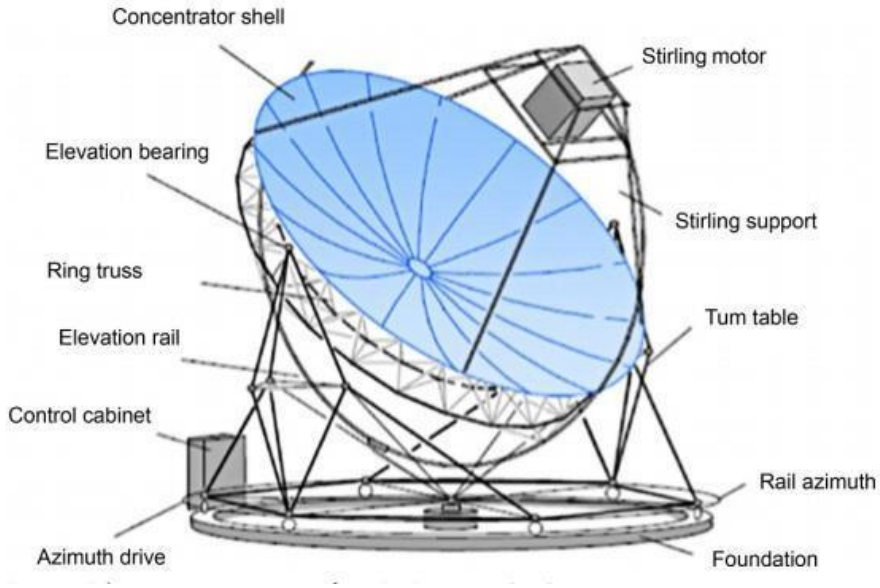

Figure 1-4.Source: Solar Cooling Technologies (Karellas et al. 2018) [4]

1.2 Solar Power Tower

Stations with solar power towers can efficiently achieve high temperatures because of the high concentration ratios they can achieve, using different configurations of the collector field and receiver. That kind of stations consist of:

- Heliostat field
- Heliostat receiver at the top of the tower
- System of Electricity Production
- Storage System (Thermal)

1.2.1 Heliostat field

As heliostat field we can consider a construction with many heliostats each of which on a visually independent axis with the main receiver of the tower. All heliostats in the solar field must reflect the sun's rays in such a way that each solar panel places its surface perpendicular to the bisector of the angle defined by the position of the sun and the solar receiver. Heliostat field along with the receiver are the most significant components of the solar power tower system, accounting in total for a 70% of the investment cost [4]. Each heliostat consists of the following elements (Κακαράς, Ε., & Καρέλλας, Σ.) (2015) [2]:

- Reflective surface
- Support system and drive mechanism
- Control system

The reflective surface of a heliostat consists of a big number of panels which can create a reflective area of up to 150m^2. The design is being done with the aim of creating a surface, which allows the highest possible reflection with the least weight of the construction. This is being done due to the willing not to harm the two-axis movement of the heliostat. In order to minimize the cost of the heliostats some theories have been developed.

First of all, the initial approach had as a target to raise the reflective surface with the use of curved surfaces made out of a big number of reflective sub-surfaces, 3 -6 square meters. Actually, the increase in the size of reflective surfaces leads to the reduce of the total cost of the heliostat, because the cost of the subsystems of it does not increase linearly with the reflective surface, due to the economies of scale. However, the above advantage of solar surfaces was limited by the increase of optical losses and their cleaning issues.

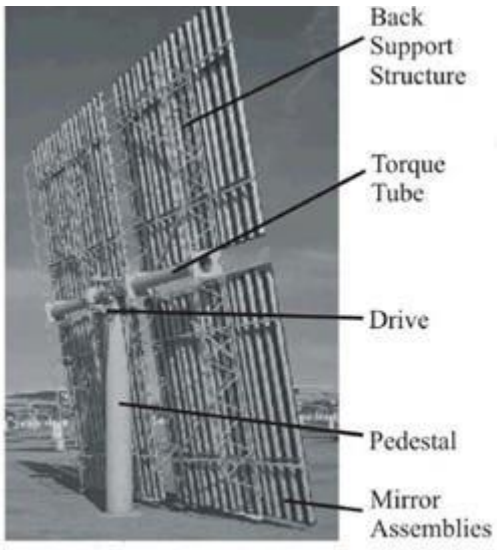

Figure 1-5. Components of an heliostat (Pitz-Paal,2007) [10]

Another technology that was developed, uses new lighter materials such as reflectors from polymers and composite materials for the construction of heliostats with strained membranes. Last but not least, BrightSourceEnergy company constructs heliostats consist of two pieces of reflective surfaces 14.4 m^2 in total aiming in high performance, less weight and cheaper construction cost.

The support system of heliostats consists of steel pillars in the shape of tau, which are embedded in the ground, constructed to endure the weight of reflective surface. The support system allows the movement of reflective surface in two individual's axes for the optimization of the position of heliostat every single moment.

The tracking mechanism of heliostats is responsible for the independent movement both in terms of azimuth angle and in terms of lifting angle so as the reflective surfaces can follow the position of the sun and reflect the incident solar radiation in the receiver point.

1.2.2 Solar receiver

The receiver is located at the top of the tower. The height of the tower is a function of the scale of the solar field. High solar towers allow to the heliostats that are positioned at a great distance from the tower to reflect their solar beams to the receiver.

The receiver is actually a specially designed heat exchanger which receives uneven intermittent heat flow. That flow can take place in a specific region or in the whole surface of the receiver. That depends on the design of the construction. The scale of the receiver is determined by the max flow thermal flow that is going to enter, in a specific period of time. Through the receiver conversion of solar energy to thermal energy takes place, which can be used in the conventional thermodynamic cycles for the production of electricity. The thermal flow and the temperatures that are being developed in the receiver are higher than those on parabolic trough collectors and thus state of the art materials have to be used for its construction. The receiver has to have ideally the behavior of blackbody in order to manage to eliminate radiation losses. To achieve this in the construction of the receivers are used cavities, pipes with black painting or porous absorbent constructions which can trap the escaped photons.

Type of receivers:

- Tubular receiver

With geometric criteria's tubular receivers have two basic categories.

i. External Receivers: The external receivers are usually made out of cylindrical tubular panels which are typical solutions for cases in which the heliostat field surrounds the tower. That kind of systems had been used in USA in Solar One and Two projects and in some experimental cases in Europe and Japan.

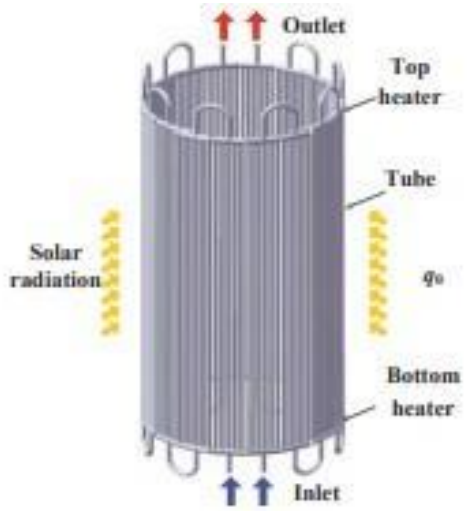

Figure 1-6. **External Receivers fluid flow (Zheng et al., 2015) (11)**

ii. Cavity receiver: In cavity receivers the reflected from heliostats radiation comes through an opening in a cuboidal construction before it hits in the surface of the heat exchanger. Due to geometrical limitations these kinds of receivers are used in North (or South) constructions of heliostat field (Themis project in France, IEA-SSPS-CRS project in Spain).

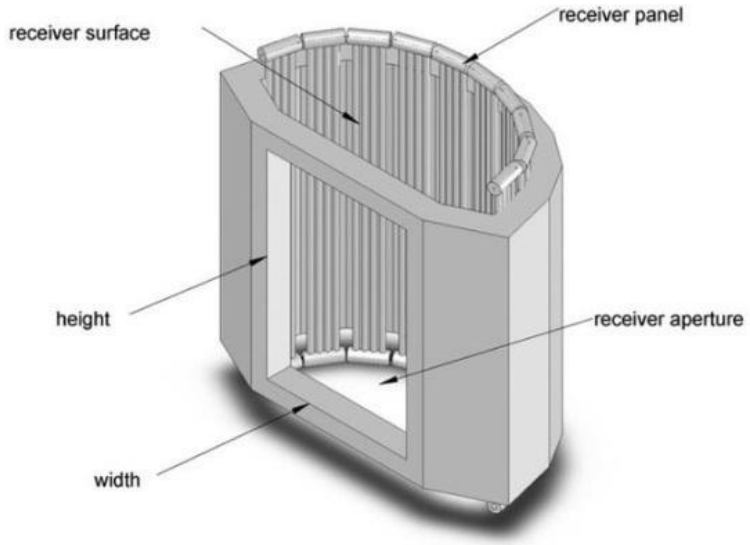

Figure 1-7. **Basic elements of a cavity receiver (Tiryaki & Camdali, 2017) [12]**

- Volumetric receiver

They have great application prospect due to the simple structure; high thermal efficiency and the air exit temperature can reach above more than 800 ^{o}C. The porous material is used instead of tube as absorber in volumetric solar receivers to heat the working medium, and the incident radiation can be absorbed gradually from outside to inside (Liu et al., 2018) [13]. The most commonly applied Heat Thermal Fluids are:

- Water (The receiver works as steam generation system)
- Molten Salts
- Air

Typical operational values of the receivers are between 500 ^{o}C and 1200 ^{o}C, and the typical thermal inlet flow is between 300 kW/m^2 and up to 1000kW/m^2.

1.3 Storage in CSP

Due to the major drawback of the of solar energy which is temporary, Thermal Energy Storage (TES) can be coupled with concentrating solar power CSP so as to offer energy dispatchability to adapt the electricity power production to the curve demand. Up to date, all the TES sub-units are based on a unique technology initially developed in Themis-France. The so called “two- tank molten salt technology” is composed of two separated tanks in which all the molten salt (mixture of nitrate salts) used at the same time as HTF and thermal storage material can be stored at the two temperature levels. The molten salt stores the thermal energy by changing its temperature and this procedure is called sensible heat approach. During the sunny hours of the day the heliostat field via tower gives heat power which is shared between the TES unit and the power block. When the produced heat power in less than the nominal that is needed to feed the power generation circuit the TES unit offers stored power in order to balance the deficit. Therefore, using the TES unit, the power block of the plant is fed at nominal power and delivers a constant electric power to the grid. As the basic binary eutectic “solar salt” made of NaNO3 and KNO3 presents a solidification temperature of 250^{o}C, the different equipment has to be maintained above this critical temperature to avoid any plug according to (Patel et.al) [14].

In order to avoid this kind of state huge efforts were done to find suitable mixtures of molten salts with lower solidification temperatures. An example can be the Themis project in France were a mixture of $NaNO_2/KNO_3/NaNO_3$ with a solidification temperature of 142 ^{o}C. The mixture issue is under study despite its optimistic aspects.

Figure 1-8. The Themis Solar Power Tower in the Eastern Pyrenees, France (Patel & Choksi, 2015) [15]

The major efforts are now have turned into replacing the two-tank storage system with one tank where the hot salt mixture would be due to its density at the top of the tank and the cold mixture at the bottom. In this "thermocline" approach, the mixtures are divided naturally. This will have as a result the reduce of overall cost of the TES unit by (30%) by using a single tank.

However, heat transfer by diffusion at the interface between the two temperature levels reduces the thermal efficiency. During the charging period, the coldest salt fraction is pumped at the bottom of the tank to be heated by the solar field through a heat exchanger and to go back to the top of the TES tank. During the discharging period, the hottest salt fraction is pumped at the top of the tank to supply the power block and the resulting coldest salt is fed back at the bottom of the tank (Py et al., 2017) [16].

1.4 Power generation cycles

As electric energy production cycles can be considered: Clausius-Rankine cycles which will be analyzed subsequently, Kalina cycle, Strirling Cycle, Joule cycle and combined circles.

Kalina thermodynamic circle is accomplished with the use of ammonia-water mixture. The mixture is zeotropic. That means that temperature and composition of the mixture are changing during the vaporization for all the possible composition of the mixtures. During the process of this cycle the mixture of NH_3-H_2O is being heated isobarically, until it reaches to a specific temperature. When temperature reaches to the boiling point, the mixture starts vaporization.

While the mixture continuously heating, it is separated to its components. As a result, the steam which have separated is richer in ammonia, rather than the rest liquid mixture. Now the steam (rich in ammonia) is superheated and uses its energy in the turbine and as a result to the generator and after that is absorbed from the weak current of NH3-H2O with heat abortion [2].

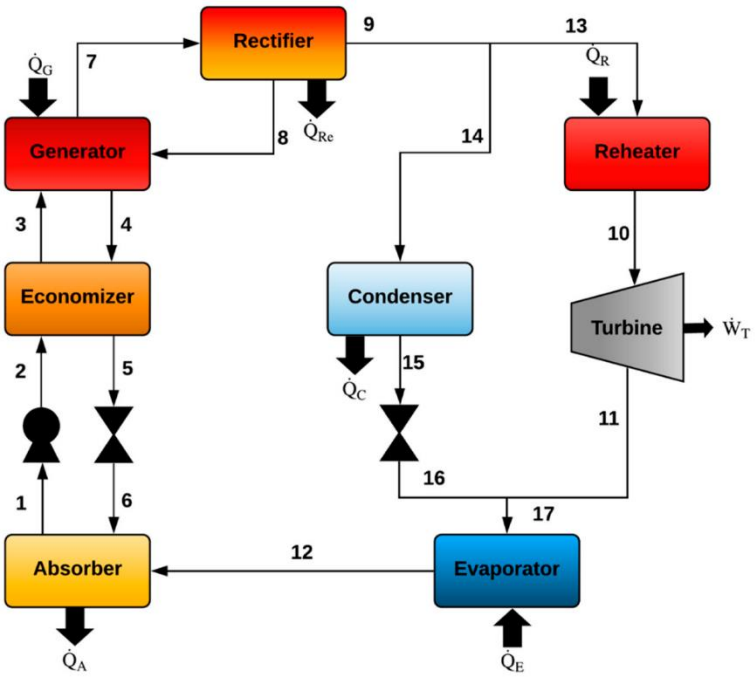

Figure 1-9. Kalina Cycle, Power and Cooling Production at the same time (Rivera et al., 2020) [17]

Joule thermodynamic cycle can be shown below. Ambient air is compressed in the compressor until it reaches a pressure between 8 and 32 bar. Due to the compression the air is heated between a temperature of 300 ^{o}C and 650 ^{o}C. By adding fuel in an adiabatic chamber, the exhaust gases enter the turbine of the construction with a temperature of 800-1500 ^{o}C. This temperature as also in the steam turbines is limited by the materials that turbine is constructed. Finally, the exhaust gas is abandoned in the environment between the temperature of 440 ^{o}C and 620 ^{o}C. The exhaust gas provision and its temperature before it enters the turbine are significant numbers in order to calculate the efficiency of the gas turbines. The turbine in a gas turbine construction is in the same shaft with the generator and the compressor [2].

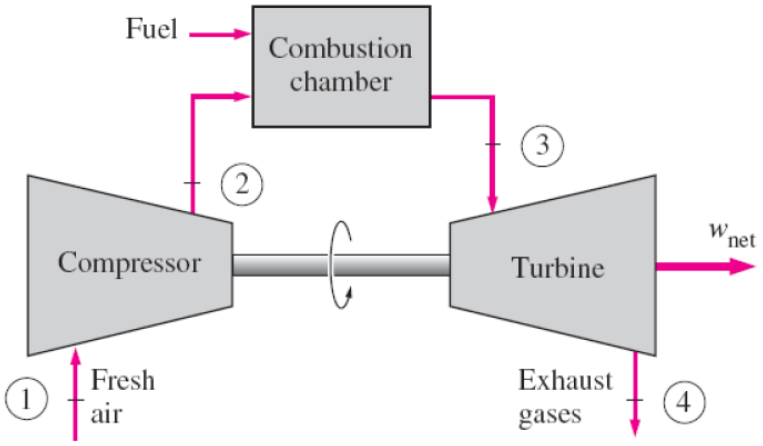

Figure 1-10.Gas Turbine parts and procedures (Cengel & Boles, 2008) [18]

1.4.1 Water-steam Rankine cycle

The thermodynamic Clausius-Rankine cycle for water-steam can be shown on the bellow scheme. In the beginning the water is pumped from low to high pressure. The simple ideal Rankine Cycle [2]:

- Process 1→2: The water is pumped from low pressure to high pressure. In this stage the water is in liquid state so it needs less energy.
- Process 2→3: The high-pressured liquid is inserted into the boiler where it is heated in constant pressure until it reaches a superheated vapor state. The input energy required can be easily calculated graphically, using an enthalpy–entropy chart (h–s chart, or Mollier diagram), or numerically, using steam tables. The boiler is practically a large heat exchanger where the heat gained from combustion gases, nuclear reactors, or renewable energy sources in transferred to the fluid.
- Process 3→4: The superheated vapor of stage 3 enters the turbine and expands isentropically, producing work by rotating a shaft connected to an electric generator. The temperature and pressure drops during this procedure to the state 4 where steam enters the condenser. At this stage steam is a saturated liquid-vapor mixture with a high quality.
- Process 4→1: At this stage mixture enters the condenser, where in constant pressure, it rejects heat in a cooling medium such as lake, river or atmosphere. Mixture lives condenser as saturated liquid and enters the pump so as to complete the cycle. In some areas the use of water is not preferred in order to cool the mixture, due to the lack of it. As a result, air is being used, the so-called dry cooling procedure.

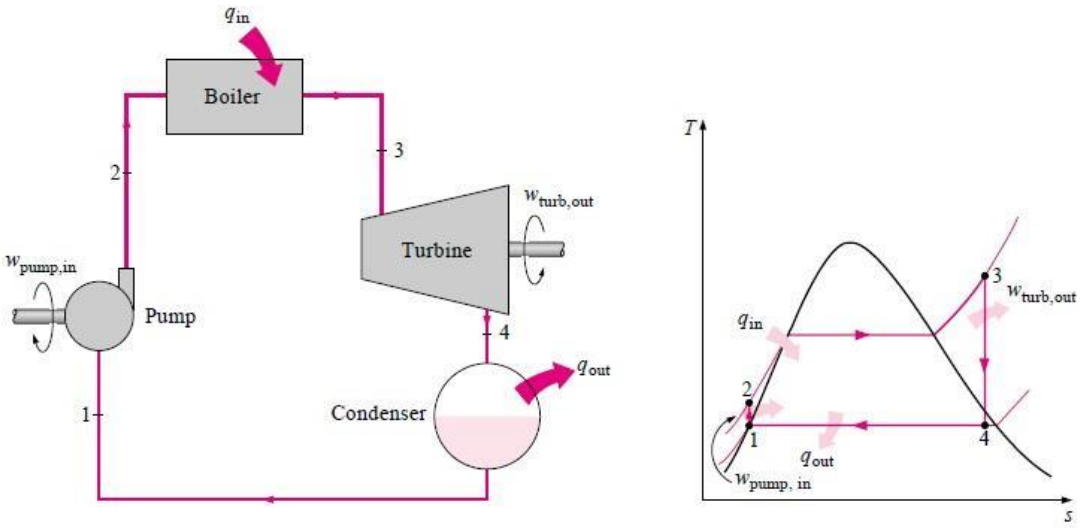

Figure 1-11. **Water-steam Rankine Cycle and procedures (Cengel & Boles, 2008) [18]**

The actual vapor power cycle differs from the ideal Rankine cycle due to irreversibilities in many components. Fluid friction and heat loss to the surroundings are the two common sources of them.

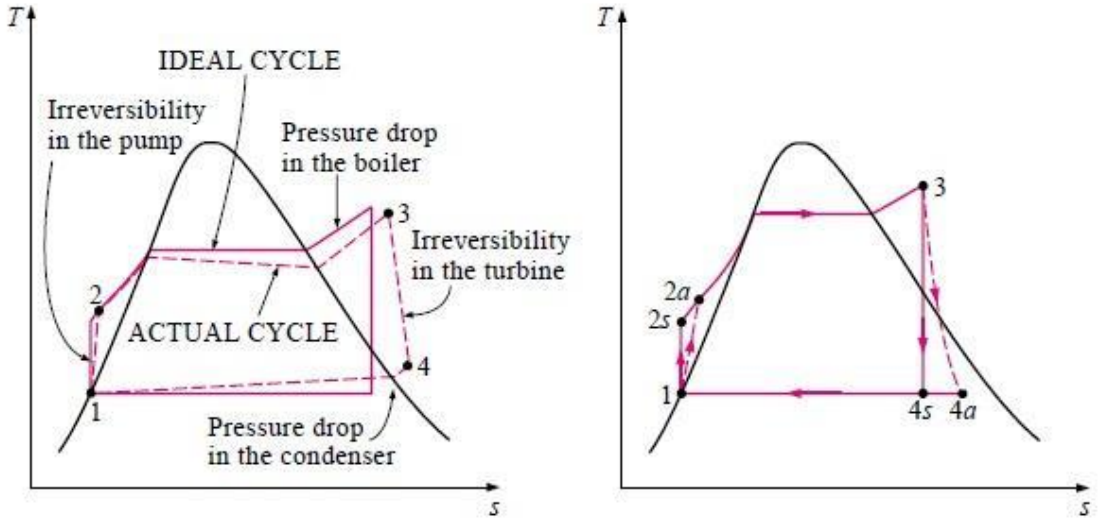

Figure 1-12. **Difference between ideal and real Rankine cycle (Cengel & Boles, 2008) [18]**

Fluid friction of the steam that is leaving the boiler causes the steam to be at a lower pressure than the pressure that was calculated in ideal cycle. What's more the steam pressure that enters the turbine is lower than that in the exit of boiler due to losses via piping components. In order

to compensate these pressure drops; the water has to be pumped at a higher pressure and thus larger pump and larger work input to the pump is needed.
Another important irreversibility is the heat loss of the steam in components of its surrounding. To tackle this problem more heat needs to be transferred to steam through the boiler. As a result, the efficiency decreases.
One more thing we have to take into consideration is that in real cycles the liquid before entering the pump is usually sub cooled in order to prevent cavitation in the low-pressure side of the pump impeller which may damage it. Additional losses occur at the bearings between the moving parts as a result of friction. Steam can also escape during the cycle but also air can be inserted in it on the condenser. Last but not least, the power that is being consumed by auxiliary systems of the cycle should also be taken into consideration when we are "measuring" the efficiency of the plant.

1.4.2 Organic Rankine cycle

The organic Rankine Cycle is similar to the Rankine-Cycle with the only difference that instead of water-steam medium is used as working medium an organic fluid, which differs in different applications. The application and construction of such systems is observed in decentralized units, due to the fact that, this particular thermodynamic cycle offers the ability of exploitation thermal energy resources of low temperature, in small scale constructions (geothermal plants co-production, concentrated solar thermal power plants, small scale biomass power plants etc.)
A very important factor that has to be taken seriously during the design of an ORC system, is to choose the right, environmentally acceptable organic fluid and its thermodynamic design so as to achieve high thermal efficiency. Below are presented some saturation curves of different working mediums [2].

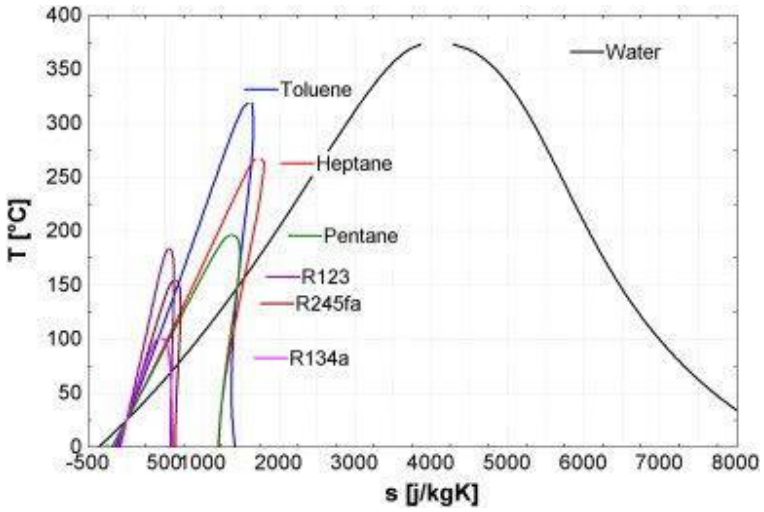

Figure 1-13. **T-s diagram for steam and different organic fluids (Quoilin, n.d.) [19]**

The choice of the working fluid is determined mainly from the heat output temperature in the circle. Apart from the thermodynamic parameters of the working fluid someone needs to keep in mind some environmental parameters such as flammability, corrosiveness and toxicity.

The most significant parameter to choose working fluid is about its environmental performance which is determined by the effect of it to the ozone layer (Ozone Depletion Potential, ODP) according to the directive 2037/2000 EU and the Global Warming Potential (GWP) which is the potential of the fluid to overheat the planet, according to 842/2006 EU.

Table 1-1. Different working medium properties (Quoilin, n.d.)[19]

Working Medium	Tc[°C]	Pc[bar]	Ts,1[°C]	$P_{s,20oC}$[bar]
R134a	101.8	40.6	-26.4	5.7
R227ea	101.8	29.3	-16.6	3.9
R236fa	129.9	32.0	-1.8	2.3
R245fa	154.0	36.5	14.8	1.2
R141b	204.4	42.1	31.7	0.7
R365mfc	186.9	32.7	39.8	0.5
cyclohexane	280.5	40.8	80.3	0.1

1.5 Solar Power Towers review

1.5.1 Ivanpah Solar Electric Generating system

The Ivanpah Solar Electric Generating System is a concentrated solar thermal plant in the desert. It is placed at the place of Clark Mountain California, across the State Line of Primm, Nevada. The gross capacity of the plant is 392 MW and the net turbine capacity is 377MW [21]. It consists of 173,500 heliostats each and every one of them focusing solar energy on boilers located on three centralized solar power towers. The plant started it's functioning on February 2014 although connection test to the grid were placed in the plant from September 2013.

The initial cost of the facility was 2.2 billion USD and the project was developed by the BrightSource Energy and Bechtel. Despite the initial design which was about to build a 440MW plant the actual project scaled down to 377 MW due to environmental aspects which are about to be developed subsequently.

Figure 1-14. **The Ivanpah Solar Electric Generating System [20]**

The turbine that was linked to the generator was a 123 MW Siemens SST-900 single-casing reheat turbine [22] Siemens also supplied instrumentation and control systems [23]. The plants use BrightSource Energy's "Luz Power Tower 550" (LPT 550) technology [24] which heats the steam to 550 °C directly in the receivers'. The plant has no storage facility [25]. In order to begin its function, the plant has to use Natural Gas. In 2014 the plant burned 254GWh of natural gas emitting 46084 metric tons of carbon dioxide, which is nearly twice the pollution threshold at which power plants and factories in California are required to participate in the United States emissions program to reduce carbon [26].

If that fuel had been used in a Combined Cycle Gas Turbine (CCGT) plant, it would have generated about 124 GWh of electrical energy [26]. The facility used that gas plus solar energy to produce 419 GWh of electrical energy (more than four times that of the referenced CCGT plant). The total construction of plant consists of 3 units. The units 1 and 3 produce 640GWh/yr and unit 2 produce 336Gwh/yr. One heliostat mirror is 7.02 m^2 reflecting surface [26], giving a total of 14.05 m^2 per heliostat because each heliostat consists of 2 pieces. The total plant heliostat reflecting surface results in 173500 heliostats × 14.05 m^2/heliostat = 2437144 m^2. If the mirrors could always be perpendicular to sun's ray, based on irradiance, the intercepted solar energy flow is 2717 MWh/m^2/yr × 2437144 m^2 = 6621720 MWh yearly.

The height of the tower is 140m [25]. The type of the receiver, is solar receiver steam generator. As a result, the steam is generated in the receiver and then it is forwarded in the turbine. The inlet temperature in the receiver is 248.9°C and the outlet temperature is 565.6°C.

Last but not least, the power cycle pressure is calculated to 160 bar and the method of cooling the water-steam mixture that comes out of the turbine is air (dry cooling).

1.5.2 Crescent Dunes Solar Energy project

The Crescent Dunes Solar Energy project is an 110MW solar thermal power project with 1.1gigawatt-hours of energy storage located near Tonopah, about 310 km northwest of Las Vegas. Crescent Dunes was the first concentrated solar power (CSP) plant with a central receiver tower and advanced molten salt energy storage technology from Solar Reserve.

It was developed by SolarReserve and owned by Tonopah SolarEnergy. The initial cost of the construction was 975 million USD 2015 values, corresponding to 1,015milion USD of 2017.This has a result of 8,864 USD/KW in 2015 values or 9,227 KW 2017 values. The heliostat solar field has an aperture area of 1,197,148 m^2, molten salt is used as heat transfer fluid, the receiver inlet temperature is 288 ^oC, and the receiver outlet temperature is 565^oC.The plant has TES and no initial ignition by NG. The TES has 2 tanks which gives storage capacity of 10 hours. The Rankine power cycle has a maximum pressure of 110 bar.

Figure 1-15. Crescent Dunes solar power tower project [5]

The project started operation in November 2015.While the planned electricity generation was 500,000MWh/year (CF 51.89%) the “real” electricity that was produced in 2016 was only 127,308 MWh/year. This particular year the plant was operated 10 months from January to October. In October 2016 the plant was shut-down due to a leak in Molten Salt tank and returned to operation in July 2017. Using the actual production of 2016, the capacity factor is only 13% (Boretti et al., 2019) [27]. The extra thermal energy is stored in the molten salt and can be used to generate power for up to 10 hours, when the direct sunlight is not available. The

storage technology eliminated the need of additional fossil fuels such as natural gas. In order to melt the working medium (salt) it took 2 months and about 32,000,000kg of it. Once it is melted it stays inside the plant for all its lifetime and is being cycled and reheated in the receiver [28].

Maximum actual energy output that accounts for maintenance (i.e., capacity factor) was re-estimated at 500 GWh annually, though the highest producing year thus far, 2018, only attained 40% of that [5]. Crescent dunes began its operation in September 2015 but went off-line in October 2016 due to a leak in a molten salt tank. It returned to operation in July 2017. Its average monthly production was about to exceed 40,000MWh until its last performance on May 2019 it never reached that value. Below can be observed the generation in MWh of Crescent Dunes Solar energy for different months between 2015 and 2019.

Year	Jan	Feb	Mar	Apr	May	Jun	Jul	Aug	Sep	Oct	Nov	Dec	Total
2015										1,703	1,831	0	3,534
2016	1,508	9,121	7,099	2,158	11,485	6,216	25,560	28,267	30,514	5,410	0	0	127,338
2017	0	0	0	0	0	0	9,420	9,192	13,666	9,263	488	0	42,029
2018	795	5,145	5,907	13,801	10,653	33,387	23,749	33,169	31,632	21,253	8,130	8,189	195,810
2019	12,889	14,431	20,041	2,807	0	0	0	0	0	0	0		50,168
Total (2015-2019)													418,879

Figure 1-16. Generation in MWh of Crescent Dunes for different months between 2015 and 2019 [29]

Despite the good aspects of this project in May 2019 the plant shut down because NV Energy who was responsible for the purchase of the electricity generated, broke the contract due to the lack of the plant to achieve the production that was firstly agreed.

1.5.3 Ashalim power station

The Ashalim Power station is a solar power station in the Negev desert south of the district of Beersheba in Israel. The electricity production began on September 2019. It has the tallest tower in the world including the boiler which reaches the height of 250 meters with the receiver's height being ~17m and receiver's diameter being ~20m. It is a 121 MW project including 55,000 heliostats. The installed capacity is enough to power 120000 homes. It is said that it will avoid 110,000 tons of CO_2 each year during its lifetime [20]. It produces 320 GWh of energy per year. The solar tower uses molten salt to allow the plant to operate for up to 4.5 hours with the absence of the solar radiation. The initial cost of the project was nearly 570 million USD and a joint venture of BrightSource Energy Inc. and Alstom SA.

Figure 1-17. **Ashalim biggest world tower and heliostat field [30]**

1.5.4 Quarzazate Solar Power Station

Quarzazate Solar power station (OSPS) also called Noor Power Station is a solar power complex located in Morocco, 10 km from Quarzazate town, in Ghessat rural council area. At 510 MW is the world's largest CSP. From these MW only 150Mw are about solar power tower with 7.5 hours capacity storage. The Characteristics of Noor III can be described in the below table

Table 1-2. Basic Characteristics of Noor III station (Relloso & Gutiérrez, 2017) [31]

Parameter	Value
Tower height	250 m
Mirror aperture area	1,3 Mm^2
Number of heliostats	7400
Heliostat type	HE54
Solar Field Area	550 Ha (5,5 km^2)
Turbine gross Power	150MW_e
Receiver Thermal Power	660MW_{th}
Storage Capacity	7.5 h
Cycle Cooling	Dry, Air Cooled Condenser
Molten Salt Maximum	565ºC
CO_2 Saving	130,000 tons/year

Vivid research upon solar towers in Ashalim has been done in order to investigate how effective the tower can work in cloudy conditions. In order to achieve stable and high-performance operation in cloudy days, spatial high resolution direct normal irradiance (DNI) measurement is vital for the control of flux in CSP towers. In Ashalim solar power plant, the Solar Receiver Steam Generator (SRSG) consists of 24 different targets each and every one of them having different load requirement and flux density limitations. That's why an exact and accurate heliostat aiming plan is required to properly use each heliostat.

In the solar field the control of a heliostat and therefore the load that can provide depends on both constant and transient parameters. Constant parameters can be heliostat's size, angle and distance from the receiver. Transient parameters can be considered heliostat's and sun's orientation and the DNI. From bibliography, can be elicited that when DNI drops solar field can compensate by using more heliostats, thus maintaining stable load. However, in this case, variations in the DNI can cause local overheating of the receiver causing permanent damage. If the exact DNI of each heliostat is ignored, a maximum number of DNI in order to avoid overfluxing of the receiver need to be assumed. This has a result of underutilization of solar irradiance and under performance during cloudy conditions. On the contrary, if DNI can be calculated with other more exact solutions, solar irradiance and solar field can be utilized in better ways.

In Ashalim each of the installed heliostats is unwired and uses a small Photovoltaic unit (PV) charging a battery which provides all the energy the heliostat need to operate (Minis et al., 2019) [32]. The new idea of DNI measurement uses this PV unit as a local isolation sensor. If these measurements are combined with some fixed sensors in the field, the short-circuit current that is measured by this PV cell is translated to the DNI available for each heliostat.

Figure 1-18. **PV is shown on the top left of the heliostat (Minis et al., 2019) [32]**

The transition from PV to DNI is based on the idea that small-circuit current on PV is proportional to the effective irradiance at the PV plane and that the irradiance is a sum of the direct, the diffusive and ground-reflected irradiance projected on the PV plane.

$$f\cdot I_{pv} = I_b \cdot \cos\cos(\theta) + I_d \cdot \frac{1+\sin\sin(\beta)}{2} + I_g \cdot \frac{1-\sin\sin(\beta)}{2} \quad (1)$$

I_{pv} is the PV short current (mA)
I_d is the diffusive irradiance(W/m^2)
I_g is the ground reflected irradiance (W/m^2)
β is the elevation angle of the heliostat, where 0° means it is vertical and 90° means it is horizontal
θ is the angle between the orthonormal vector of the heliostat's plane and the normal vector of the sun
f is the proportion constant factor to convert from irradiance on the PV panel to short-circuit current. (f depends on the properties of PV panels and may differ from one to another; f is a unit converter from mA to Watt.)

The angles β, θ and the PV current I_{pv} are known and collected from the solar field heliostats during real time operation. The irradiance that is being reflected from the ground can be

predicted, by good approximation, to be isotropic and calculated as I_g=ρ*G*H*I where ρ =0.3 in desert sand soil (Ineichen et al., 1990) [33].

When there are no clouds I_b can be retrieved from dedicated sensors located in the solar field central weather station. What's more when the sky is clear DNI is even enough across the solar field area. It needs to be mentioned that when the sky is cloudy the diffusive radiation is uniform across the solar field area. Thus, I_d can be found from Pyranometer instruments placed at the boundary of solar field.

This has a result of only unknown f when the sky is clear and in this way can be found. Later, when the sky is cloudy f can be used to solve for I_b:

$$I_b = \frac{(f \cdot I_p - I_d \cdot \frac{1 + \sin\sin(\beta)}{2})}{\cos(\theta)} \quad (2)$$

In the process that is described above there are some inaccuracies that can occur. A significant one is sensor inaccuracies and one more is model inaccuracies due to oversimplification of the phenomena involved. Below can be detected the 3 types of solar radiation measurement instruments that were used in Ashalim:

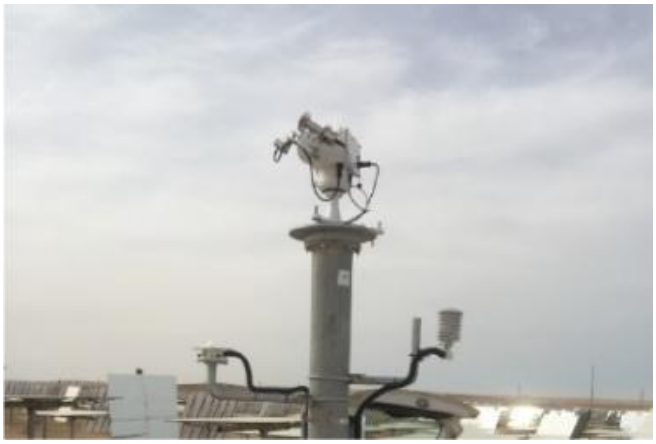

Figure 1-19. Epply Model sNIP Pyrheliometer in Ashalim (Minis et al., 2019) (Minis et al., 2019) [32]

Figure 1-20.Pyranometer, used to measure the global irradiance, leveled on a horizontal plane in Ashalim (Minis et al., 2019) [32]

Figure 1-21. A patented instrument that can measure global and diffused insolation. 4 SPN1 instruments are installed, in the 4 corners of the perimeter of the solar field (Minis et al., 2019) [32]

1.5.5 Khi Solar One

Khi solar One is a solar thermal power station located in the Northern Cape region of South Africa. Khi Solar One has a 50MW installed capacity and is the first solar power plant in Africa. It aims to deliver 186 GWh per year that will prevent approximately 183,000 tons of CO_2 emissions per year and will support with energy 45,000 households. The height of the tower is 205 m and 30 meters in diameter at the top and 40 m at the base. The solar field covers more than 576,800 m^2 and allocates 4530 mobile heliostats with a curved reflective surface to concentrate solar radiation on a receiver at the top of the tower.

Figure 1-22. **Khi Solar One Power Cycle [34]**

The solar receiver consists of a series of tube panels operating at high temperature and reusing pressurized water. The steam produced is partially stored in storage tank located partially at the top of the tower in order to be used when not enough steam is generated. What is left is being sent in a turbine to generate electricity. This construction consists of two different receivers. The first receiver (evaporator) converts water to steam which is led into the second receiver where steam is reheated thus allowing reaching higher temperatures (540^{o}C at 130 bar) and increasing the efficiency of the power cycle. Despite the modern trend to store energy with molten salts Khi Solar One uses its superheated steam to store energy up to 2 hours and in tanks of 247 m^{3}.

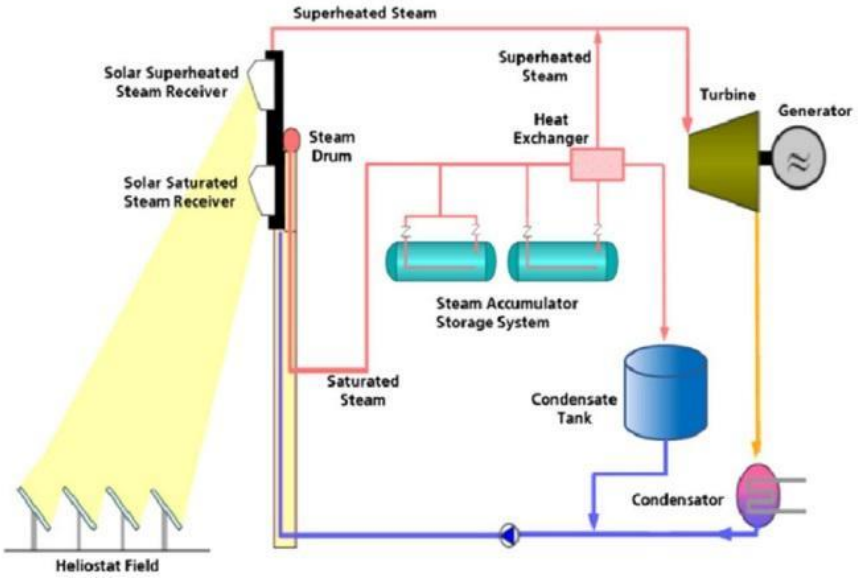

Figure 1-23. Scheme of 50 MW Khi Solar One plant with steam accumulator TES system (Falcoz et al., 2018) [35]

1.6 Thesis scope

This study aims to examine from both an energetic/exergetic as well as an economical point of view the operation of a coupled system of solar power tower, thermal energy storage, and power plant and identify its viability as an application in four different climate zones of Greece.

In the next chapters are going to be addressed the below questions:

- How the 3 different parts can be modelled in order to work properly as a unity and give results?
- How efficient from an Energy and Exergy point of view is the coupled system?
- What is the total capital cost of the whole investment but also the economic indexes for such a project?
- How applicable is the model that will be created in the regions of Greece?

In order to answer to all these questions a thorough analysis is going to be realized. Each single model will be coupled to an entire unity which will be implemented in different case scenarios in order to find the best match combination of payback period, Net Present Value and Levelized Cost of Energy.

2. Modelling of Solar Power Tower System

2.1 Solar Power Tower

The heat source for the TES and Power Block system comes from the receiver of the Solar Power Tower. For the modelling of the SPT and the rest equipment of the plant (Mostafavi Tehrani & Taylor, 2016) [36] equations were used. The analysis of the researchers is based on a cavity receiver mathematical model which leads to a non-linear equations set, that was solved using MATLAB. It is known that the direct sunbeams hit the heliostats and reflect to the cavity receiver on top of the tower. Depending on the distribution of the heliostats and distance from the tower base each heliostat has its own efficiency. With equation (1) below can be defined an average efficiency for the whole solar field. It is made the assumption that the average field efficiency is 60%.Once the efficiency and the total area of the heliostat field is defined the total incident energy on the cavity receiver can be found:

$$\eta_{field} = \eta_{cos} * \eta_{shadow} * \eta_{block} * \eta_{ref} * \eta_{att} * \eta_{spill} \quad (3)$$

$$Q_{field} = DNI * A_{field} \quad (4)$$

$$\eta_{field} = \frac{Q_{rec,in}}{Q_{field}} \quad (5)$$

The total energy balance of the molten salt cavity receiver can be written as proposed by (Li et al., 2010) [37] and (Benammar et al., 2014) [38].While the heat transfer fluid absorbs energy, it is continually lost by different sources such as reflection, conduction, radiation, natural and forced convection.

$$Q_{rec,in} = Q_{loss,total} + Q_{abs} \quad (6)$$

$$Q_{loss,total} = Q_{ref} + Q_{cond} + Q_{rad} + Q_{nc} + Q_{fc} \quad (7)$$

$$\eta_{rec,energetic} = \frac{Q_{abs}}{Q_{rec,in}} \quad (8)$$

In order to calculate the energy balance of the receiver, an extra equation has been provided by Winter et al. [39] where $T_{rec,sur}$ is the average receiver surface temperature and T_{ms} is the average temperature of the molten salt in the receiver. Concentration ratio C and view factor Fr are constant design parameters while receiver surface area, the receiver aperture area, and the total heliostatic field area are parameters that has to be defined. The assumption is made, that the width (W) of the aperture is half of the receiver's aperture height (H).

$$Q_{rec,in} = \frac{T_{rec,sur} - T_{ms}}{\frac{d_0}{d_i * h_{ms}} + \frac{d_0}{2 * \lambda_{rec,tube}} \ln\frac{d_0}{d_i}} = \frac{Q_{rec,in}}{A_{rec,sur}} \quad (9)$$

$$Nu_{ms} = 0.023 * Re_{ms}^{0.8} * Pr_{ms}^{0.4} = \frac{h_{ms} * d_i}{\lambda_{ms}} \quad (10)$$

$$Re_{ms} = \frac{2 * \dot{m}_{ms}}{\pi * N_{rec,tube} * r_i * \mu_{ms}} \quad (11)$$

$$T_{ms} = \frac{T_{rec,out} + T_{rec,in}}{2} \quad (12)$$

$$F_r = \frac{A_{rec,ap}}{A_{rec,sur}} = \frac{H * W}{A_{rec,sur}} \quad (13)$$

$$W = 0.5 * H \quad (14)$$

$$C = \frac{A_{field}}{A_{rec,ap}} \quad (15)$$

At the design point, the total energy that is absorbed by the cavity receiver is the same that is needed to run the Power Block system. This energy, depends on the mass flowrate of the molten salt and the Power blocks inlet/outlet temperatures. It should be mentioned that the Rankine cycle inlet and outlet temperatures correspond to the cavity receiver outlet and inlet temperatures, respectively.

$$Q_{abs} = Q_{PB} = \dot{m}_{ms} * C_{p,ms} * (T_{PB,out} - T_{PB,in}) \quad (16)$$

$$N_{rec,tube} = \frac{4 * \dot{m}_{ms}}{\rho_{ms} * V_{max,ms} * \pi * d_i^2} \quad (17)$$

According to (Li et al., 2010) [37], the cavity receiver only exchanges heat between the receiver surface and the ambient environment, so the radiative heat loss can be found by equation (16).

$$Q_{rad} = \varepsilon_{avg} * \sigma * \left(T^4_{rec,sur} - T^4_{amb}\right) * A_{rec,sur} * Fr \quad (18)$$

$$\varepsilon_{avg} = \frac{\varepsilon_w}{\varepsilon_w + (1 - \varepsilon_w) * Fr} \quad (19)$$

Where σ is Stefan-Boltzmann constant:

$$\sigma = 5.67 * 10^{-8} \quad \mathrm{W/(m^2K^4)} \tag{20}$$

Another great loss of the cavity receivers which is considered to be the highest share of loss is the reflection of the incident arrays escaping from the aperture. It is assumed that the receiver reflectivity is not temperature dependent so the reflection heat loss can be calculated by equation (19).

$$Q_{ref} = \rho * Q_{rec,in} * Fr \tag{21}$$

According to Siebers and Kraabel [40] forced convective heat loss in cavity receivers was found to be similar to forced convection loss from a flat plate, if the size of the aperture area and the average receiver surface temperature of receiver surface are used in equations (20) and (21), (22).Natural convection in the cavity receiver was also considered to be similar to flat plate and the empirical correlations in (23) and (24) prove that. The reference length in calculations is the height, H.

$$Q_{fc} = h_{fc} * \left(T_{rec,sur} - T_{amb}\right) * A_{rec,ap} \tag{22}$$

$$Nu_{fc} = 0.0287 * {Re_{fc}}^{0.8} * {Pr_{air}}^{1/3} = \frac{h_{fc} * H}{\lambda_{air}} \tag{23}$$

$$Re_{fc} = \rho_{air} * V_{wind} * \frac{H}{\mu_{air}} \tag{24}$$

$$Q_{nc} = h_{nc} * \left(T_{rec,sur} - T_{amb}\right) * A_{rec,sur} \tag{25}$$

$$h_{nc} = 0.81 * \left(T_{rec,sur} - T_{amb}\right)^{0.426} \tag{26}$$

Heat conduction has a minimal effect in the performance of the cavity receivers. There are three parallel conductive loss sources: conduction through the insulation layer, through support structure and air convection between the insulation layer and receiver panel.

$$Q_{cond} = \frac{\left(T_{rec,sur} - T_{ins}\right) * A_{rec,sur}}{\frac{\delta_{ins}}{\lambda_{ins}}} = \frac{(T_{ins} - T_{amb}) * A_{rec,sur}}{\frac{1}{h_{mix}}} \tag{27}$$

In the above equation h_{mix} is a combined heat transfer coefficient that can be calculated with the bellow formula:

$$h_{mix} = \left({h^a}_{air,fc} - {h^a}_{air,nc}\right)^{1/a}, a = 1 \tag{28}$$

$$\mathrm{Nu_{air,fc}} = 0.0239 * \mathrm{Re_{air,fc}}^{0.805} * (\frac{0.785 * \mathrm{T_{ins}}}{\mathrm{T_{amb}}})^{0.2} * 1.167 * \mathrm{Pr_{air}}^{0.45} = \frac{\mathrm{h_{air,fc}} * \mathrm{H}}{\lambda_{\mathrm{air}}} \quad (29)$$

$$\mathrm{h_{air,nc}} = 1.24 * (\mathrm{T_{ins}} - \mathrm{T_{amb}})^{1/3} \quad (30)$$

Regarding energetic analysis of the cavity receivers, the exergetic analysis of this component can be written as follows (Xu et al., 2011) [41], and (Le Roux et al., 2012) [42]:

$$\mathrm{Ex_{rec}} = \mathrm{Ex_{rec,abs}} + \mathrm{Ex_{rec,loss}} + \mathrm{T_{amb}}\dot{\mathrm{S}}_{\mathrm{gen}} \quad (31)$$

$$\mathrm{Ex_{rec,abs}} = \dot{m}_{ms} * C_{p,ms} * (T_{rec,out} - T_{rec,in} - T_{\mathrm{amb}} ln \frac{T_{rec,out}}{T_{rec,in}}) \quad (32)$$

$$\mathrm{Ex_{rec,loss}} = Q_{loss,total} * \left(1 - \frac{\mathrm{T_{amb}}}{\mathrm{T_{rec,sur}}}\right) \quad (33)$$

$$\dot{\mathrm{S}}_{\mathrm{gen}} = \frac{-\mathrm{Q_{rec,in}}}{T_{sun}} + \frac{\mathrm{Q_{loss,total}}}{\mathrm{T_{amb}}} + \dot{m}_{ms} * C_{\mathrm{p,ms}} * \ln\left(\frac{T_{rec,out}}{T_{rec,in}}\right), T_{sun} = 5778K \quad (34)$$

$$\eta_{\mathrm{rec,energetic}} = \frac{\mathrm{Ex_{rec,abs}}}{\mathrm{Ex_{rec}}} \quad (35)$$

In the table below are mentioned thermo-physical properties of solar salt and air used in simulations:

Table 2-1. Average thermo-physical properties of solar salt and air used in simulations [36]

HTF and PCMs thermal properties	Unit	Solar Salt	Air
Dynamic Viscosity	$Kgm^{-1}s^{-1}$	0.00326	0.00002285
Density	Kgm^{-3}	1820	0.88
Specific Heat Capacity	$Jkg^{-1}K^{-1}$	1553	1014
Thermal Conductivity	$Wm^{-1}K^{-1}$	0.52	0.03

2.2 Dynamic Modeling of Thermal Energy Storage System

Generally, there are different types of heat energy storage systems and thus different scientific approaches. A TES system allows exploiting surplus of thermal production during low demand periods and using it when high demand occurs. As a result, discharging phase occurs in different period than the charging one. Thermal Energy Storage systems can offer environmental and economic benefits by reducing the needs for burning fuel and improving the use of cogeneration plants. There are mostly three types of storing heat: sensible, latent and chemical heat storage [8]. In this diploma thesis sensible heat storage is going to be examined. In this very situation thermal energy can be stored by increasing the temperature of a substance, i.e., by increasing its internal energy. Sensible thermal energy storage (STES) consists of a container, for example a tank, and a storage medium, in this case alumina that operates in temperatures that do not permit phase change and breakage of chemical bonds.

Usually a two-tank construction is used to store sensible thermal energy. In these configuration HTF is at the same time transfer fluid and storage medium. The heated fluid is stored in a hot tank and used during demanding periods (discharging phase). The cooled fluid is then stored via pumps in a cold tank, 'waiting', until next charging phase of it.

Alternatively, a single-tank construction can be used to avoid the empty volumes of the two-tank configurations in order to reduce investment costs. In this thesis a single tank configuration will be used in which a thermocline is maintained within the tank due to buoyancy effect and thermal stratification which creates an effective separation between warm fluid at the top and cold fluid at the bottom. Single phase solid will be used to fill most of the tank volume, and act as primary thermal storage medium (packed bed systems).

In this phase, it is going to be presented the zero-dimensional model which was used for the calculations of charging and discharging phase. The model of (Raccanello et al., 2019) [10] was used for the below calculations.

- Zero-Dimensional Model: Also called perfect mixing model is considered as a unique fully mixed region having uniform temperature. The dynamic behavior of the storage is described by the time steps of the uniform temperature inside the tank and can be calculated by solving ordinary differential equations of energy balance.
- Sensible Packed Bed System: Our tank is filled with no-phase change material (alumina). The filler particles are considered homogenous, continuous, isotropic, uniformly distributed without temperature gradients.

2.2.1 On Design Analysis

To start with, it is considered that the results of the previous chapter are datum to this chapter in order to validate the code model that was created. It is considered that:

- Void Fraction: ε =0.4
- Diameter of the filler material: d_p=0.055 mm
- Height of the tank: L=10.5 m [43]
- Diameter of the tank: D=23 m [43]
- Thickness of insulation: thickness=0.62 m
- Acceleration due to earth's gravity: g=9.81 m/s²
- Density of filler material (alumina): ρ=3550 kg/m³
- Density of stainless-steel tank: ρ_{ap}=8050 kg/m³
- Density of molten salt: ρ_{ms}=1820 kg/m³
- Dynamic viscosity of molten salt: μ_{ms}=0.00326 kg/(m·s)
- Specific heat capacity of molten salt: Cp=1553 J/(kg·K)
- Thermal conductivity of molten salt: λ_{ms}=0.52 W/(m·K)

In order to calculate the internal convective heat transfer coefficient a_i between the storage medium and the tank walls the below formula is used:

$$D_i = D - 2 * \text{thickness} \tag{36}$$

Where D_i is the inner dimension of the diameter of the cylindrical vertical tank.

The heat transfer coefficient, β, is calculated with the assumption of constant pressure:

$$\beta = -\frac{\rho_{ap} - \rho}{\rho * (T_{ap} - T)} \tag{37}$$

Where T_{ap} is the internal temperature of the steel tank and T is the temperature of the fluid which is inserted in the tank and had been mentioned in previous chapters as $T_{f,in}$.

The kinematic viscosity of the fluid is calculated below:

$$\nu = \frac{\mu_{ms}}{\rho_{ms}} \tag{38}$$

The Grashof number need to be calculated in order to find the Nusselt number and finally to calculate the a_i:

$$Gr = \frac{(g * b * T - T_{ap}) * D^3}{v^2} \tag{39}$$

The Prandtl number calculated for the molten salt:

$$\mathrm{Pr} = \frac{\mu_{ms} * C_p}{\lambda_{ms}} \quad (40)$$

The multiplication between Prandtl and Grashof number was calculated and it was found out that the flow is turbulent inside the tank so the suitable equation for the Nusselt number will be used.

$$\mathrm{Nu} = 0.13 * (\mathrm{Pr} * \mathrm{Gr})^{1/3} \quad (41)$$

The thermal conductivity of the tank shell was set λ=50 W/mK for steel tank.

$$a_i = \frac{\mathrm{Nu} * \lambda}{L} \quad (42)$$

Now it is time for the (a_e) external convective heat transfer coefficient to be calculated.
In order to calculate β_e (heat transfer constant for the external convection) REFPROP of NIST program is used. In order to go on with the calculations the properties of air from the Table 2.1 of previous chapter were used.

$$v_{air} = \frac{\mu_{air}}{\rho_{air}} \quad (43)$$

$$\mathrm{Gr}_e = \frac{(g * \beta_e * T - T_{ap}) * L^3}{{v_{air}}^2} \quad (44)$$

$$\mathrm{Pr}_e = \frac{\mu_{air} * Cp_{air}}{\lambda_{air}} \quad (45)$$

$$\mathrm{Nu}_e = 0.13 * (\mathrm{Pr} * \mathrm{Gr})^{1/3} \quad (46)$$

Where the L in the above equation is the vertical height of the tank. As a result, the external heat transfer coefficient was calculated.

$$a_e = \frac{\mathrm{Nu}_e * \lambda}{L} \quad (47)$$

All configurations have a vertical cylindrical geometry. Accordingly, the overall heat loss coefficient UA (W/K) is obtained from:

$$UA = \left(\frac{1}{\pi * D_i * L * a_i} + \frac{\ln\left(\frac{D_i}{D_e}\right)}{2 * \pi * \lambda * L} + \frac{1}{\pi * D_e * L * a_e} \right)^{-1} \quad (48)$$

Where L, D_i, D_e are the height, internal and external diameter of the tank respectively.

In the case of filler material, the heat transfer coefficient between filler material and HTF is calculated by the equations of Nusselt number provided in (Wakao & Funazkri, 1978) [44] using Reynolds number of particles.

$$\mathrm{Nu} = \frac{a_{fg} \cdot d_p}{\lambda_f} = 2 + 1.1\mathrm{Re_p}^{0.6} + \mathrm{Pr}^{1/3} \quad (49)$$

For the spherical geometry of filler particles, the total heat transfer coefficient A_{fg} is calculated as:

$$A_{fg} = V_s \cdot a \quad (50)$$

Where a is the surface area of the particles per unit of volume which is calculated as a function of the void fraction ε:

$$a = \frac{6 \cdot (1 - \varepsilon)}{dp} \quad (51)$$

The effective thermal conductivity is obtained by weighing the thermal conductivities of solid material and HTF:

$$\lambda_{eff} = \varepsilon\lambda_f + (1 - \varepsilon)\lambda_g \quad (52)$$

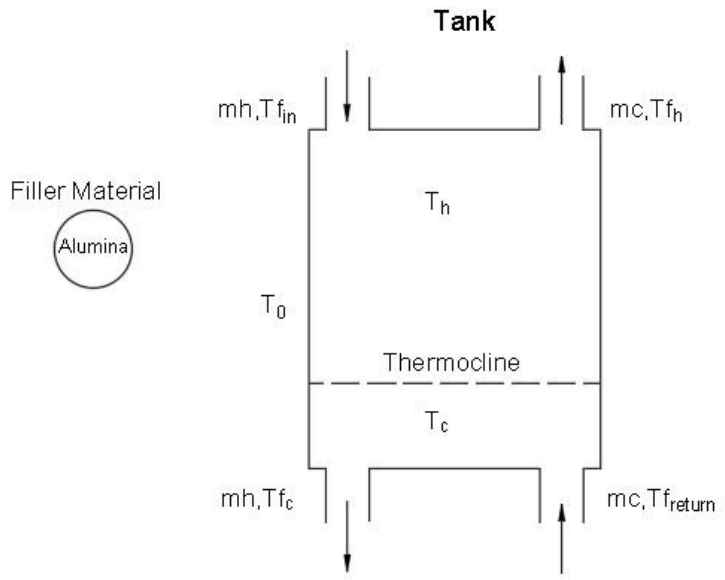

Figure 2-1. **Sketch of the thermal energy storage tank**

In order to solve the problem of charging and discharging the tank two ordinary differential equations were solved.

$$\varepsilon * V * \rho_f * C_{p,f} * \frac{dT_f}{dt} = \dot{m}_h * C_{p,f} * \left(T_{f_{in}} - T_f\right) + \dot{m}c * C_{p,f} * \left(T_{f,_{return}} - T_f\right) - a_{fg} * A_{fg} * \left(T_f - T_g\right) - UA * (T_f - T_0) \quad (53)$$

$$(1 - \varepsilon) * V * \rho_g * C_{p,g} * \frac{dT_g}{dt} = a_{fg} * A_{fg} * \left(T_f - T_g\right) \quad (54)$$

Computational iterative method was used to solve the above equation. Particularly, explicit finite difference scheme was used. In these kind of schemes the temperature at time n+1 depends explicitly on the temperature at time n. The explicit finite difference discretization of the above equations can be seen below:

$$T_{f_i}^{j+1} = T_{f_i}^{j} + \frac{Dt * \dot{m}h * \left(T_{f_{in}} - T_{f_i}^{j}\right)}{\varepsilon * V * \rho_f} + \frac{Dt * \dot{m}c * \left(T_{f_{return}} - T_{f_i}^{j}\right)}{\varepsilon * V * \rho_f} - \frac{Dt * a_{fg} * A_{fg} * \left(T_{f_i}^{j} - T_{g_i}^{j}\right)}{\varepsilon * V * \rho_f * C_{p,f}} - \frac{Dt * UA * \left(T_{f_i}^{j} - T_0\right)}{\varepsilon * V * \rho_f * C_{p,f}} \quad (55)$$

$$T_{g_i}^{j+1} = T_{g_i}^{j} + \frac{Dt * a_{fg} * A_{fg} * \left(T_{f_i}^{j} - T_{g_i}^{j}\right)}{(1 - \varepsilon) * V * \rho_g * C_{p,g}} \quad (56)$$

Below can be observed that the flow chart of the code that was used to solve the above equations and below this very chart, the flow charts of the functions that were used to solve the problem.

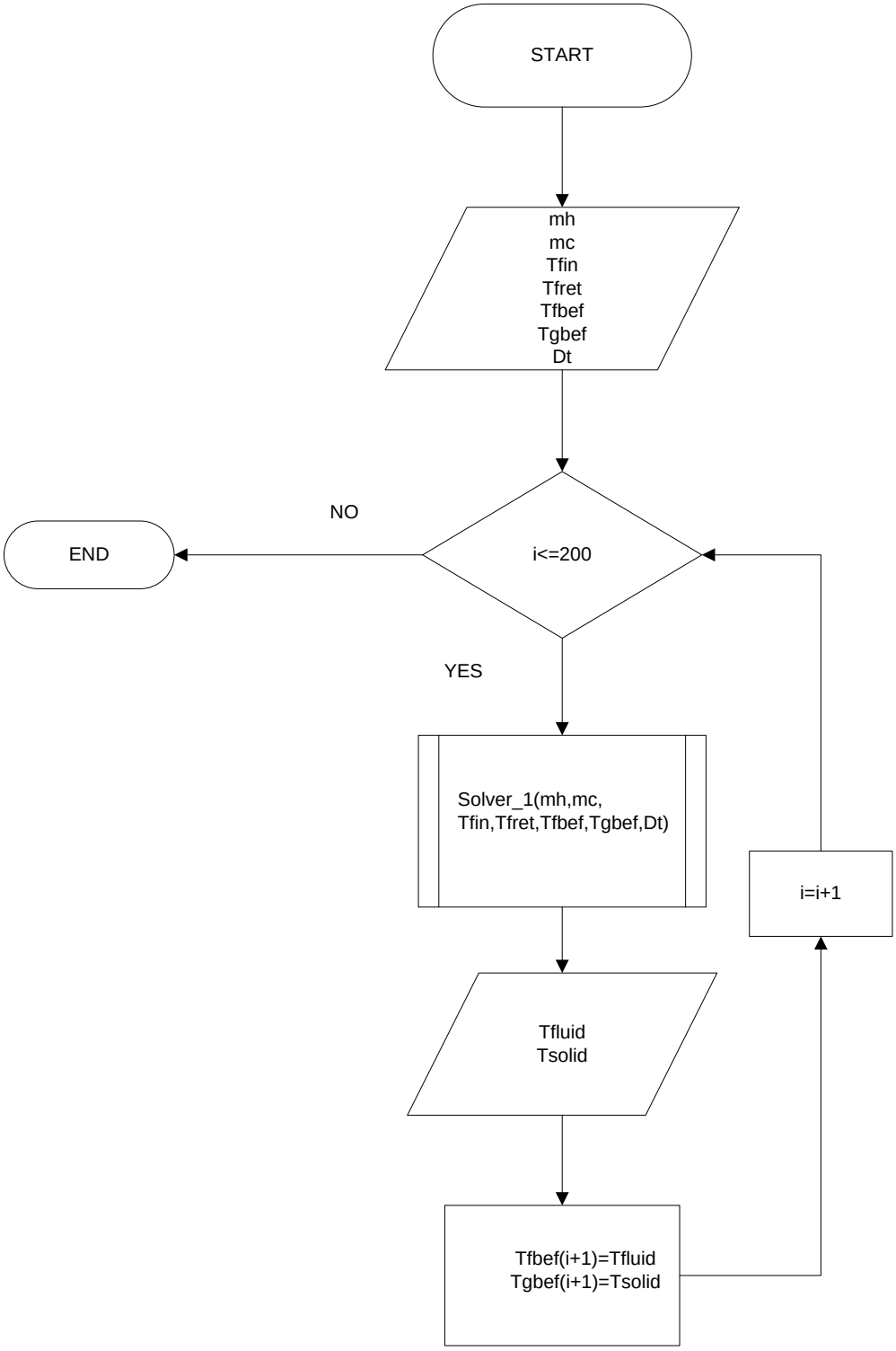

Figure 2-2. Main flowchart that solves the storage tank equations

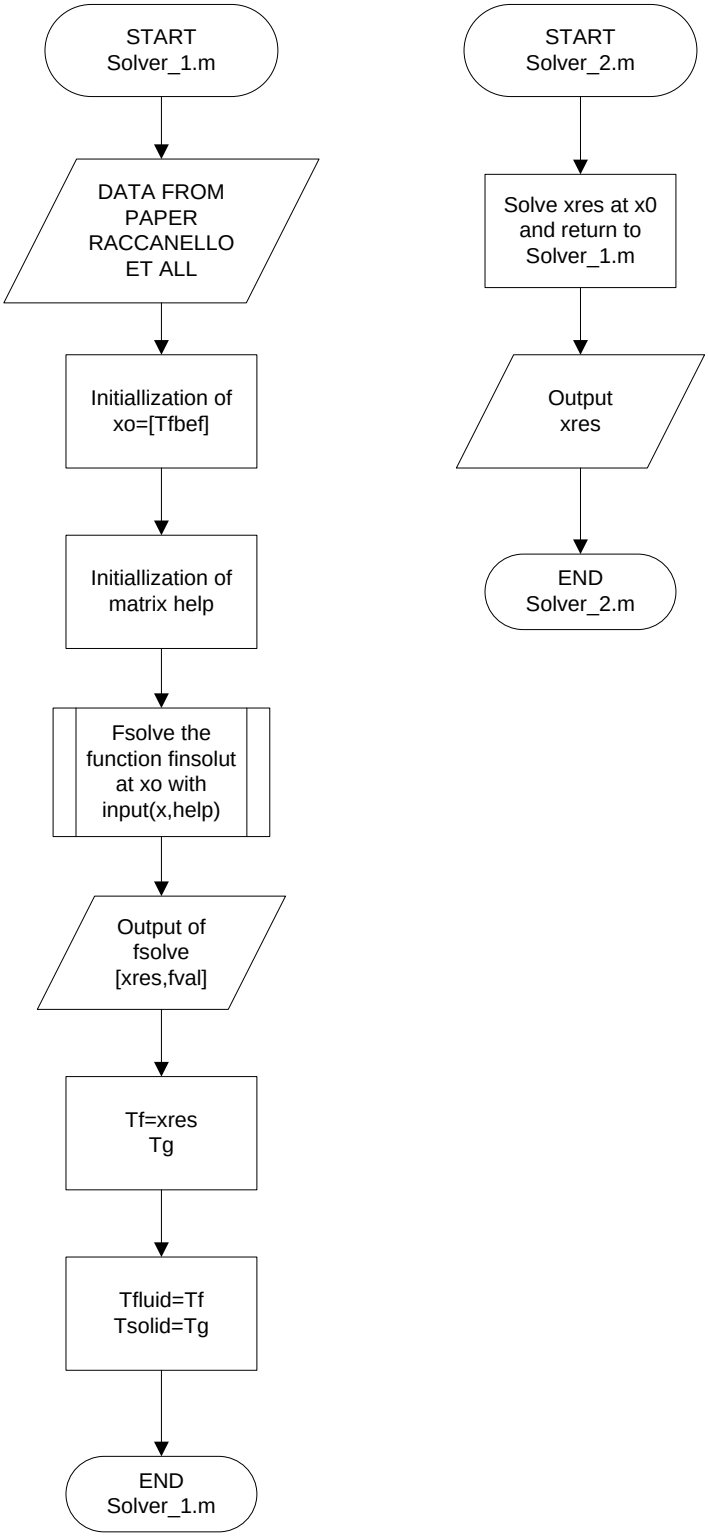

Figure 2-3. **Secondary functions that calls the main program to solve the storage tank problem**

2.3 Power Plant Modelling

The power plant construction which is coupled with the Solar Power Tower and TES unit is the basic component for the production of electricity through its coupling with the generator and then its connection with the grid. The heat of the molten salt that has been gained through the receiver of the tower is either transferred directly through the heat exchanger in the power block when the TES unit is fully stored or it is driven through the piping system to be stored in the thermal storage container. For the modeling of the system water-steam Rankine Cycle Plant due to the high temperatures arising from the solar tower.

For the Power Plant the below assumptions were made:

- Pth=80% of the produced power in the receiver
- Cpwater=4.187 KJ/kg
- Heat exchange: ΔT=279 K
- Condensation Pressure: 0.042105 bar
- Condensation Temperature: 303 K
- Mechanical efficiency: η_{mech}=0.98
- Electrical efficiency (Generator): η_g=0.98
- Density ρ of water is calculated in the point before the pumps entrance at 30°C
- It is considered ΔT_{cond}=10K temperature drop at the condenser.

It is needed to be mentioned here, that all the thermodynamic properties in each position of the power block were calculated using REFPROP program of NIST (e.g. enthalpy, entropy).

From the energy balance on the heat exchanger the mass supply can be found that is datum to the problem:

$$\dot{m}_{ms} * Cp_{ms} * \Delta T = \dot{m} * Cp * \Delta T \quad (57)$$

Where can be determined easily the mass flowrate $\dot{m}$ (kg/s) of the water-steam cycle.

According to the above calculation can be determined the volume flowrate $\dot{Q}$ (m^3/s)

From the equation:

$$\dot{Q} = \frac{\dot{m} \cdot 3600}{\rho_{water}} \tag{58}$$

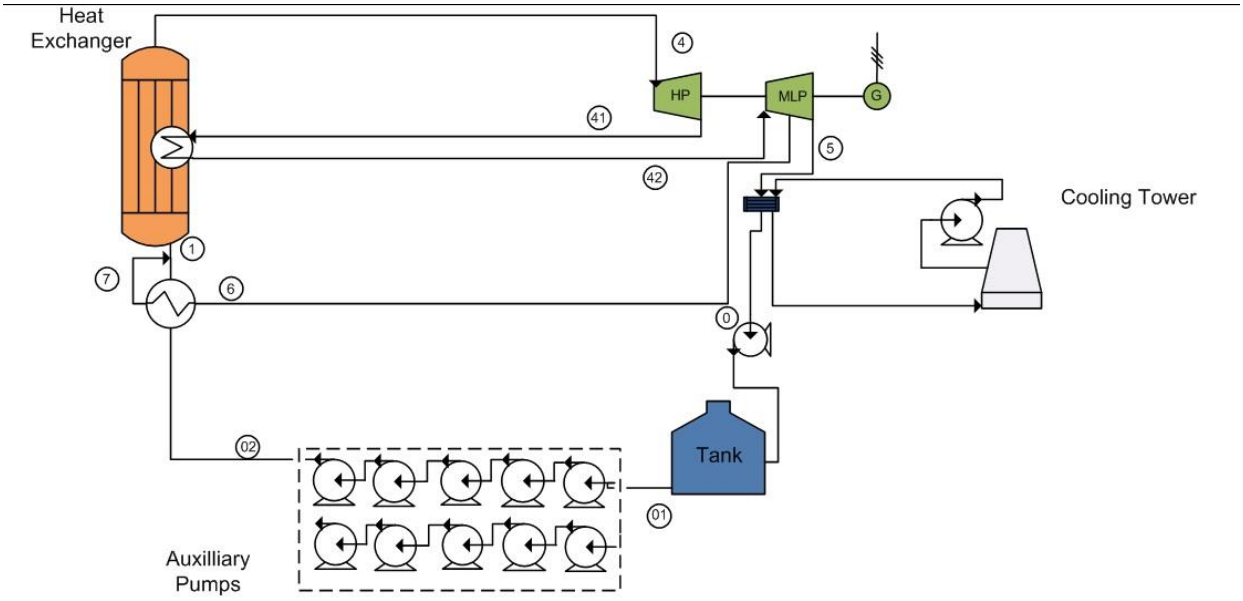

Figure 2-4. Schematic diagram of the power plant created for the project

Using the condensation pump at **0,** the pressure is increased from 0.042105 to 6.46 bar before entering the connection of the pumps in line. Doing so the phenomenon of cavitation at the first pump can be avoided.

As it can be seen above, the steam is reheated to the heat exchanger from **41** to **42** at constant pressure, the pressure is lowered to the condenser and the water is pre-heated before entering the heat exchanger in order to achieve better thermal efficiency.

For the analysis two turbines were used with 3 stages each that can succeed pressure ratios of up to 3000 bar. The turbine's isentropic efficiency is important for the calculations of enthalpy in order to create the code for the modeling of the power plant.

Below can be depicted the effect of number of stages in the isentropic efficiency of the turbine.

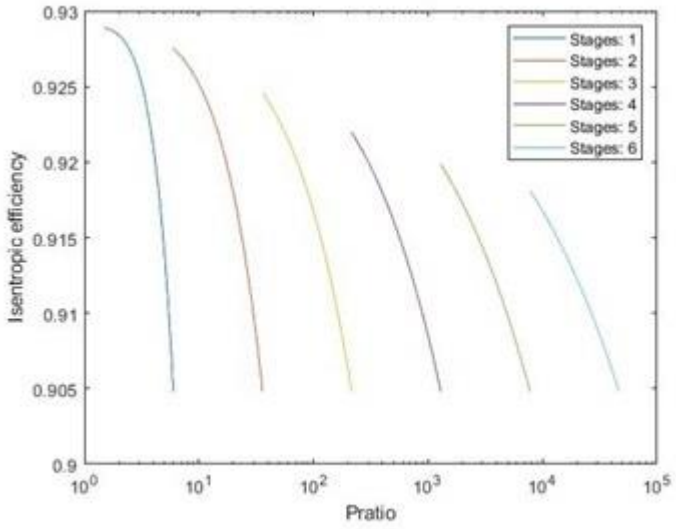

Figure 2-5 **Isentropic efficiency vs. Pressure ratio for different number of stages of turbines**

Here it needs to be mentioned that the characteristic curve for the pumps that were used, can be shown below. Firstly is presented the condensate pump and then the water-feed pumps.

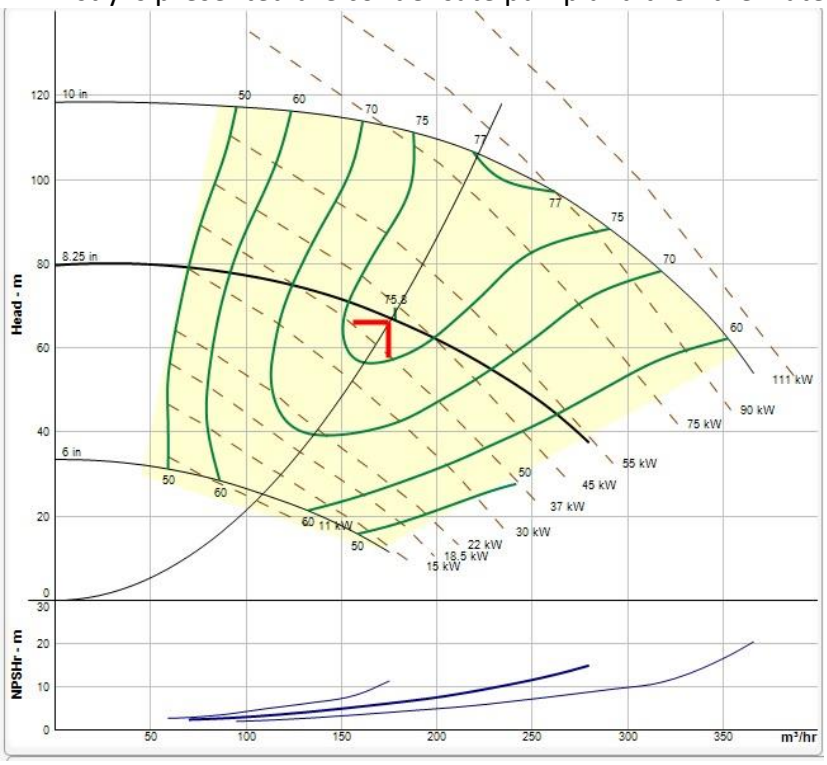

Figure 2-6. **Characteristic curves and operating point of condensate pump**

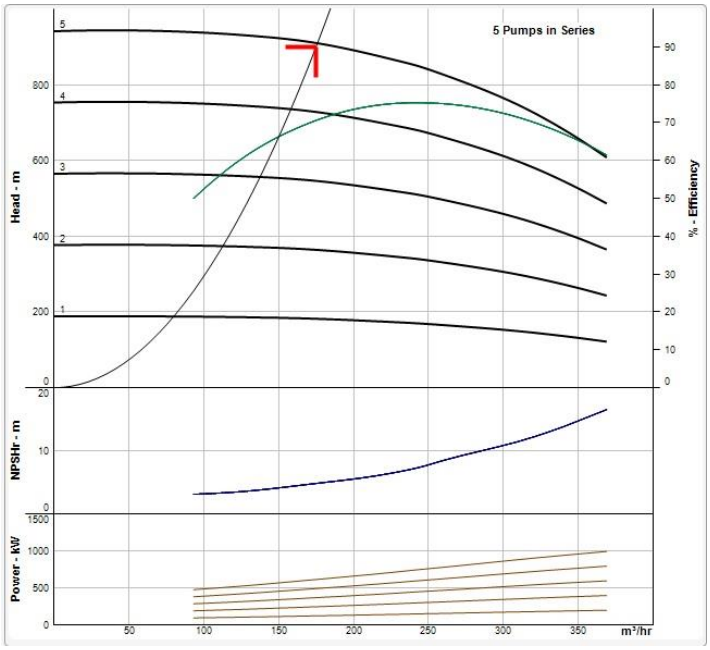

Figure 2-7. **Characteristic curves and operating point of 5 feed-water pumps in series**

From the energy balance on the pre-reheater can be obtained the mass flow $\dot{m}_1$ that is drawn-off from the turbine at the position **6**.

$$\dot{m}_1 * (h_6 - h_7) = \dot{m} * (h_1 - h_{02}) \quad (59)$$

In order to calculate the electrical power, produced in kW the below equation is used:

$$P_{el} = [\dot{m} * (h_4 - h_{41}) + \dot{m} * (h_{42} - h_6) + (\dot{m} - \dot{m}_1) * (h_6 - h_5)] * \eta_g * \eta_{mech} \quad (60)$$

From the energy balance on the condenser can be retrieved the mass flow rate of the water that comes from the cooling tower. It is assumed that the drop of the temperature of the cycle water ΔT_h is at 10 Kelvin.

$$\dot{m}_w * C_{p,water} * \Delta T_{cond} = (\dot{m} - \dot{m}_1) * (h_5 - h_0) \quad (61)$$

Last but not least, can be calculated the thermal efficiency of the whole Power Block:

$$\eta_{th} = \frac{(h_4 - h_{41}) + (h_{42} - h_6) + \frac{(\dot{m} - \dot{m}_1)}{\dot{m}} * (h_6 - h_5) - (h_{02} - h_0)}{(h_4 - h_{02}) + (h_{42} - h_{41})} \quad (62)$$

2.4 Summary Analysis – Coupling of different parts

In order to sum up the previous analysis that was made, a new code was "born" which can produce results for the Gemasolar Plant in Seville. This code will be later used in order to depict results for different climate zones in Greece.

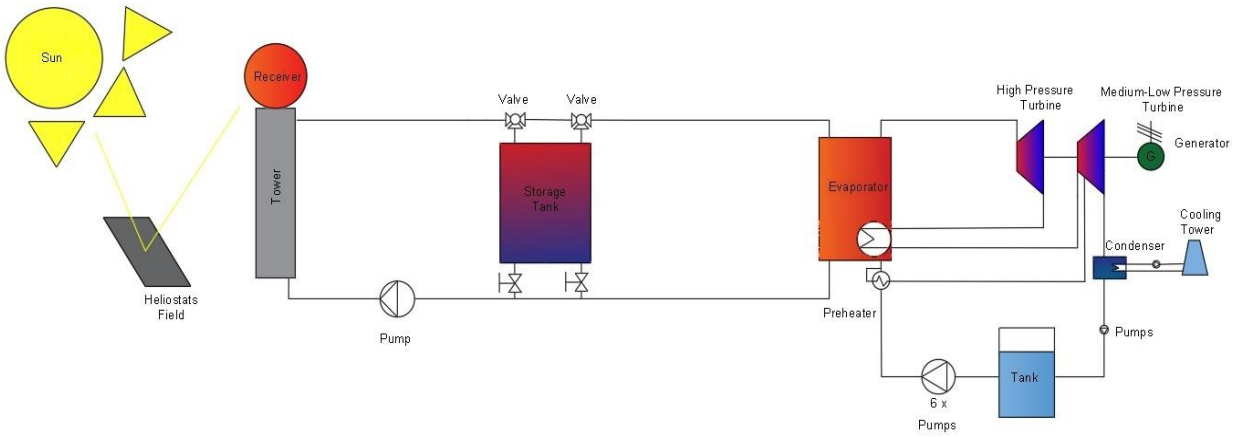

Figure 2-8. Schematic diagram of the whole construction used for this thesis

Firstly, the flowchart of this code will be presented and then some comments will follow that will explain the different scenarios that were made.

First of all, all the matrices are initialized with zeros in order to make the code run faster. A limit for the temperature that is driven through the evaporator is taken. It is assumed to be 600K.
The iterations began with a time step of one hour and are going through a whole year. The calculations that are made for each iteration, are based on the equations of Tehrani et al[36] and Raccanello et al[10] that were used in the previous chapters. In order to model the whole plant and produce electricity four basic scenarios were picked up. In order to be intelligible, the symbols i and i+1 are the current and the next time step, respectively.

1st scenario

If the temperature that comes out of the receiver and is symbolized with (T_{rec_out}) is much bigger than the temperature that already exists inside the storage tank (T_f) then, if the (T_{rec_out}) temperature is above the limit of 600K the temperature that is reached in the evaporator is the (T_{rec_out}). It is then that Rankine_solver function is called in order to calculate the electricity that is produced, the efficiency of Rankine Cycle and the value of heat that is taken from the warm current that comes directly from the tower. In the opposite case that the temperature (T_{rec_out}) is lower than the limit, the warm molten salt flow from the solar receiver ends up in the tank in

order to raise its temperature and finally the temperature that returns in the receiver and symbolized with ($T_{rec\_in(i+1)}$) ,because it represents the next time step, takes the value of ($T_{fret(i)}$).

2nd scenario

Secondly, if the temperature of the tank is much bigger than the temperature coming out of the receiver, and if it is also bigger than 600K it enters the evaporator (T_{fin}=T_f) and comes out of it with smaller temperature (T_{fret}) due to the heat exchange that takes place in this part. If it does not exceeds the limit, (T_{fret}) takes the value of (T_{fin}) that already existed and the warm fluid that comes out of the receiver is headed to the tank in order to raise its internal energy. It is now that the function called in order to calculate the temperature of the tank not only for the fluid inside but also for the storage medium (alumina).The temperature of the fluid that returns to the receiver ($T_{rec\_in(i+1)}$) is equal to the temperature of ($T_{rec\_out(i)}$) the previous time moment.

3rd scenario

The temperature of the warm fluid that is coming out of the receiver (T_{rec_out}) is higher than the temperature of the fluid inside the tank (T_f).In this case the flow is splitted in two currents one that is heading to the tank and one that is heading to the evaporator. If the (T_{rec_out})is higher than the limit then (T_{fin}) is actually equal to(T_{rec_out}) and the function is called which calculate the electricity production, efficiency and the heat absorbed by the evaporator. In different case the heat absorbed by the evaporator is equal to zero. After this part the temperature of the fluid that returns from the evaporator is calculated (T_{fret}). Here ,is called another function that calculates the temperature of the fluid inside the tank and the temperature of storage medium using the (T_{fret}), and (T_{hin}) which is the temperature of the fluid that inserting the tank from the side of receiver output and is equal to (T_{rec_out}) in this case. Now the temperature for the next time step that inserts the receiver is equal ($T_{rec\_in(i+1)}$=$T_{f(i)}$).

4th scenario

Last but not least, in the last scenario the temperature of the fluid inside the tank (T_f) is higher than the temperature of the receiver (T_{rec_out}).In this case is considered that the Tf is higher than the (T_{rec_out}) but not enough so as to go to evaporator directly. So, if the Tf is higher than limit then (T_{fin}) is equal to (T_f) and the function for the calculations of the Rankine Cycle is called. In different case if the (T_f) is lower than limit, a current coming from the solar tower heads to storage tank in order to raise its temperature .The return temperature is calculated after that which feeds the storage tank and in combination with the Thin which is equal to (T_{rec_out}) give the new values for (T_f) and (T_g) the temperature of the fluid inside the tank and of storage medium, respectively. The temperature that returns to the receiver is taken equal to the ($T_{rec\_in(i+1)}$=$T_{rec\_out\ (i)}$).

In this step some diagrams of the design point of the plant in Seville are going to be presented.

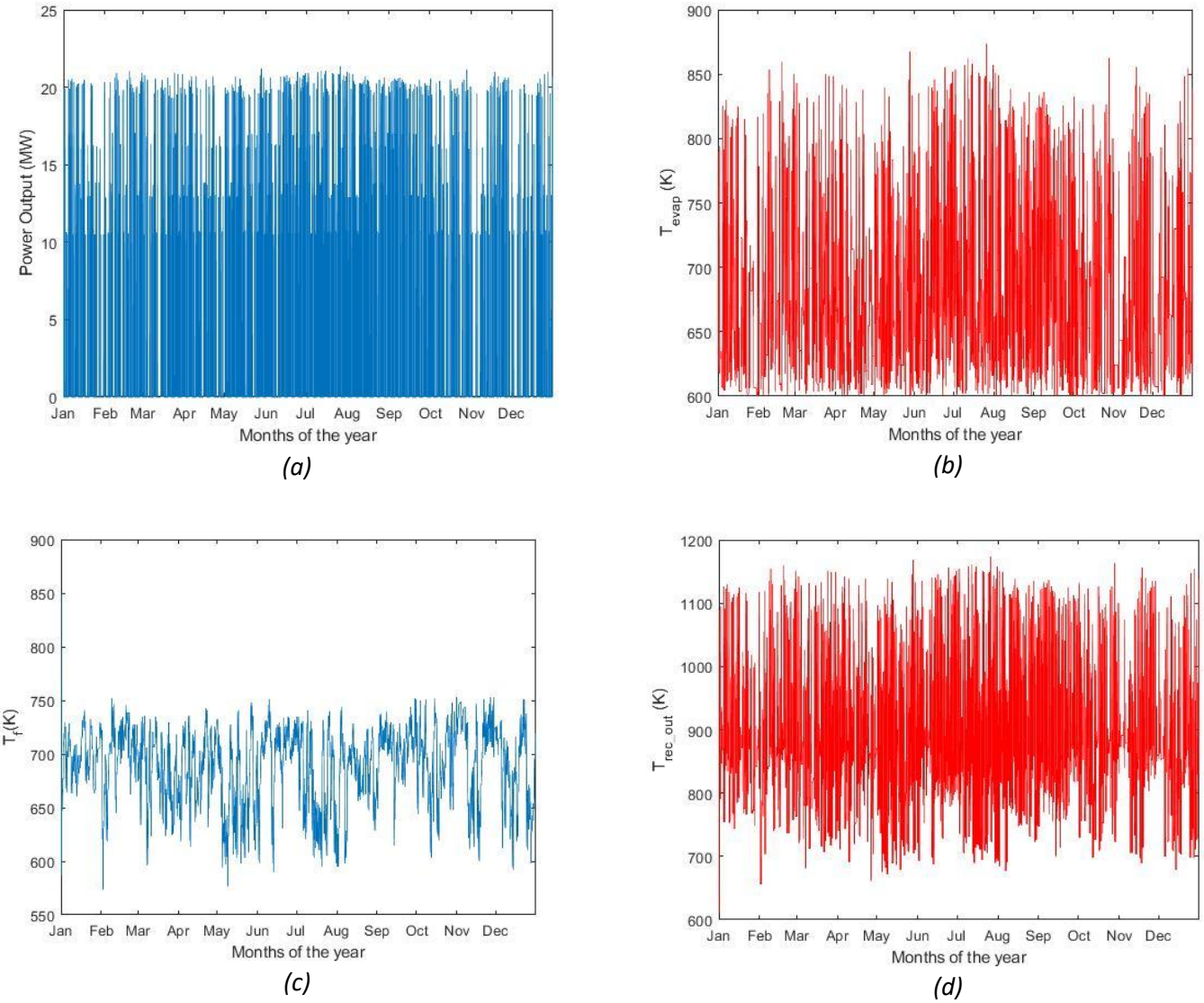

Figure 2-9. **(a) Power Output for 8760 hours, (b) Temperature inserting the evaporator for 8760 hours, (c) Temperature of the fluid inside tank for 8760 hours (d) Temperature output of the receiver for 8760 hours**

As it can be observed from the above diagrams the Power Output (a), $T_{evaporator}$ (b), $T_{receiver\_out}$ (d) are thicker from June to October as it was expected. This is due to the fact that, in those months high number of sunshine hours and high-temperatures are datum. As a result more power is produced and higher temperatures leave the receiver and 'insert' to the evaporator.

Now the basic output values of the design point in the reference plant of Seville are going to be presented.

Table 2-2. Basic output values of the design point in the reference plant of Seville

Plant in Seville	Output Values	Units
Total Pel	$6.2299*10^{10}$	[We]
Total DNI	$5.2296*10^{11}$	[W]
SolarToEnergyEfficiency	0.1191	[-]
SystemExergy	0.3955	[-]

Below is presented the basic flowchart for the code that was written in MATLAB and represents the design point in the reference plant of Seville. In this code which is described by the below chart were based the results of different scenarios that were placed in different cities in Greece.

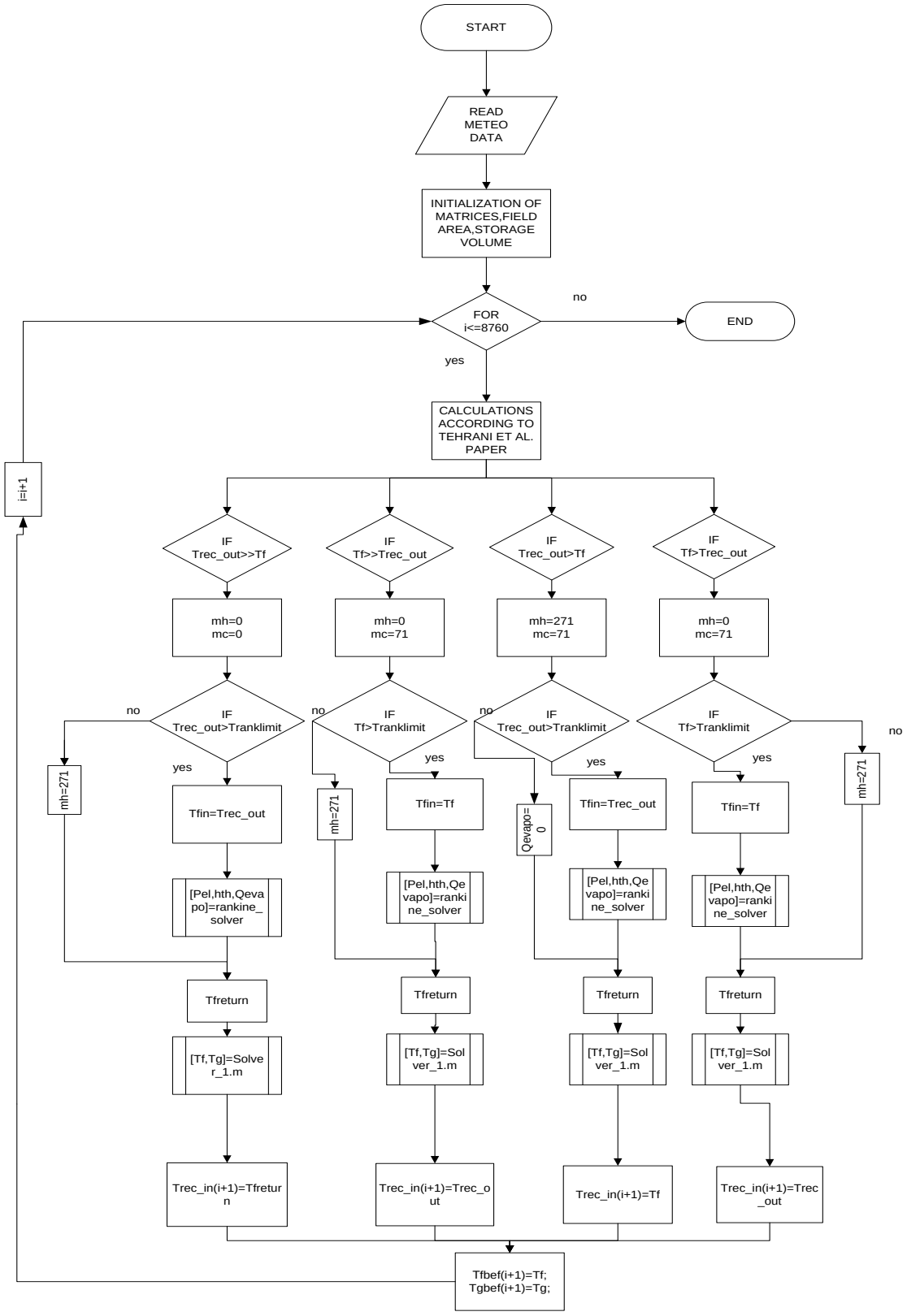

Figure 2-10. **Flowchart for the summary analysis code**

After this flowchart another one is going to be presented that shows the procedure that was followed in order to reach to the results of this thesis. The code that was written was run by this strategy. First of all the design point heliostat field which was found to be 295,000 m² was reduced by 5%,10% and raised by 5%,10% and 15% percent respectively. At the same time the design point storage volume was reduced by 5%, 10% and raised by 5%, 10% and 15% percent respectively.
Bellow the results of this strategy are presented for the design point plant that is located in Seville.

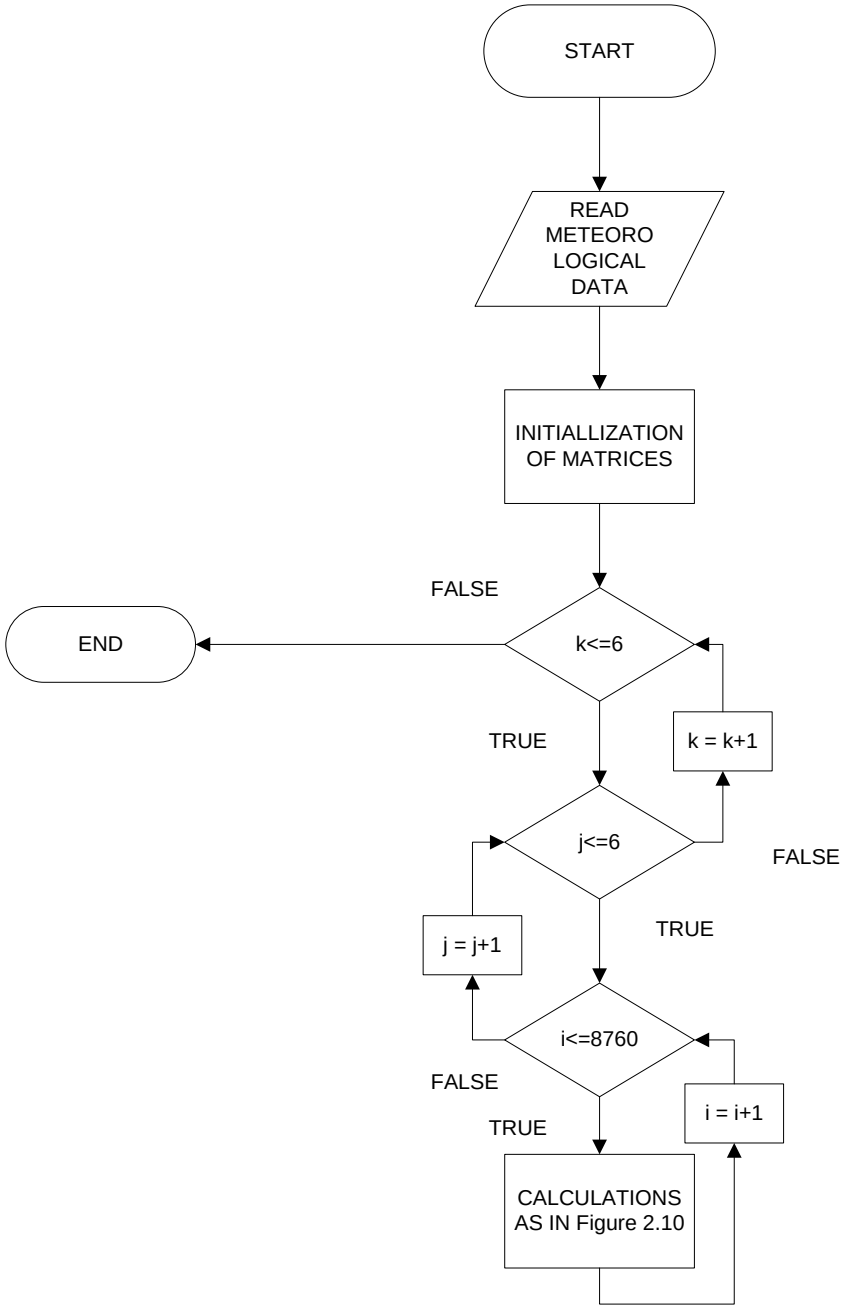

Figure 2-11. **Flowchart according to the strategy analysis that was followed**

2.5 Design Point Technical Results

In this section are going to be presented the results of the Seville which is considered to be the design point for this project. The analysis is based on 6 different Reflector Areas and 6 different storage tank volumes .In total there are 36 different situations to be examined. The 6 different reflector areas occur if the design point area is reduced by 5%,10% and raised by 5%,10%,15% and the design point storage tank volume by 5% and 10% and raised by 5%,10% and 15% respectively.

In the below tables can be observed the different situations examined:

Table 2-3.Different Heliostat Field Areas that were examined for the analysis

Afield	Value	Unit
A1	265500	[m^2]
A2	280250	[m^2]
A3	295000	[m^2]
A4	309750	[m^2]
A5	324500	[m^2]
A6	339250	[m^2]

Table 2-4.Different storage tank volumes that were examined for the analysis

Vstorage	Value	Unit
V1	3926,24	[m^3]
V2	4144,37	[m^3]
V3	4362,49	[m^3]
V4	4580,62	[m^3]
V5	4798,74	[m^3]
V6	5016,87	[m^3]

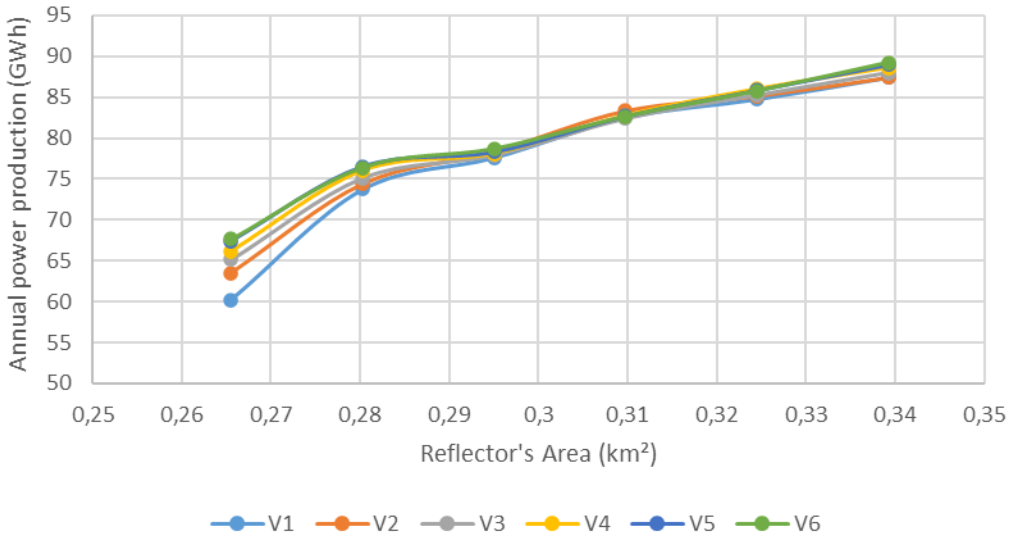

Figure 2-12. **Annual power production as a function of different Reflector's Areas and different storage tanks in Seville**

It can be observed from the above Figure2-12 that the annual power production in Seville is 90GWh for heliostat field area of 339250m² and tank storage volume of 5016,87 m^3

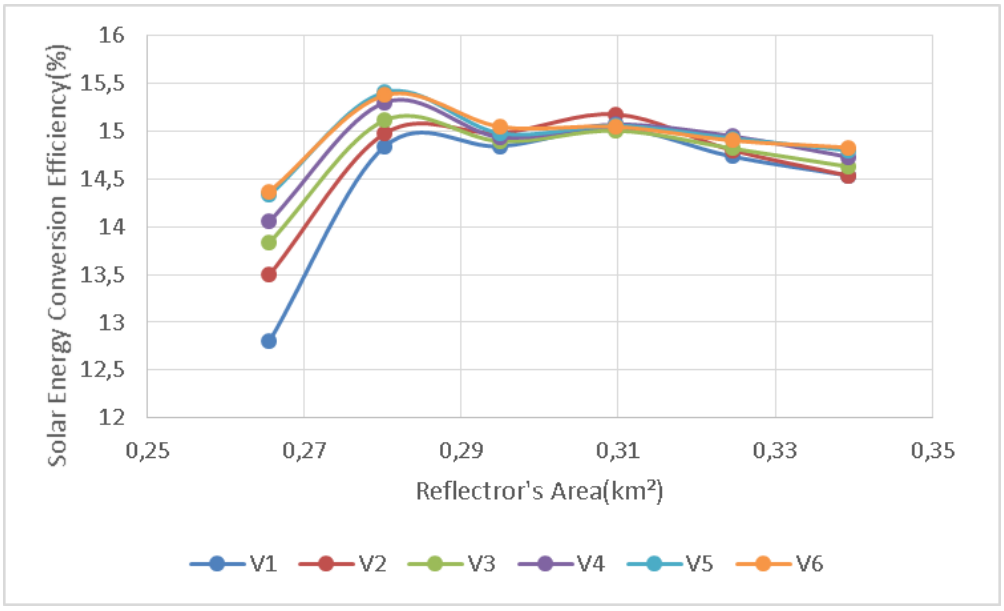

Figure 2-13. **Annual Solar Energy Conversion Efficiency as a function of heliostat field area and storage tank volume**

As it can be seen on the above Figure 2-13 the highest solar energy conversion efficiency is succeeded at 0,28km² for the biggest tank volume V6 but also V5 can be used to reach this efficiency.The fluctuation of the curve is vivid until it end with a negative gradient at 14,5% for heliostat field area of A6.

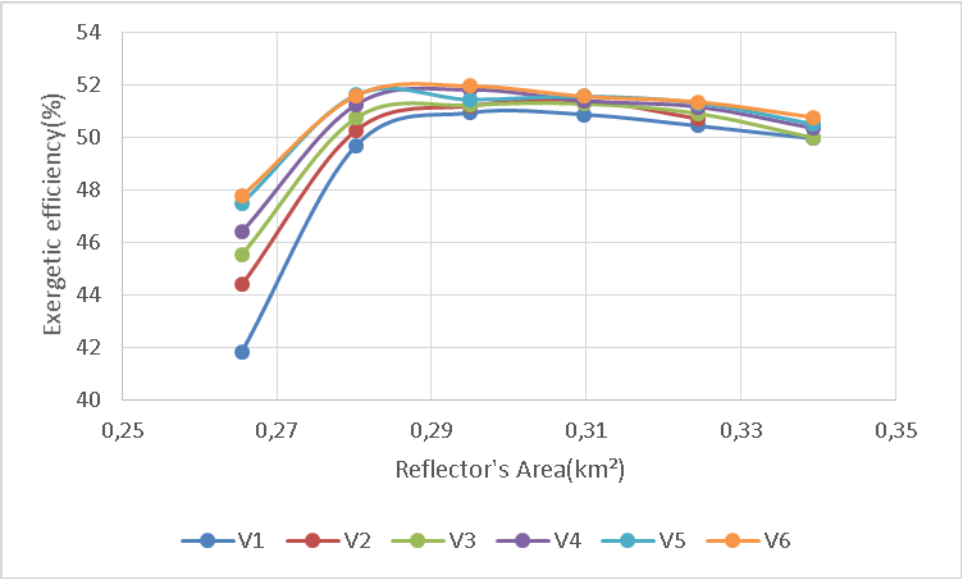

Figure 2-14. **Annual total Exergetic Efficiency as a function of heliostat field area and storage tank volume**

It can be observed from the Figure 2-14 that the max exergetic efficiency is at 0,28km² and for V6 storage tank volume which is the highest tank volume. It can be monitored also that for constant heliostat field area as the tank volume increase the exergetic efficiency also increases. From 0,29km² the increase in efficiency with the increase in volume is negligible. At huge heliostat field areas it tends to take constant values.

3. Economic Analysis on the whole Plant

3.1 Introduction to the Economic Analysis

Upon the last decade vivid research has been done on the economics of CSP projects in order to determine whether they are more viable than their fossil fuel competitors. Electricity prices from renewable sources have fallen matronly over the last decade due to the improved technologies, economies of scale, increasingly competitive supply chains and growing development experience. According to International Renewable Energy Agency (IRENA), the global weighted-average Levelized cost of Electricity (LCOE) of CSP fell by 47%.[45]

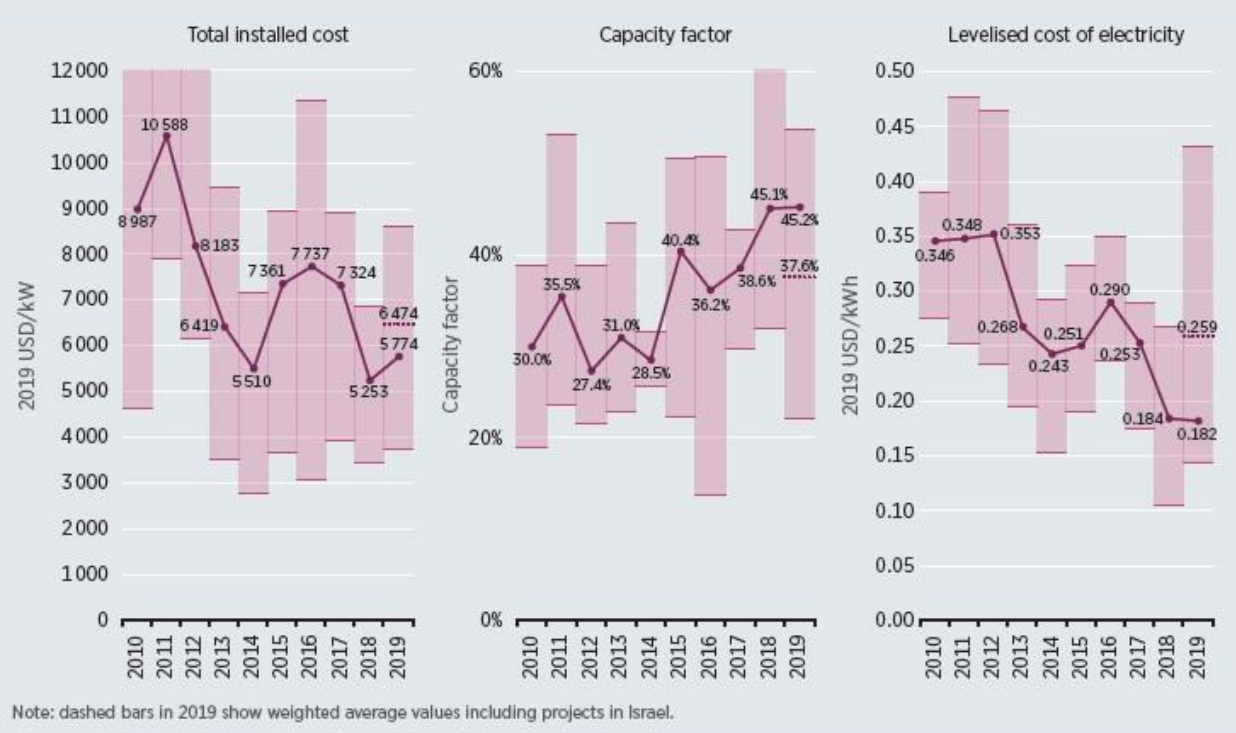

Source: IRENA Renewable Cost Database.

Figure 3-1. Total Installed Cost, Capacity factor and Levelized Cost of Energy fluctuation from 2010 to 2019.

In the above figure, can be monitored the global weighted average installed costs, capacity factors and LCOE from 2010 to 2019. According to the same research done by IRENA, the evolution of the specific cost per KWh from 2010 until the most recent value of 2019.

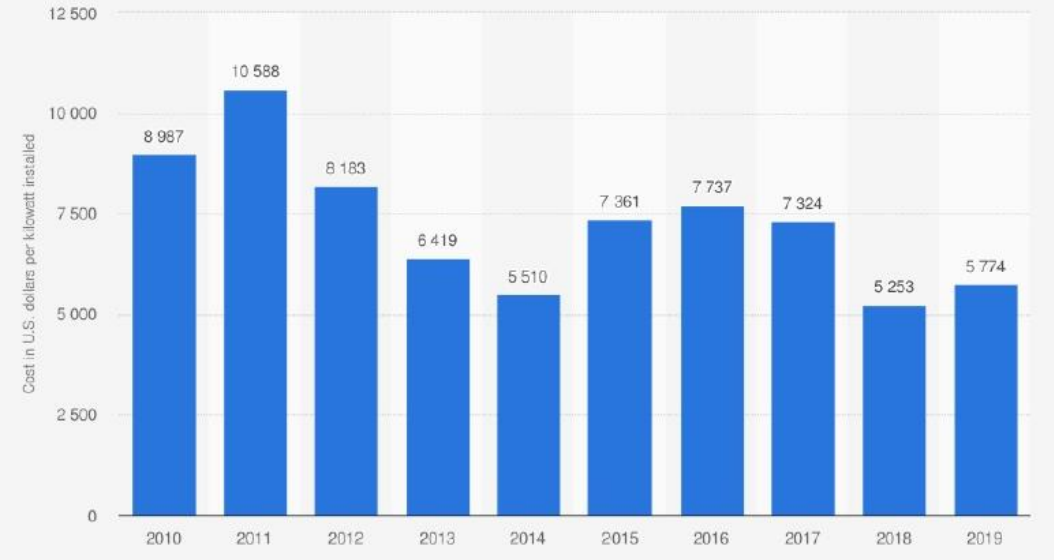

Figure 3-2.Fluctuation of specific cost for CSP projects from 2010 to 2019

Furthermore, it is worth mentioning a research that was conducted by the New Energy Update's Today, using data from news reports, company statements and Yang et.al [46] that present costs for different solar power tower applications including TES systems and different locations of the plants.

Project	Country	$/kW	Capex (Y)	Capex ($M)	Size (MW)	TES (h)	Type
Qinghai Gonghe	China	3,910	1,222	196	50	6	Tower
Golden (Three Gorges)	China	4,000	2,500	400	100	8	Tower
Yumen Town East	China	4,304	1,345	215	50	9	PT
Aurora	Australia	4,333		650	150	8	Tower
Urat Middle Banner	China	4,480	2,800	448	100	10	PT
Zhongyang Zhanjiakou	China	4,500	1,800	288	64	16	PT
Shouhang Dunhuang	China	4,864	3,040	486	100	11	Tower
Hami	China	5,056	1,580	253	50	8	Tower
Dacheng Dunhuang	China	5,376	1,680	269	50	13	LF
DEWA Phase IV	UAE	5,529		3,870	700	11 (PT) & 15 (Tower)	PT (600 MW), Tower (100 MW)
Yumen	China	5,728	1,790	286	50	9	Tower
Huaqiang Zhaoyang Zha	China	5,760	1,800	288	50	14	LF
Tamarugal	Chile	6,000		2,700	450	13	Tower
Likana	Chile	6,154		2,400	390	13	Tower
CGN Delingha	China	6,202	1,938	310	50	9	PT
Gansu Akesai	China	6,355	1,986	318	50	15	PT

Figure 3-3. Study of specific cost for different CSP technologies in different countries (Yang et.al) [46]

3.2 Total Capital Cost

In order to carry out an economic analysis on the plant, some investment performance indexes need to be introduced. These are Payback Period (PB), Net Present Value (NPV) and of course the Levelized Cost of Energy (LCOE).

Firstly, needs to be defined the total investment cost of the whole plant also known as total capital cost, because it is needed in the calculations of the above indexes. In order to depict the total capital cost of the whole plant NREL-SAM program was used. For the on-design analysis, spatial data from the Gemasolar Power Plant in Spain, combined with assumptions on the previous chapters were used. The data that had been taken for granted for the program are shown below in the table:

Table 3-1.Reference Solar Power Tower Station that was for calculations in NREL program

Project Power Plant	Input Values	Units
Design Turbine Gross Output	20	MWe
Design Thermal Power	60	MW-t
Full Load Hours of TES	12	Hr
Total Land Area	520	Acres (1acre ~ 4047m^2)
Total Reflective Area	295,000	m^2
Receiver Design Thermal Power	142	MW-t
Area	412	m^2
Tower Height	140	m
Inflation Rate	0,025	-
Sales Tax	0,05	-
User Variable 1	2021	-
User Variable 2	1	-

According to the above data a pie chart produced in order to show the direct and indirect costs that have been emerged from the on-design analysis.

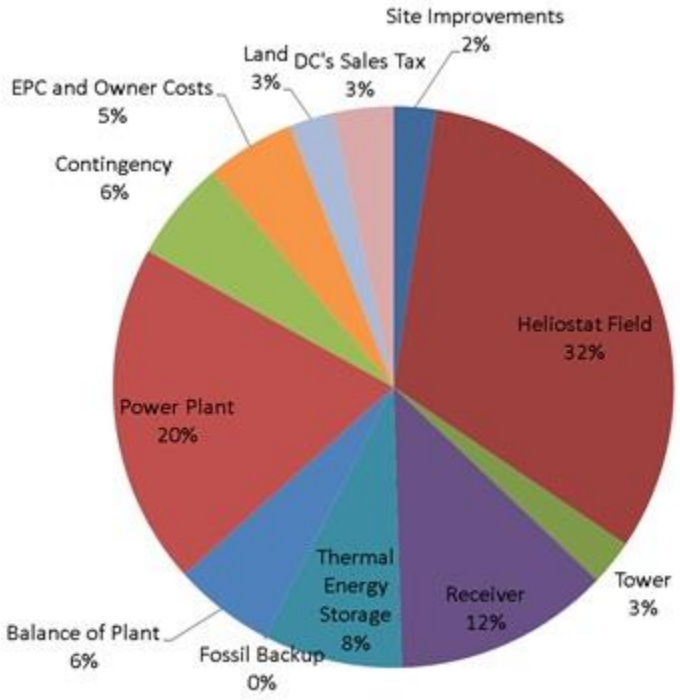

Figure 3-4. Breakdown of the total capital cost for the on-design analysis in Seville

In this part we will analyze the different parts that consist the direct and indirect costs of the above pie-chart that will also be used to our analysis.

3.2.1 Direct Capital Costs

Site-Sector

Site consist of site preparation, clearing and Grubbing, Grading, Drainage, Remediation, Retention and Detention, Evaporation Pond, Roads, Parking and Fencing, Water Supply Infrastructure.

Heliostat-Sector

Heliostat Sector consist of Mirrors, Drives, Pedestal, Mirror Support, Foundation, Controls and Wired Connections, Field Wiring and Foundations Labor, Installation and checkout.

Tower Sector

Tower Sector consist of Tower, Riser and down comer, Piping and Insulation.

Receiver

Receiver Direct cost consist of the Receiver, Horizontal Piping and Insulation, Cold Salt Pump(s), Controls, Instruments, Heat Trace, Spare Parts.

Thermal Energy Storage

Thermal Energy Storage (TES) consist of a Tank, Media, Piping, Insulation, Valves and Fittings, Foundations, Support Structures, Instrumentation and Controls.

Fossil

Fossil direct costs is zero in this very project.

Balance of Plan -**Defined as Steam Generation System**

Balance of Plant consist of Steam Generation Heat exchangers and Equiment, hot salt pumps, steam Piping, Insulation, Valves and Fittings, Electrical, Instrumentation and Control System, Foundations and Support Structures.

Power Plant

Power Plant sector consist of the following parts: Steam Turbine Generator Island, Blowdown System, Cooling Systems, Condensate System, Feedwater System, Auxiliary Cooling Water System, Steam Piping, Insulatiton, Valves and Fittings, Fuel Gas Handling and Metering System ,Water Treatment System, Power Distribution Systems, Backup Power Systems, Instrument and Control Systems, Fire and Protection System, Foundation and Support Structures, Buildings, BOP Mechanical Systems BOP Electrical Systems.

3.2.2 Indirect Capital Costs

In this category they are included the so called no-hardware project costs such as permitting ,land, legal fees, geotechnical and environmental surveys ,taxes, interest during construction and the owner's engineering and project management activities. Some of these categories are listed explicitly, while many are simply lumped into the EPC and Owner's Cost category.

The capital costs that occurred were calculated by SAM-NREL model at 2013 dollar currency. In order to update the costs in 2021 prices in euros, the exchange rate according to the European Central Bank [47] was calculated.

$$\text{Prices}(€)_{2013} = 0{,}72 * \text{Prices}(\$)_{2013} \quad (63)$$

After this conversion the values of money from 2013 were transferred to 2021 by the below calculation:

$$\text{FutureValue} = \text{CurrentValue} * (1 + \text{i})^{n} \quad (64)$$

Where i is the inflation rate set to be 5% in Greece and n are the years that need to pass until 2021.

The program of NREL that was used follows the philosophy that will be described next. Program contains cost information for two different plants a 'reference plant' and a 'project plant'. The reference plant matches the default molten salt power tower in SAM 2012-11-30.

Table 3-2. Reference Plant characteristics as they were in SAM-NREL program

Reference Parameters	Input Values	Units
Power Block gross rating	115	MWe
Thermal Storage	10	hours
Solar Multiple	2.4	-
Design conditions dry-bulb temperature	42	^{o}C
Location	Daggett,CA	-
Tower Height	203	m
Receiver Design Thermal Power	670	MWt
Solar Field area	1289000	m^2
Thermal Storage salt volume	13,000	m^3
Net Capacity annual average	105	(MWe)
Annual net electricity generation	539,700	MWh
Capacity Factor	58.9%	-

For each cost, two parts, direct and indirect costs were calculated. Direct and indirect costs consist of (each one) material and labor costs. Size scaling exponent parameters were used in order to calculate the capital costs in 2021 in euros. The prices of the material and those of labor costs correspond to the costs of SAM-NREL database that were retrieved from [48] and [49].The exponent values are shown below.

Table 3-3. Scaling factors that were used for the calculations in SAM

Scaling Values	Values
Site	1.8
Heliostat	1.2
Tower	0.0326
Receiver	1.2
TES	1.6
BOP	1.6
Power Plant	1.8
EPC and Owners Costs	1.4

The Materials and Labors costs of the reference plant were retrieved by the SAM-NREL database.

Table 3-4. Different coefficients that were used for the calculations of costs

Parameters	C1	C2
Material_Site	1.214	1.8
Labor_Site	0.986	1.8
Material_HeliostatField	1	1.2
Labor_HeliostatField	1	1.2
Material_Tower	1.120	-
Labor_Tower	0.982	-
Material_Receiver	1.120	1.2
Labor_Receiver	1.120	1.2
Material_TES	1.124	1.6
Labor_TES	0.982	1.6
Material_BOP	1	1.2
Labor_BOP	1	1.2
Material_Power Plant	1	1.6
Labor_Power Plant	1	1.6

- **Direct Cost**

$$\text{MaterialCost}_{proj} = \text{MaterialCost}_{ref} * \text{C}_1 * (\frac{Project\ \ area}{Reference\ \ area})^{C_2} \quad (65)$$

$$\text{LaborCost}_{proj} = \text{LaborCost}_{ref} * \text{C}_1 * \left(\frac{Project\ \ area}{Reference\ \ area}\right)^{C_2} * 0{,}99 \quad (66)$$

In order to find the total Direct Costs all the above costs are summed, material and labor, for each and every part of the above table.

- **Indirect Costs**

$$\text{Cost}_{proj} = (\text{Cost}_{ref} * 0.022 * 1 * \left(\frac{Projectarea}{Referencearea}\right)^{1.4} + \text{fixedvalue}) \quad (67)$$

The price of the fixed value is set by NREL program and depends on the country that the project is going to be constructed.

Here it needs to be mentioned that in every subtotal cost of the direct costs a contingency of 7% is calculated and added to the final total direct cost. Cost of land was calculated and found 2% of the total direct cost by multiplying the total 520 acres with the land cost in Greece.

The strategy that was followed in order to trace the capital cost of the whole plant is going to be described in this step. First of all, the model and the capital cost of the plant were calculated with the weather conditions and concepts that are valid in Seville. This was considered the design and validated point of this project. With the knowledge of the Gemasolar plant in Seville, the project was further developed by adding cities of Greece that depict the 4 different climate zones such as Athens, Thessaloniki, Kozani and Chania in Crete.

The field area (Afield) is kept constant and at the same time for the period of one year, the storage's tank volume changes its value between minus 10% and plus 10% from the value of volume tank on the design point. By changing the volume and keeping steady the heliostats field area, different values of capital cost occur. In order to have a better result at this study, the heliostat's field area changes also from minus 10% to plus 10% of the field area on design point and this happens on a year basis scenario.

3.3 Levelized Cost of Energy (LCOE)

Levelized Cost of Energy (LCOE), also referred to as Levelized Cost of Electricity is a performance index used in energy applications and measures lifetime cost of an investment divided by energy production. In other words, it calculates the cost for the production of 1 KWh_e.

$$\text{LCOE} = \frac{\text{IC} * \text{R} + \text{OMC}}{\text{E}_{el,net,total}} \quad (68)$$

- IC: Investment Cost

- OMC: Annual Operational and Maintenance Cost

$$\mathrm{OMC} = \frac{\mathrm{IC}}{236} \tag{69}$$

- $\mathrm{E}_{el,net,total}$: is the annual net electricity production by the whole plant

- R:coefficient calculated as follows

$$\mathrm{R} = \frac{\mathrm{i}}{1 - (1 + \mathrm{i})^{-n}} \tag{70}$$

- i:Discount rate equals to 6%

- n=30 years is the expected lifetime of the investment

What is more needed to be mentioned about the LCOE is that is a measurement used to assess and compare alternative methods of energy production.

According to the Greek legislature under the Greek name “ΦΕΚ 213/A/24-12-2019”[50] the price that was used for the calculations was set to be 268€/MWh for the electricity sold by concentrated solar power systems with a thermal energy storage system of at least 2 hours availability.

3.4 Net Present Value (NPV)

The Net Present Value (NPV) of a system calculates the value of all future cash flows during the lifetime of an investment, discounted to the present. As was mentioned before the expected lifetime of this project was set to be n=30years and the discount rate was set to be equal to i=6%. The equation that calculates the Net Present Value is given below.

$$\mathrm{NPV} = -\mathrm{IC} + \sum_{n=1}^{n=30} (\mathrm{E}_{el,net,total} * Pr_{el} - OMC) * (1+\mathrm{i})^{-n} \quad (71)$$

At the beginning of time period it is assumed that the net cash flow is negative and it's absolute value is equal to the investment cost. That's why the first term of the above equation is negative. It depicts the year 0 for the calculations.

- $\mathrm{Pr_{el}}$: this term is the price of electricity

$$annual\ net\ cash\ flow = \mathrm{E}_{el,net,total} * Pr_{el} - OMC \quad (72)$$

This term calculates the net cash flow for n years starting from the first year because as it was mentioned before the zero year we have negative cash flow.

- $\mathrm{E}_{el,net,total} * Pr_{el}$= is the income from power production of n year
- OMC: Annual Operational and Maintenance Cost as aforementioned.

3.5 Simple Payback Period (PB)

Simple Payback period refers to the amount of time it needs to recover and investment. As was mentioned before the investment lifetime is set to be n=30 years and the discount rate equal to i=6%. For this reason, if the payback period is greater than 30 years this means that the application is not economically sustainable for the expected lifetime. The Payback period is the cost of the investment divided by the annual cash flow. The shorter the payback period the more desirable is the investment. Here it needs to be mentioned that the simple payback period is an index of low quality because it does not consider the changing value of money through the years via the inflation rate .That is why it is used only to have a general overview of the plant that will be constructed. It is calculated using the below equation:

$$\mathrm{PBP} = \frac{\mathrm{IC}}{\text{Net annual revenue}} \quad (73)$$

Where Net annual revenue is the income of the plant minus the operational and maintenance costs for the period of one year.

Below, are presented the performance indexes of the design point plant in Seville in the current situation.

Table 3-5. Performance indexes of the design point in Seville

Design Point	AN/VN	Unit
Total Capital Cost	209674328,3	€
Specific cost €/Kw	5003.56	€/KW
LCOE	0.2069	€/KWh
NPV	150606282	€
PBP	8,12	years

4. Results-Comments

4.1 Technical Performance Results

In the chapters that are going to follow, the results of the total power generation in the period of one year, the solar energy conversion efficiency but also the exergetic efficiency are going to be presented. Here it needs to be mentioned that the Gemasolar Power Plant located in Seville was used, with it's characteristics, as the design point plant. A code in Matlab was created in order to take technical results out of this very plant. The code included three different parts. The part of receiving solar energy via heliostat field into the receiver, the part of storing this energy in a storage tank and finally the part of producing electricity via a water-steam Rankine cycle. After this modelling the plant that was created was "transferred'' in 4 different regions of Greece. These regions were not picked up randomly. These 4 regions depict the 4 different climate zones of Greece. With the created code formula and by using different climatic values for weather conditions in Athens, Chania, Thessaloniki and Kozani the below technical results were occurred.

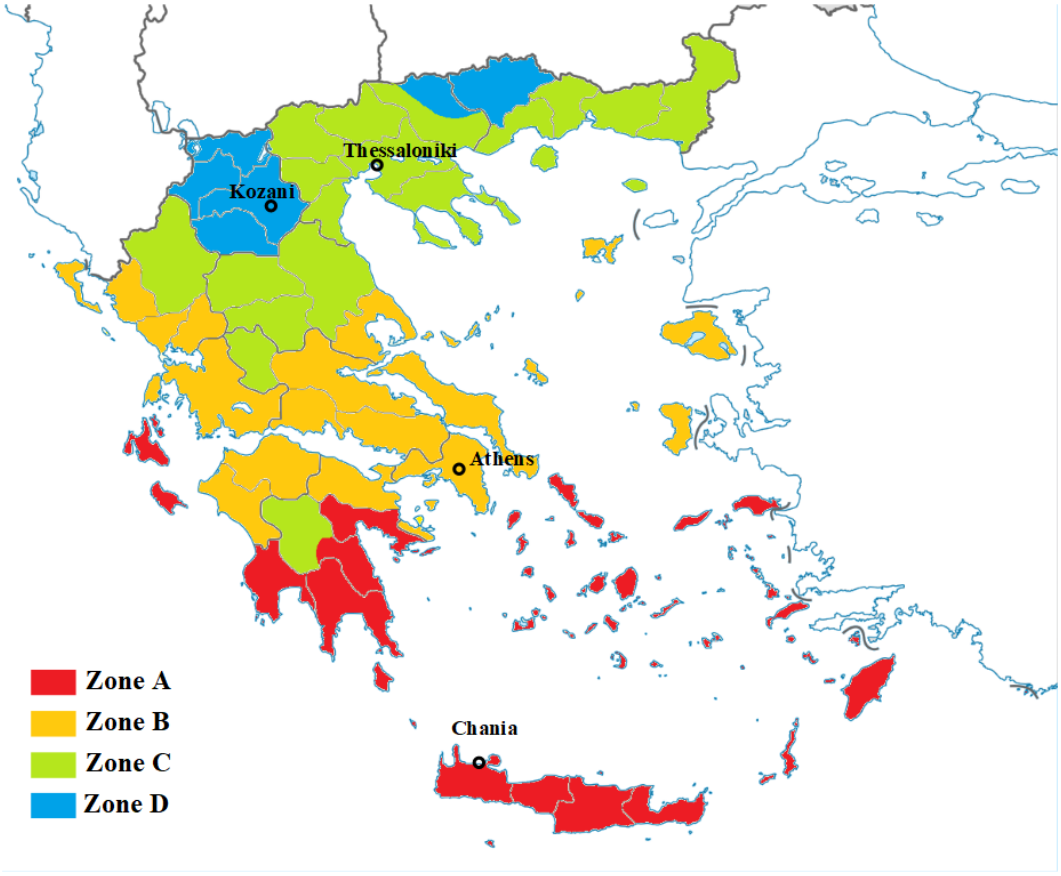

Figure 4-1. The Four different climate zones of Greece and the four different cities for the thesis analysis

In the above figure can be spotted 4 different climate zones of Greece and the cities that were used in order to trace the performance of the modeled power plant per climatic zone.

In the table 6 different heliostat field areas and 6 different storage volumes can be spotted that were used for the analysis.

Table 4-1. Different Heliostat Field Areas that were examined for the thesis analysis

Afield	Value	Unit
A1	265500	[m^2]
A2	280250	[m^2]
A3	295000	[m^2]
A4	309750	[m^2]
A5	324500	[m^2]
A6	339250	[m^2]

Table 4-2. Different storage tank volumes that were examined for the thesis analysis

Vstorage	Value	Unit
V1	3926,24	[m^3]
V2	4144,37	[m^3]
V3	4362,49	[m^3]
V4	4580,62	[m^3]
V5	4798,74	[m^3]
V6	5016,87	[m^3]

4.1.1 Athens

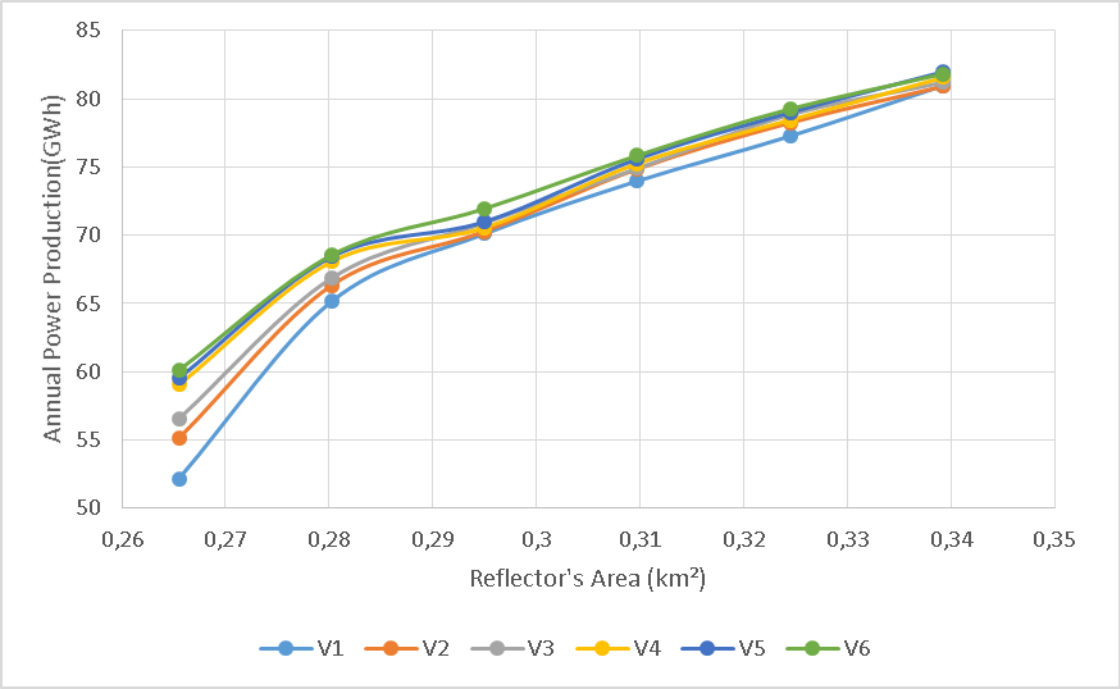

Figure 4-2. Annual total Power Production as function of different Reflector's Areas and different storage tank volumes in Athens

If Figure 4-2, it can be seen that the highest annual power production is 82 GWh for the biggest heliostat field area of 339250 m² .Also it can be monitored that in constant heliostat field area the total power output is rising with the increase in the storage tank volume. This effect is negligible from an heliostat field area of 0,31 km² and beyond.

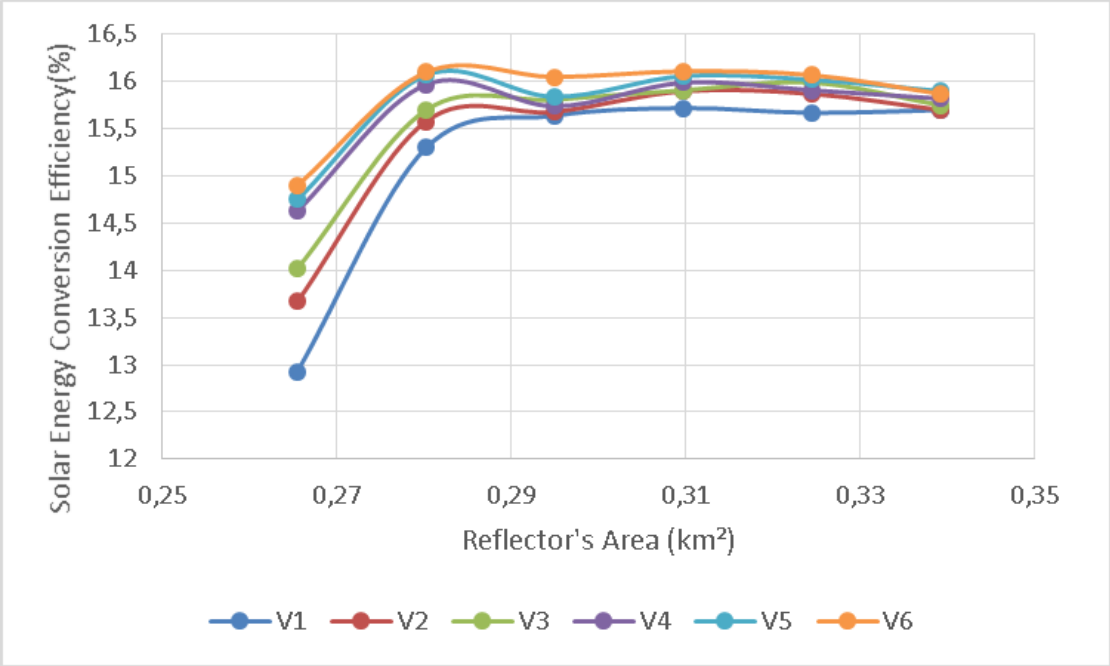

Figure 4-3. Annual Solar Energy Conversion efficiency as a function of different Reflector's Areas and different storage tank volumes in Athens

From Figure 4-3 it can be observed that the biggest efficiency is achieved for the biggest storage tank volume V6 but in a heliostat field area of 0,28 km² which is below the design point area of 295000 m² .Also it can be monitored that for constant heliostat field area the efficiency rises with an increase in storage tank volume until the biggest heliostat area where from that point and beyond the efficiency turns to be steady.

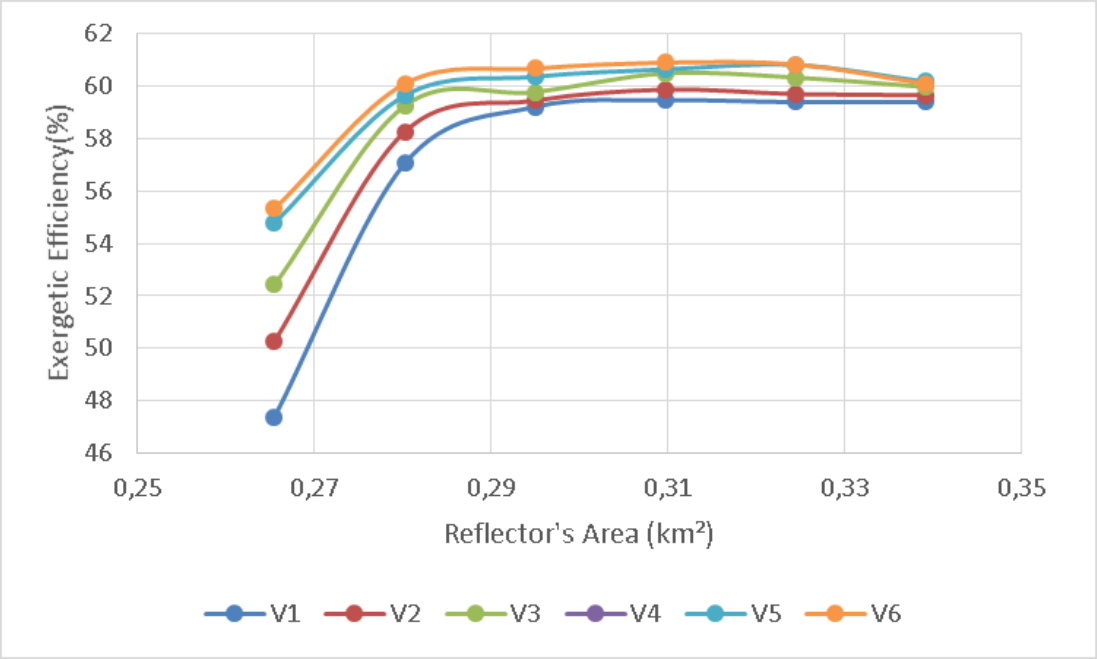

Figure 4-4. Annual Exergetic Efficiency as a function of different Reflector's Areas and different storage tank volumes in Athens.

In the above Figure 4-4. It can be observed that the biggest exergetic efficiency for Athens is achieved at 0,29km² close to the value of design point and from that point and on the exergetic efficiency is constant. In the diagram of solar conversion efficiency but also on that of exergetic efficiency it can be seen that as the heliostat field increases the efficiencies tend to fall steadily after their constant route.

From the above figures of Athens it can be seen that for constant Reflector's Area while the storage tank volume is increasing , the annual power production, the solar to energy conversion efficiency but also the exergetic efficiency also increase. What's more while the Reflecting Area increases ,it can be seen that the increase in power output ,solar conversion efficiency and exergetic efficiency with the simultaneous increase in tank volume is smaller. It can be seen also that as the heliostat collectors area grows despite the simultaneous increase in volume, from a field size and then all the above performance indexes tend to constant values.

4.1.2 Chania

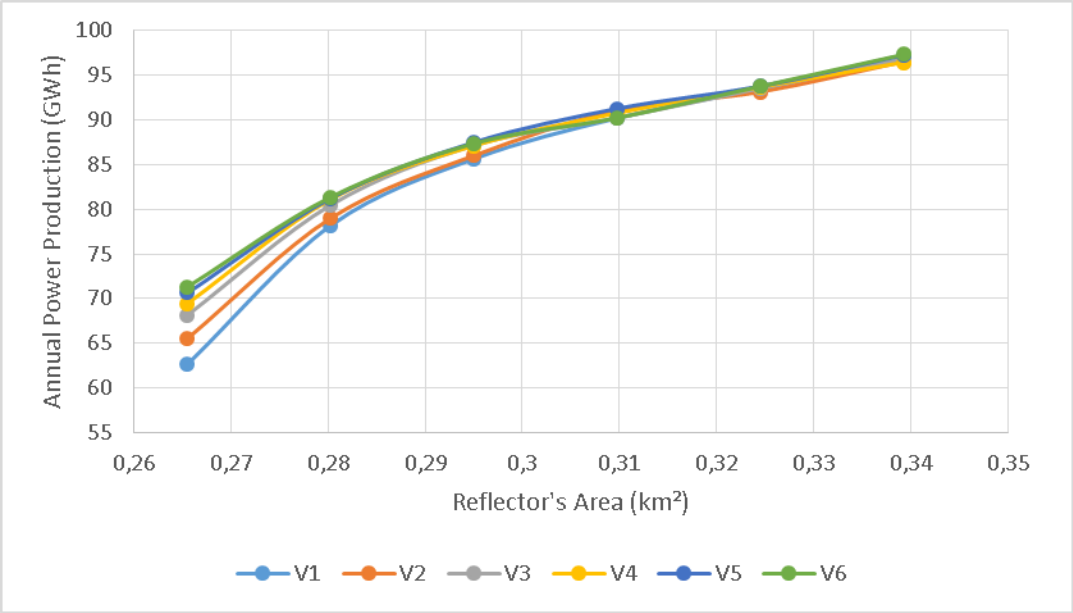

Figure 4-5. Annual total Power Production as function of different Reflector's Areas and different storage tank volumes in Chania.

From the above Figure 4-5. It can be observed that the highest annual power output of 96 GWh for Chania can be achieved with the biggest heliostat field area as in Athens but in Chania we have bigger power output. Also it can be seen that for particular heliostat field areas the annual power output is higher while the tank volume getting bigger and bigger, but this phenomenon is negligible after 0,29 km² which is the design point heliostat field area.

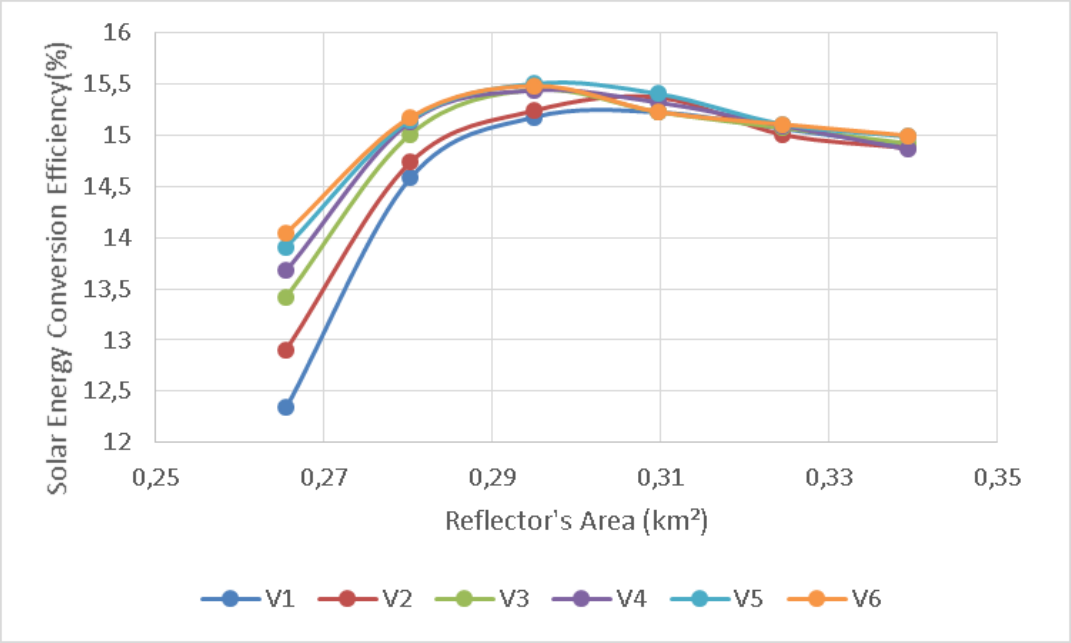

Figure 4-6. Annual Solar Energy Conversion efficiency as a function of different Reflector's Areas and different storage tank volumes in Chania.

As far as Figure 4-6. Is concerned ,can be monitored the facts that mentioned before but also here needs to be mentioned that the peak efficiency is after 0,29km² while in Athens it was before that value. While the heliostat field area increases the efficiency take steady values.The peak efficiency here is 15,5% while in Athens it was higher and around 16%.This is due to the fact that Athens has fewer sunny hours throughout a year.

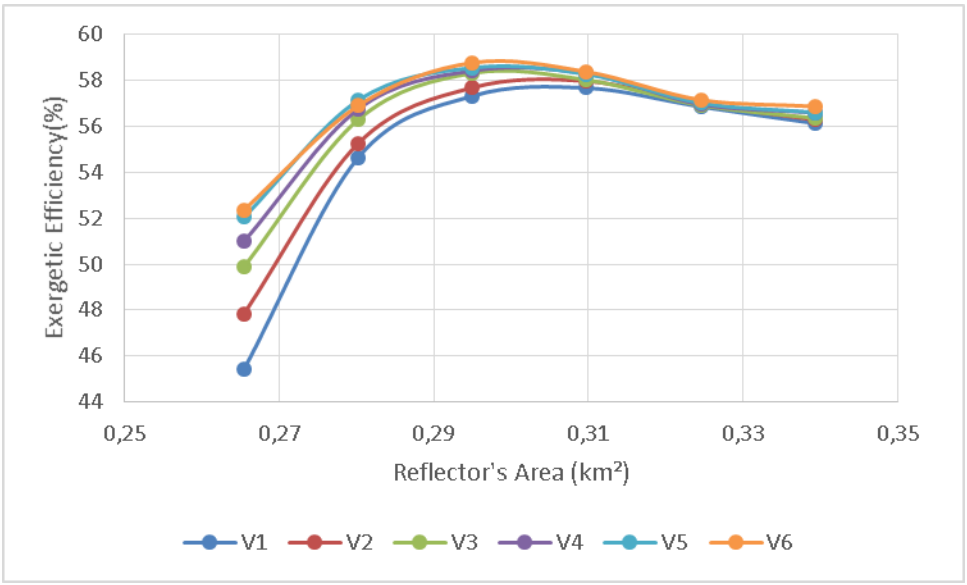

Figure 4-7. Annual Exergetic Efficiency as a function of different Reflector's Areas and different storage tank volumes in Chania.

In the Figure 4-7 can be observed that the max exergetic efficiency of Chania is 58% and achieved close to the design point .This exergetic efficiency is lower than in Athens for the aforementioned reason.

Comparing Chania to Athens it is observed that they have big annual power output due to higher DNI values, but solar energy conversion efficiency and exergetic efficiency is bigger in Athens due to lower availability of sunny hours throughout the year. In other words it is logical if plant operates fewer hours a year to be more efficient.

4.1.3 Thessaloniki

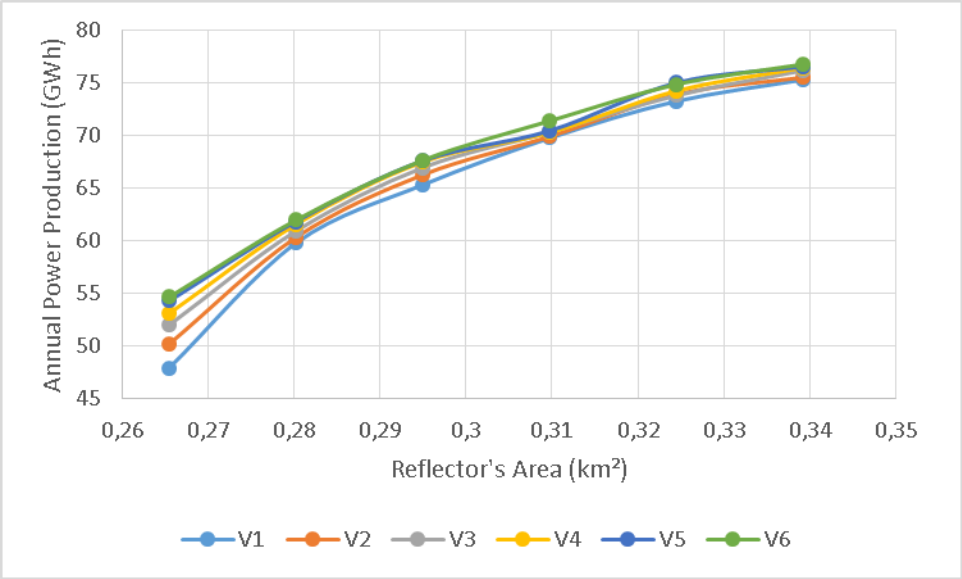

Figure 4-8. Annual total Power Production as function of different Reflector's Areas and different storage tank volumes in Thessaloniki.

As it can be seen for Thessaloniki the max total annual Power output is achieved for the biggest heliostat area named as A6 in the previous chapter. It is obvious that the curves in Figure 4-8 are smoother and less fluctuated than that of Athens but also it is obvious that from a Reflector Area of 0,28km² despite the increase in the storage tank volume the annual power output does not increase as much. The total GWh are fewer than that of Athens due to less sunny days throughout the year.

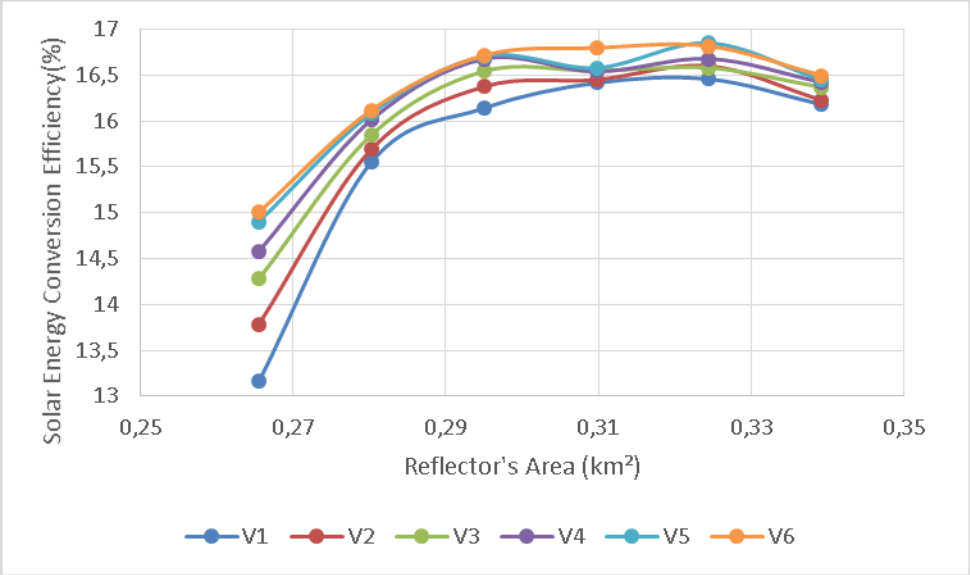

Figure 4-9. Annual Solar Energy Conversion efficiency as a function of different Reflector's Areas and different storage tank volumes in Thessaloniki.

In above Figure 4-9 can be monitored that max efficiency is at 16,5% and achieved for an heliostat field area of 0,31km² and a volume of V6 which is the bigger tank .If it is compared with the results of Athens , Athens has max efficiency at 16% for a heliostat field area of 0,28km² and for volume V6.

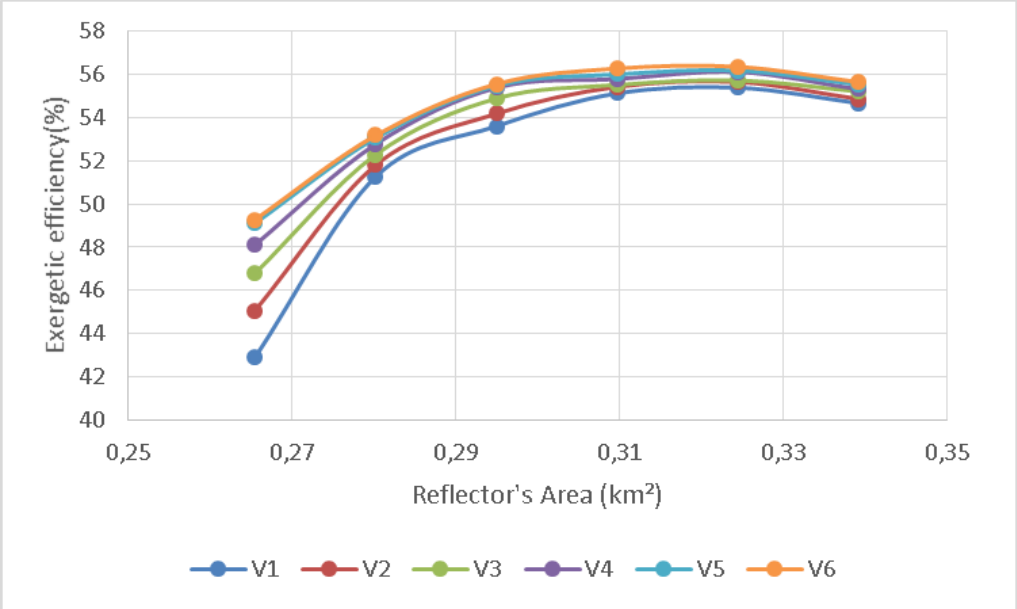

Figure 4-10. Annual Exergetic Efficiency as a function of different Reflector's Areas and different storage tank volumes in Thessaloniki.

It can be observed from the above Figure 4-10 that the exergetic efficiency has its max value at 56% for a V6 storage volume and for a Heliostat Field area of 0,31km² and after that value its value drops slightly. Athens did have its max exergetic efficiency at 0,29km² and was at 61%.

Comparing Thessaloniki and the Athens because it is no sense to compare with Chania due to bigger DNI previous cities it is observed that the production of power yearly is lower but the exergetic efficiency and solar energy conversion efficiency is higher due to the lower temperatures and the fewer annual operating hours of those plants.

4.1.4 Kozani

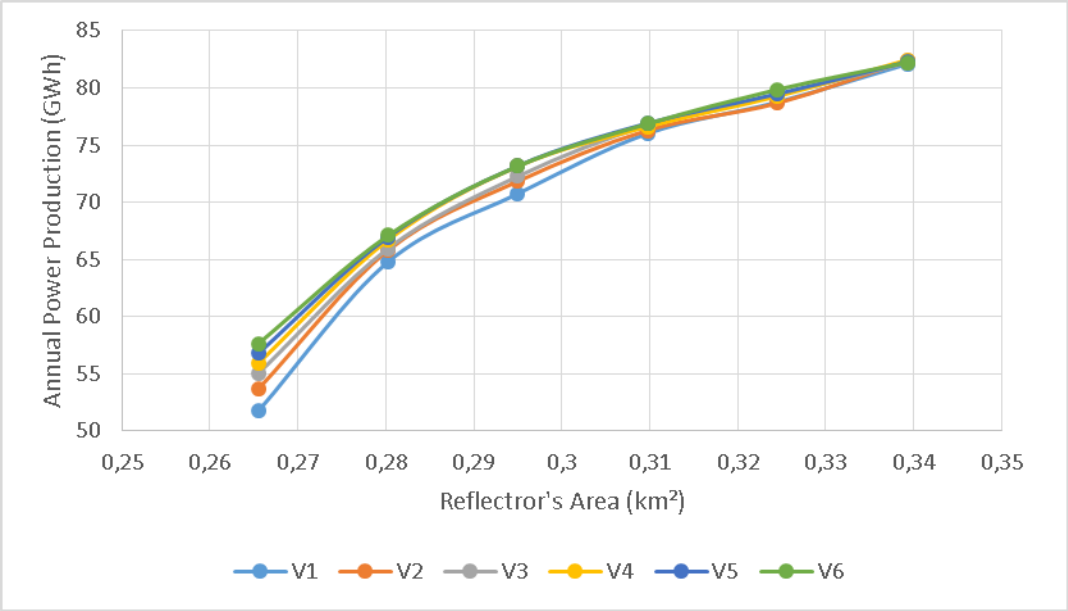

Figure 4-11. Annual total Power Production as function of different Reflector's Areas and different storage tank volumes in Kozani.

In Figure 4-11 can be spotted that Kozani has its biggest annual power output for all storage tank sizes but for the biggest heliostat field area. The effect of bigger storage tank is negligible from 0,31km² and on. Kozani's biggest annual power output is at 82GWh which is bigger than that of Thessaloniki. The curve is also steeper that means the power output raise quicker than the power output of Thessaloniki.

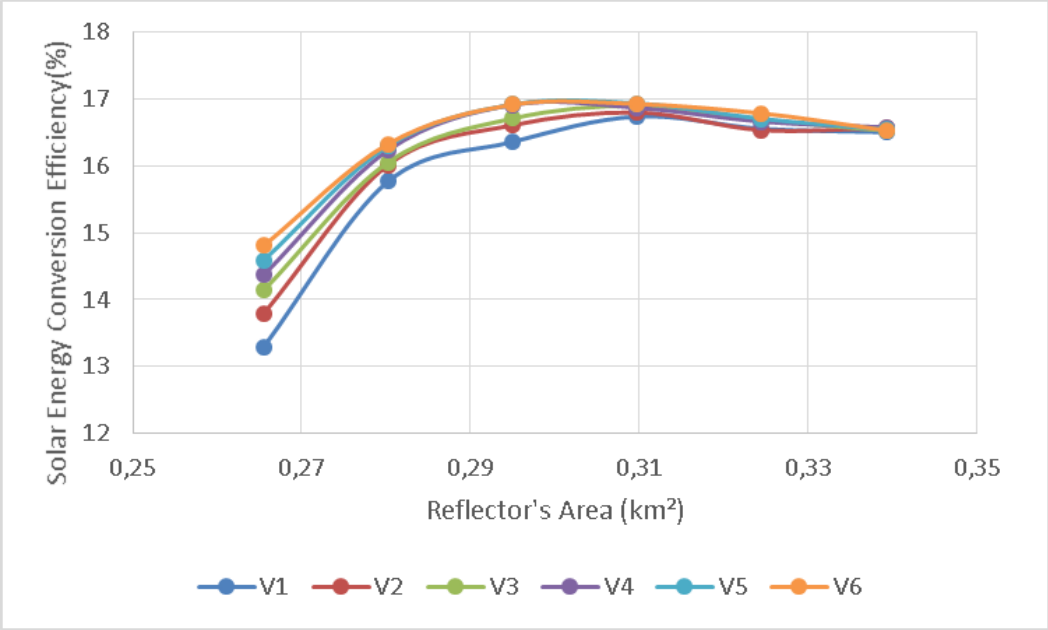

Figure 4-12. Annual Solar Energy Conversion efficiency as a function of different Reflector's Areas and different storage tank volumes in Kozani.

In Figure 4-12 can be spotted the highest solar energy conversion efficiency for Kozani that is 17% higher than that of Thessaloniki due to the low temperatures and the shorter fluctuation in the temperature.

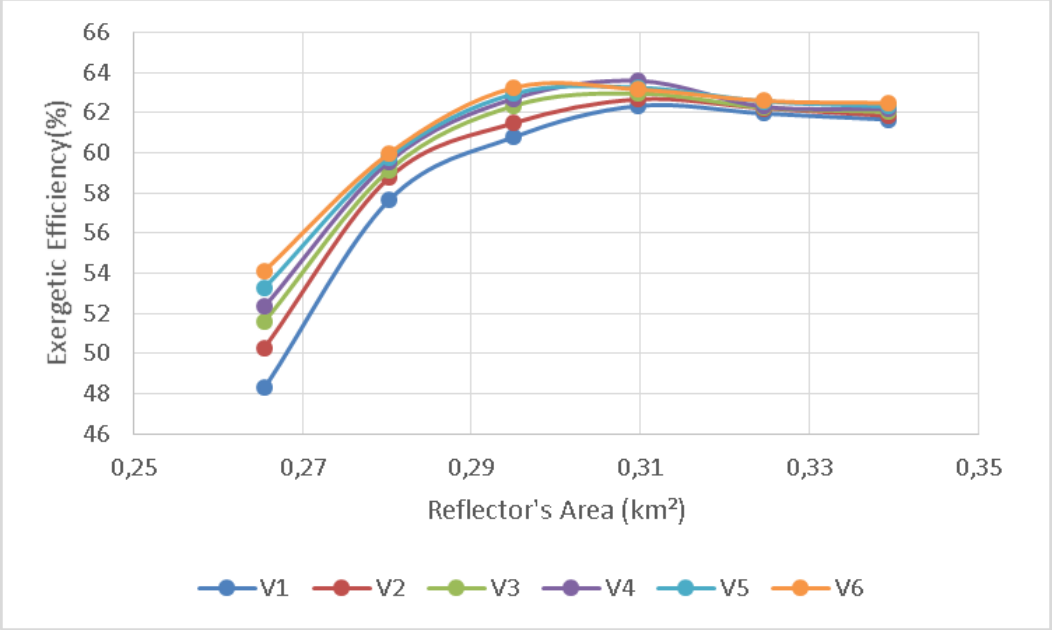

Figure 4-13. Annual Exergetic Efficiency as a function of different Reflector's Areas and different storage tank volumes in Kozani.

The exergetic efficiency is higher than those of Thessaloniki and other cities and reach the value of 64% at 0,31km² heliostat field area but with a smaller storage tank of volume V4 which is close to the design point.

By observing the results of Kozani city it can be seen that the annual power production is similar to the power produced by Athens despite the difference in temperatures, but higher than that of Thessaloniki. What's more the exergetic efficiency and solar energy conversion efficiency of Kozani is higher than those of the other cities because Kozani does not have big fluctuation in temperature throughout the year. All year round has low temperatures.

4.2 Economic Results

According to the Greek legislation [50] the feed-in Tariff for CSP with at least 2 hours of storage is datum in Greece and set to be 0,278€/KWh. With this feed in tariff are going to be presented the results of Payback period, Net Present Value, LCOE and specific cost. The strategy that was followed as was aforementioned is as follows. First of all the design point heliostat field which was found to be 295,000 m² was reduced by 5%,10% and raised by 5%,10% and 15% percent respectively. At the same time the design point storage volume was reduced by 5%, 10% and raised by 5%, 10% and 15% percent respectively.

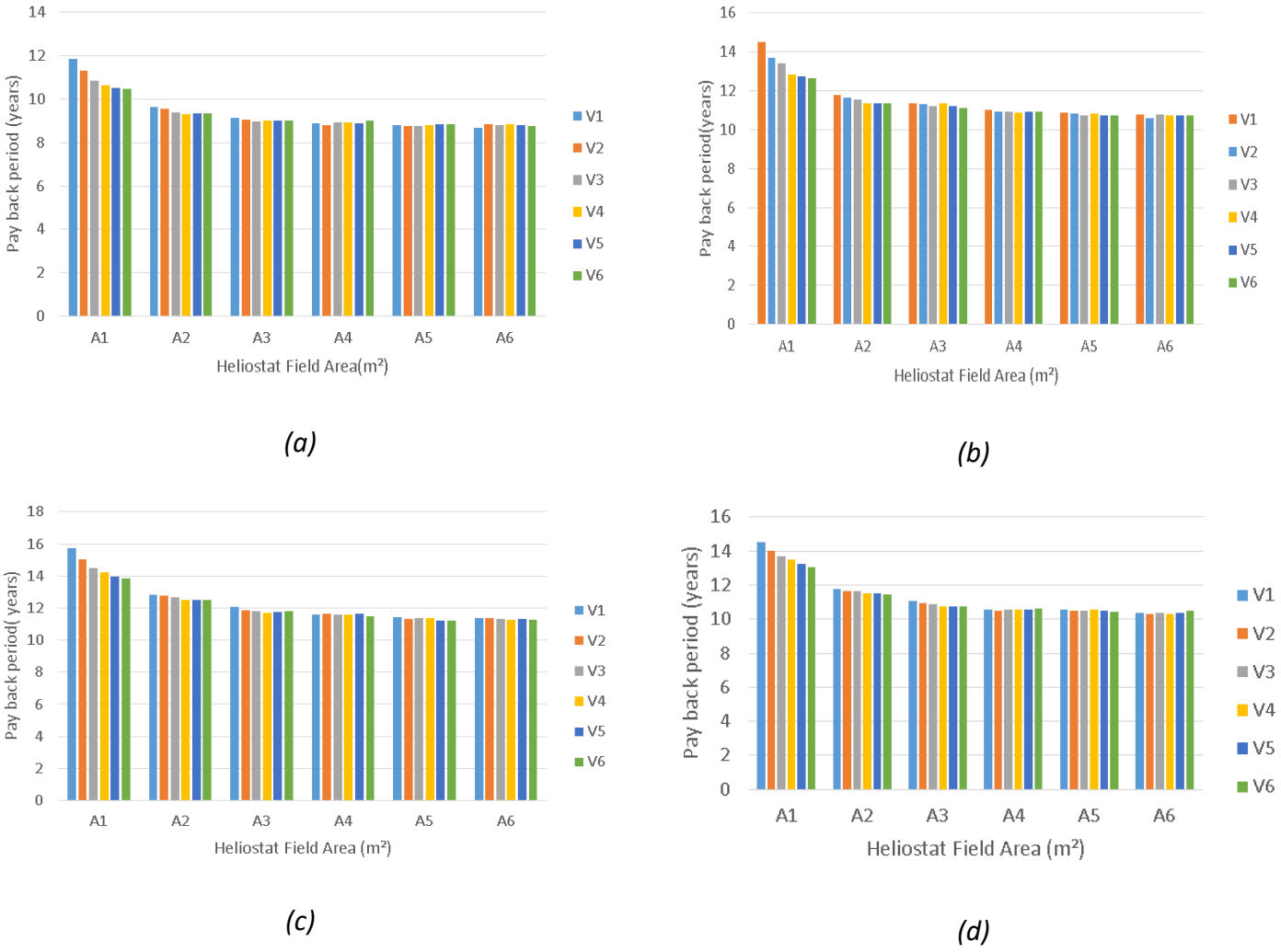

Figure 4-14. On the (a) side is depicted PBP of Chania on the (b) side PBP of Athens ,on the (c) side PBP of Thessaloniki and on the (d) side PBP of Kozani.

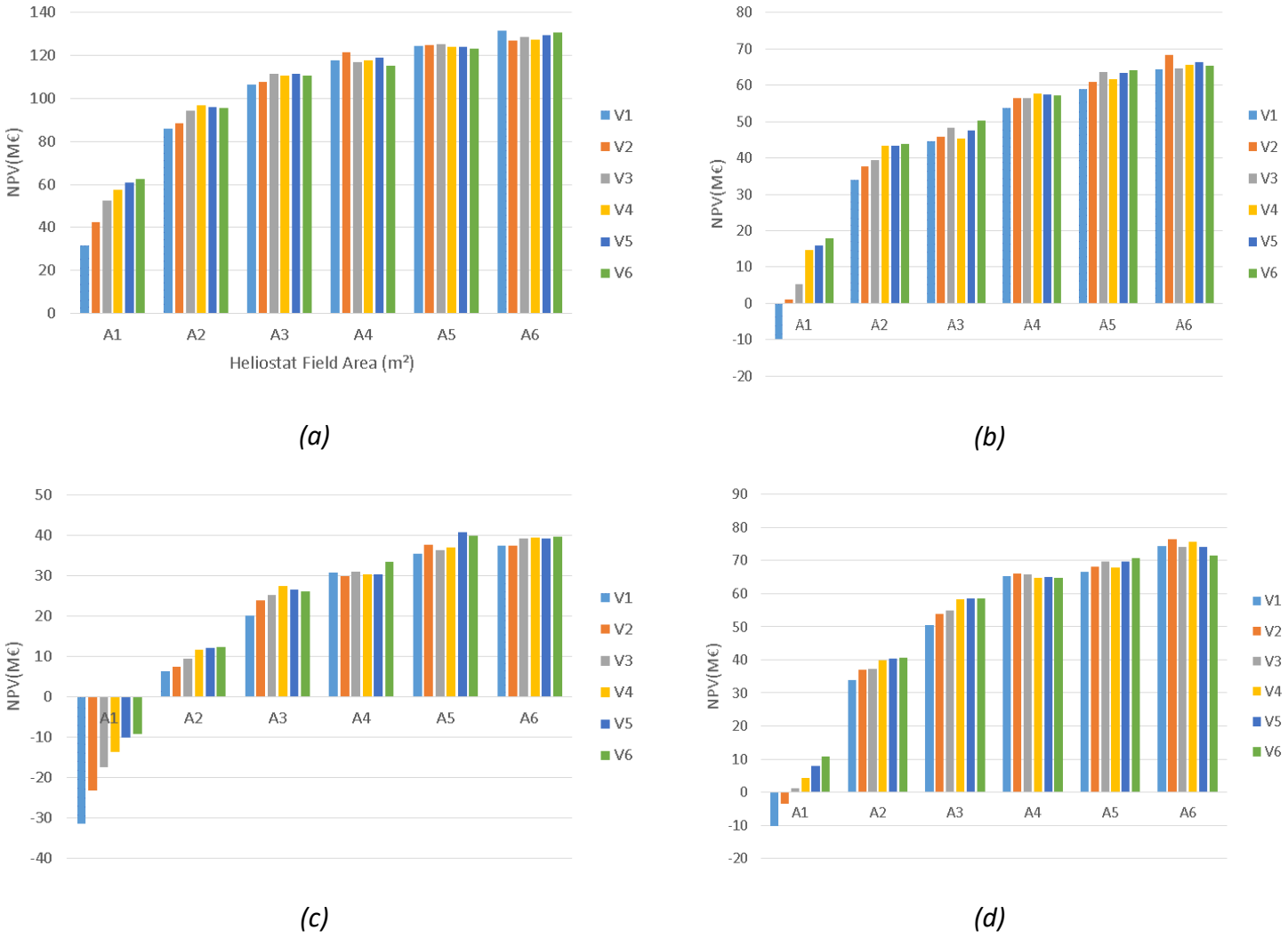

Figure 4-15. **On the (a) side is depicted NPV of Chania on the (b) side NPV of Athens ,on the (c) side NPV of Thessaloniki and on the (d) side NPV of Kozani.**

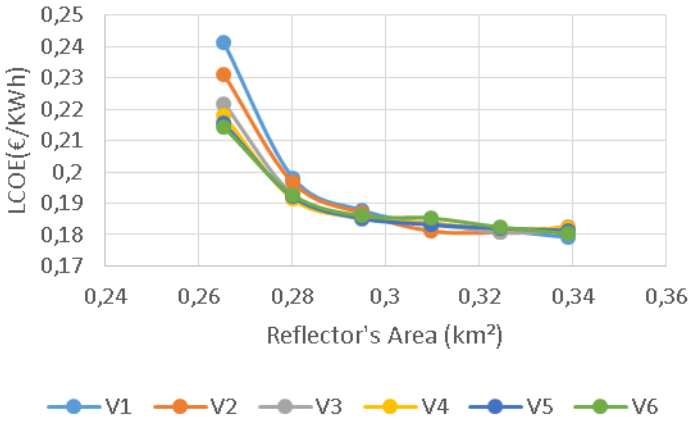

(a)

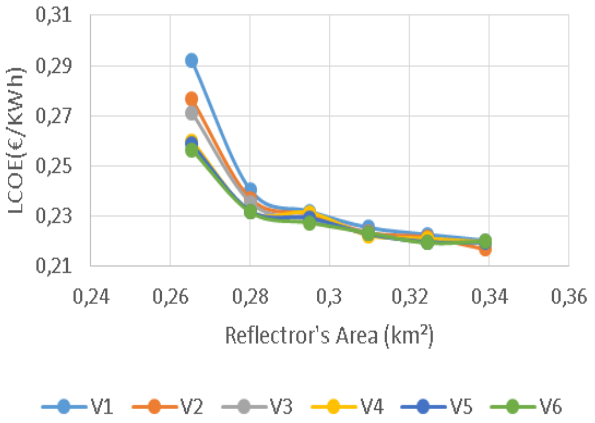

(b)

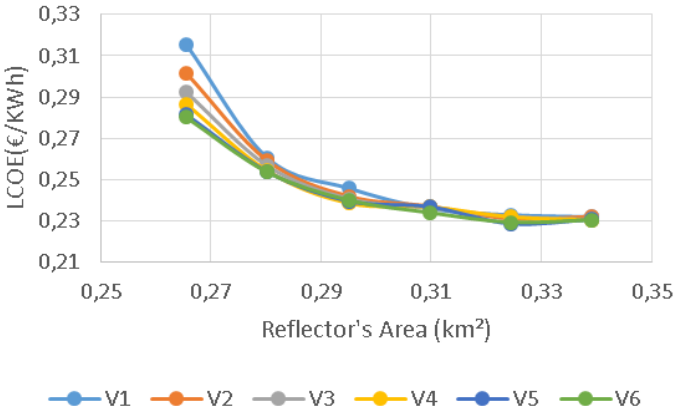

(c)

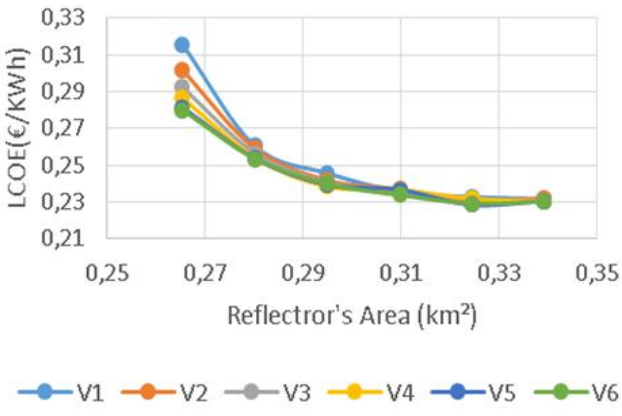

(d)

Figure 4-16. On the (a) side is depicted LCOE of Chania on the (b) side LCOE of Athens ,on the (c) side LCOE of Thessaloniki and on the (d) side LCOE of Kozani.

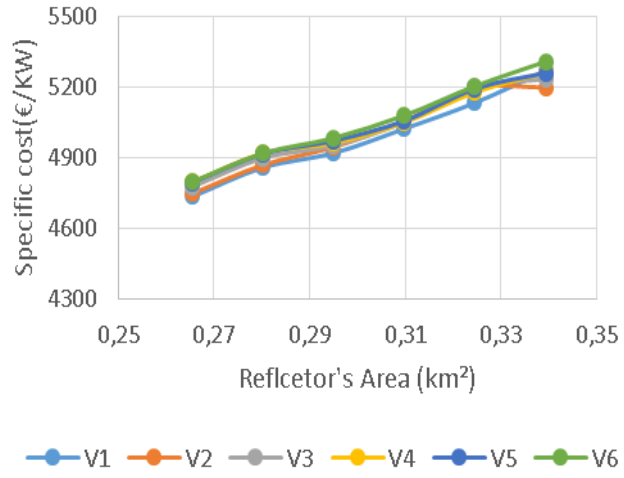

(a)

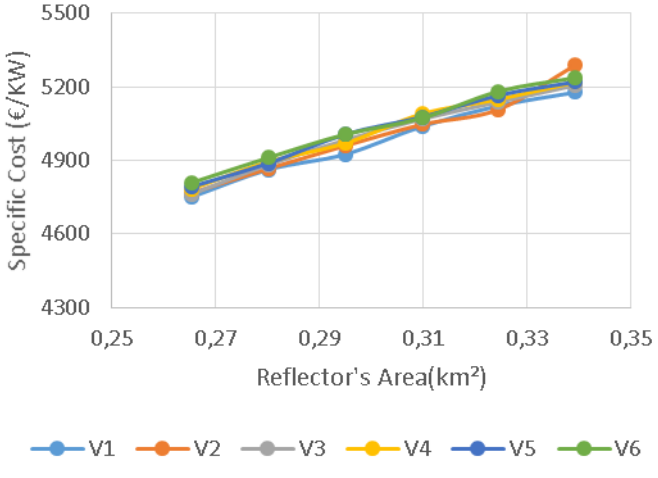

(b)

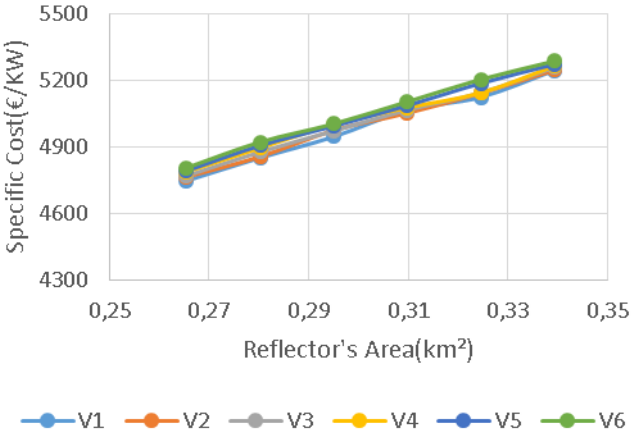

(c)

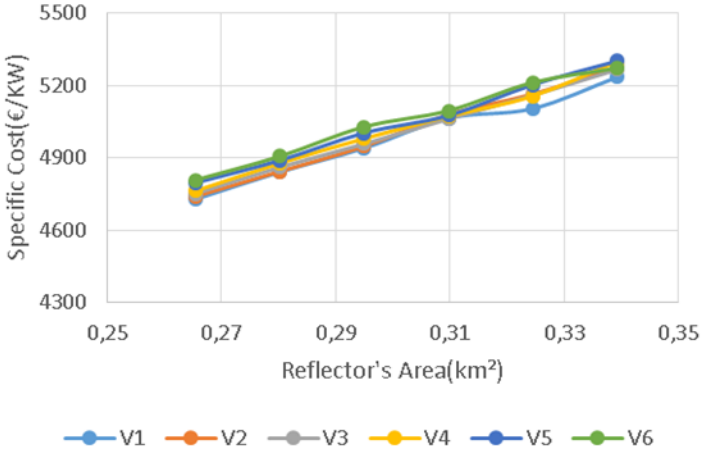

(d)

Figure 4-17. On the (a) side is depicted specific cost of Chania on the (b) side the specific cost of Athens, on the (c) side the specific cost of Thessaloniki and on the (d) side the specific cost of Kozani.

According to the above results the best by far option is the investment in Chania city. Below is depicted a table in which the results are gathered. The LCOE is better in Chania, the payback period is lower and the Net Present Value is higher. This was as expected due to the biggest total annual Direct Irradiance.

Table 4-3. Economic Results for feed-in Tariff of 0,278€/KWh

Cities	PBP	NPV	Combination	LCOE
Chania	8.69	131626258,7 €	A6-V1	0,1791 €/KWh
Athens	10.59	68375787,1 €	A6-V2	0,2166 €/KWh
Thessaloniki	11.20	51114312,01 €	A5-V5	0,2285 €/KWh
Kozani	10.29	76347445,59 €	A6-V2	0,2107 €/KWh

The best case scenario occurred for Chania city with a payback period of 8.69 years and a Net Present Value of 131626258,7 €. The combination of Reflector's area and storage tank volume is A6-V1.The storage volume is the smaller possible due to the more sunny hours throughout the year and as a result the less need for storing energy.

4.3 Sensitivity Analysis-Total Capital Cost

The evaluation that was accomplished before is affected by possible changes of some basic parameters of the problem. These parameters for example are the total capital cost, the inflation rate, the total power produced by the plant and many others that affect the lifetime of the investment and its efficiency.

By changing the total capital cost and reducing it by 5% percent and at the same time keeping the value of feed-in tariff constant and also the rest aspects constants the below diagrams occurred.

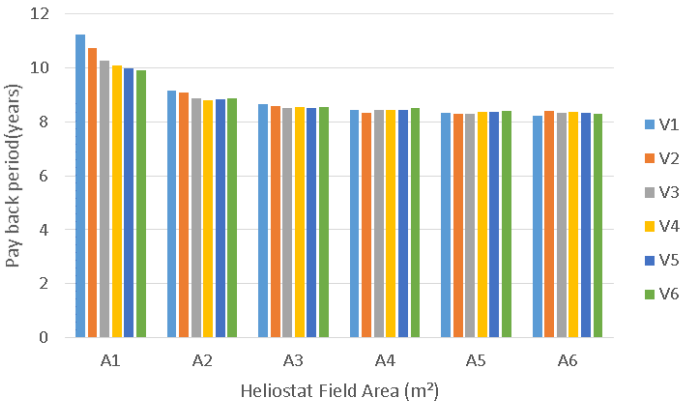

(a)

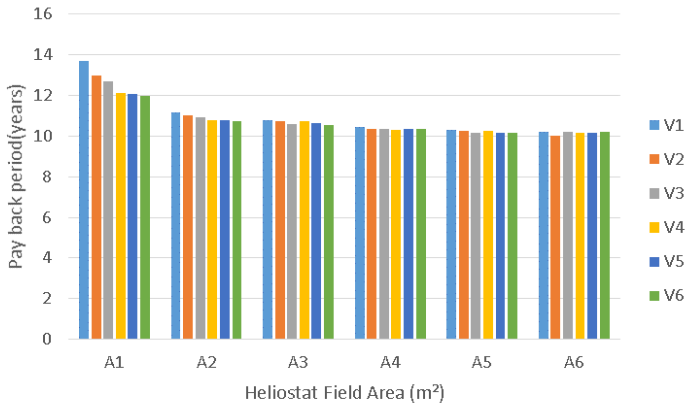

(b)

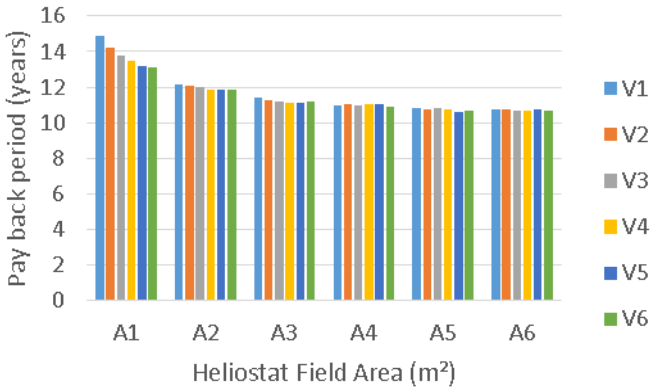

(c)

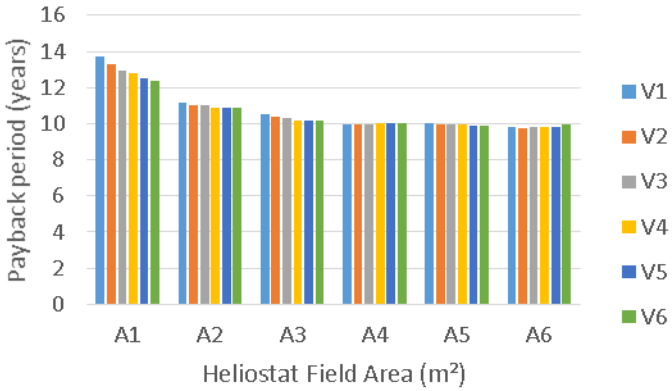

(d)

Figure 4-18. On the (a) side is depicted PBP of Chania on the (b) side PBP of Athens ,on the (c) side PBP of Thessaloniki and on the (d) side PBP of Kozani.

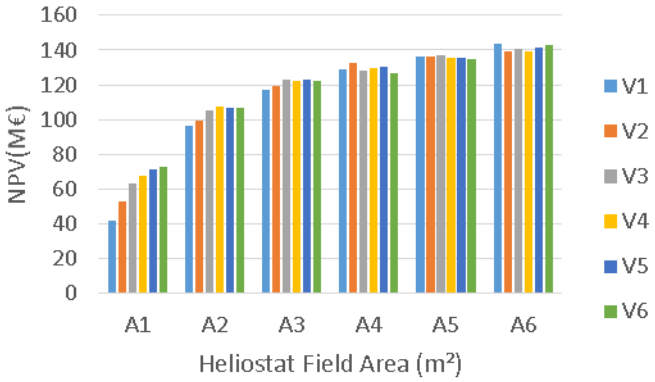

(a)

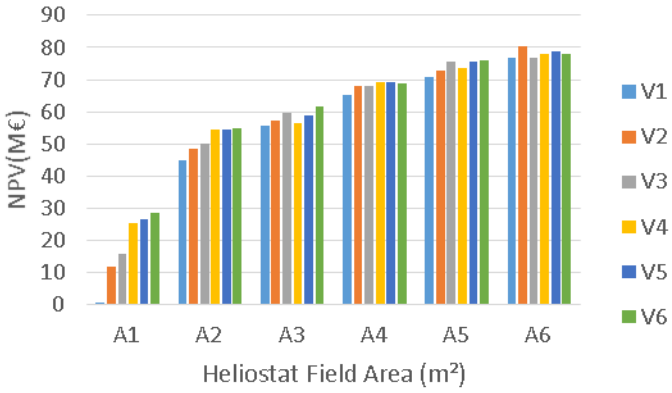

(b)

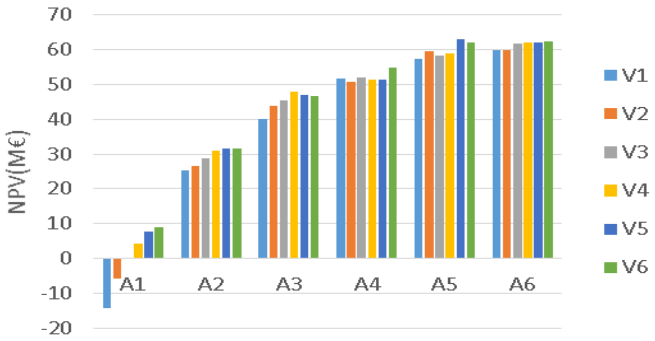

(c)

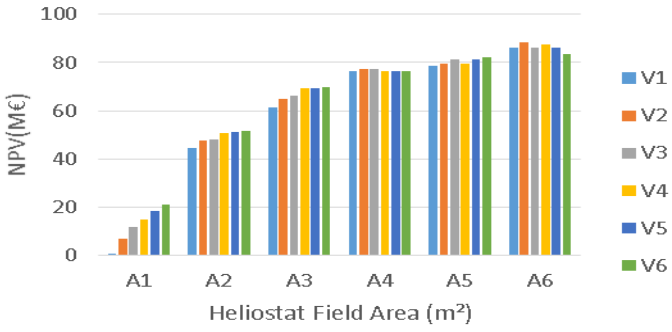

(d)

Figure 4-19. On the (a) side is depicted PBP of Chania on the (b) side PBP of Athens ,on the (c) side PBP of Thessaloniki and on the (d) side PBP of Kozani.

Table 4-4. Economic Results for feed-in Tariff of 0,278€/KWh

Cities	PBP	NPV	Combination	LCOE
Chania	8.24	143546127,2 €	A6-V1	0,1702 €/KWh
Athens	10.04	80440471,3 €	A6-V2	0,2058 €/KWh
Thessaloniki	10.61	62921260,34 €	A5-V5	0,2171 €/KWh
Kozani	9.75	88296409,13 €	A6-V2	0,2002 €/KWh

Again ,from this analysis Chania is the winning situation with the lowest LCOE, the smallest payback period and the biggest NPV.

4.4 Sensitivity Analysis-Annual Power Production

By keeping constant the feed-in Tariff in Greece and by increasing the total annual power production by 6% of the calculated in the four different cities that depict four different climate zones the below results occurred:

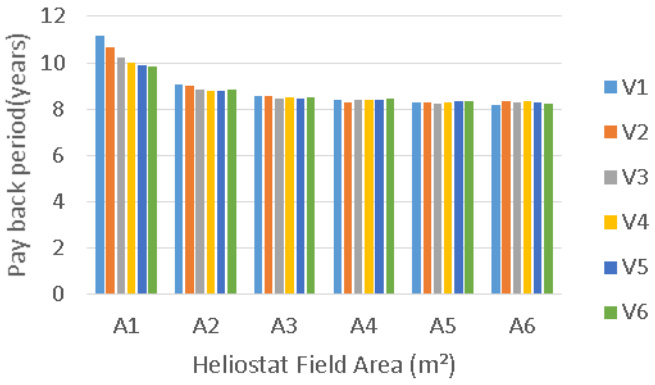

(a)

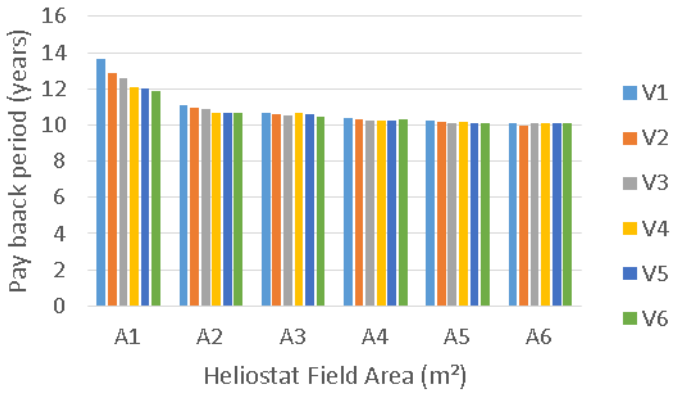

(b)

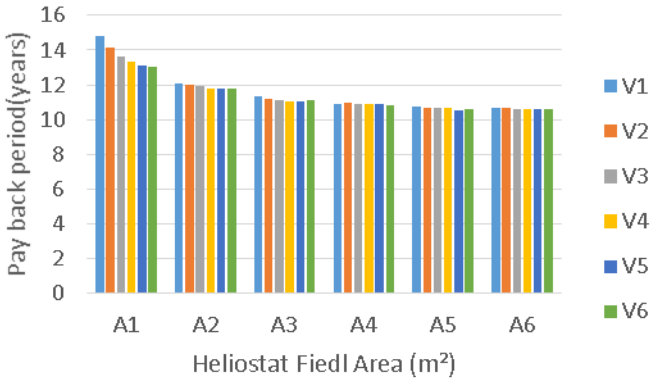
Pay back period(years)
16
14
12
10
8
6
4
2
0
A1
A2
A3
A4
A5
A6
Heliostat Fiedl Area (m²)
V1
V2
V3
V4
V5
V6

(c)

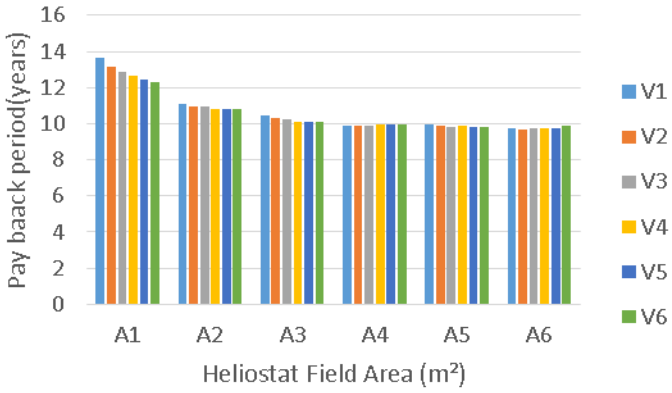
Pay baack period(years)
16
14
12
10
8
6
4
2
0
A1
A2
A3
A4
A5
A6
Heliostat Field Area (m²)
V1
V2
V3
V4
V5
V6

(d)

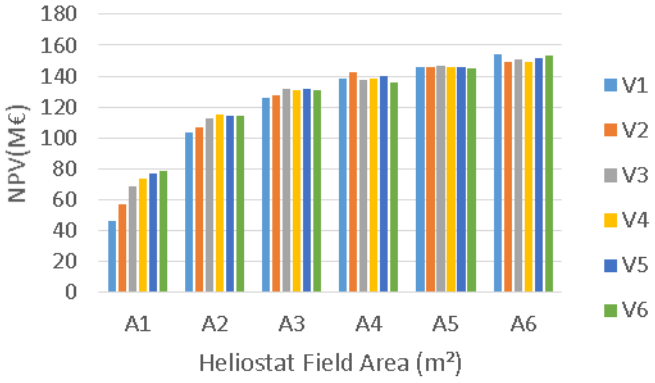
NPV(M€)
180
160
140
120
100
80
60
40
20
0
A1
A2
A3
A4
A5
A6
Heliostat Field Area (m²)
V1
V2
V3
V4
V5
V6

(e)

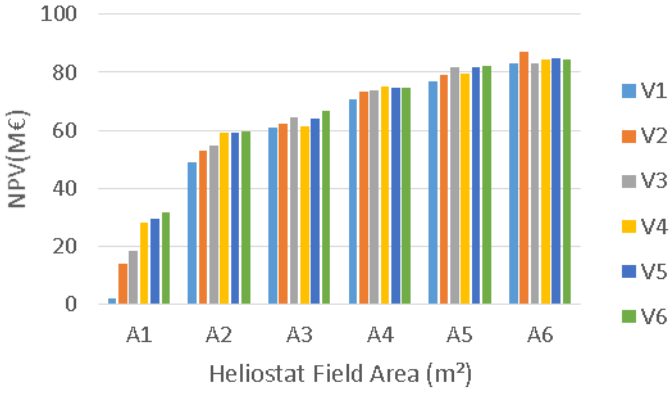
NPV(M€)
100
80
60
40
20
0
A1
A2
A3
A4
A5
A6
Heliostat Field Area (m²)
V1
V2
V3
V4
V5
V6

(f)


NPV(M€)
80
70
60
50
40
30
20
10
0
-10
-20
A1
A2
A3
A4
A5
A6
V1
V2
V3
V4
V5
V6

(g)

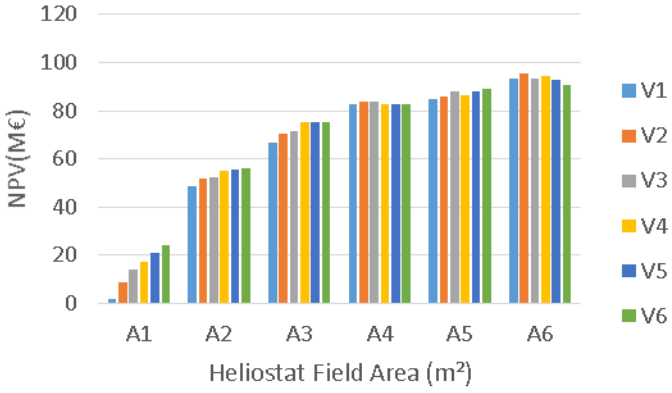
NPV(M€)
120
100
80
60
40
20
0
A1
A2
A3
A4
A5
A6
Heliostat Field Area (m²)
V1
V2
V3
V4
V5
V6

(h)

Figure 4-20. On the (a) side is depicted PBP of Chania on the (b) side PBP of Athens ,on the (c) side PBP of Thessaloniki and on the (d) side PBP of Kozani, on the € side is depicted the NPV of Chania ,on the (f) side the NPV of Athens ,on thet (g) side the NPV of Thessaloniki and on the (h) side the NPV of Kozani.

Table 4-5. Economic Results for feed-in Tariff of 0,278€/KWh

Cities	PBP	NPV	Combination	LCOE
Chania	8.18	153827676,4 €	A6-V1	0,1690 €/KWh
Athens	9.96	86955955,37 €	A6-V2	0,2043 €/KWh
Thessaloniki	10.54	68349508,73 €	A5-V5	0,2156 €/KWh
Kozani	9.68	95267048,58 €	A6-V2	0,1988 €/KWh

Comparing the results of the 3 strategies that were presented before it can easily be reached the conclusion that Chania had better results in all cases scenarios with the best case scenario to be by increasing the total annual power generation by 6%.The smallest LCOE occurred 0,1690 €/KWh with the smallest payback period and the highest NPV.

4.5 Sensitivity Analysis-Feed-in Tariff

By changing the value of feed-in tariff with a lower bound of 0,248€/KWh and an upper bound of 0,288€/KWh and keeping constant values to other aspects the below results occurred.

4.5.1 Athens

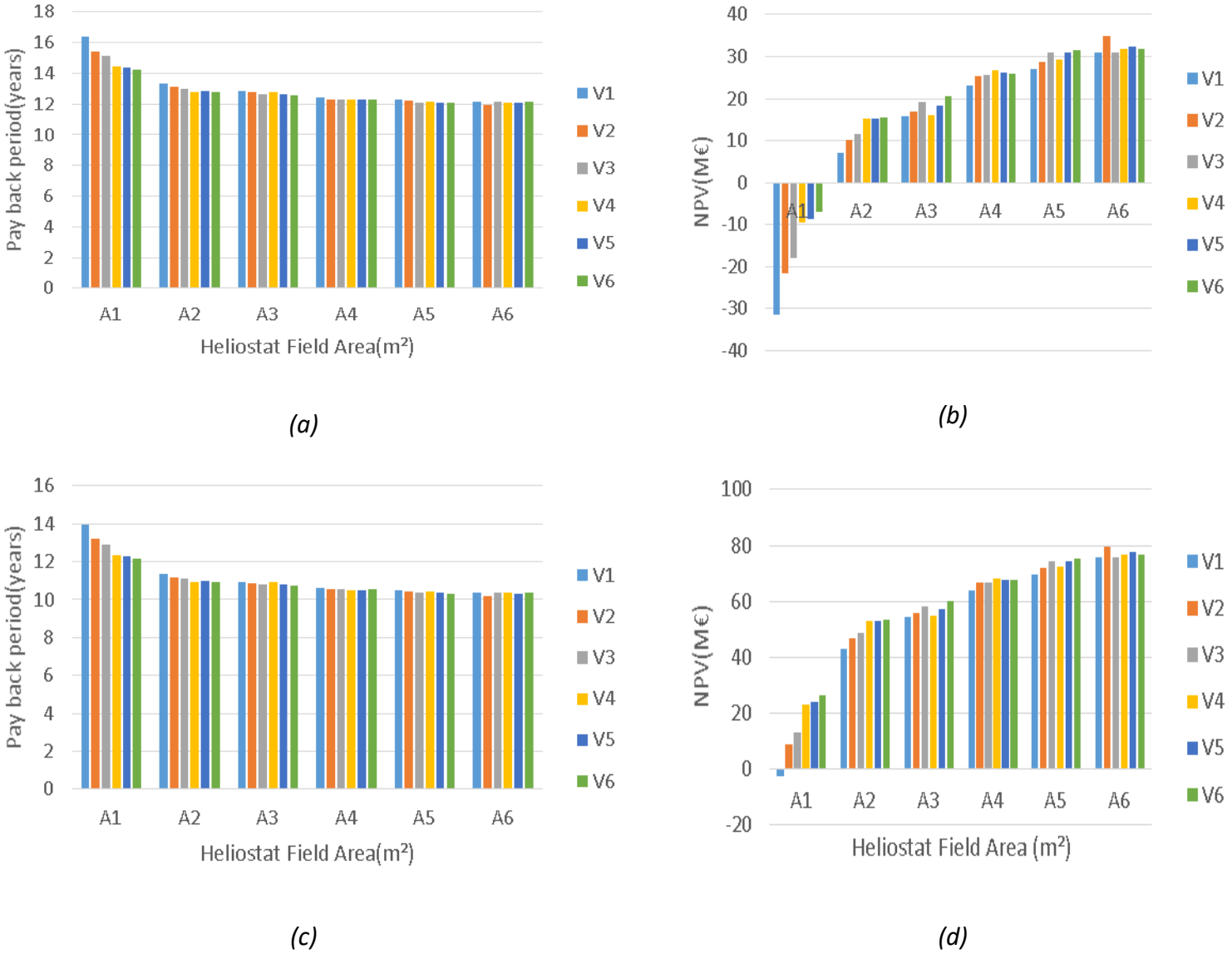

Figure 4-21. On the (a) and (b) can be depicted the PBP and NPV for 0,248€/KWh marginal price cost of the system and on (c) and (d) PBP and NPV for 0,288 €/KWh in Athens.

From the above Figure 4-14 can be reached easily the conclusion that while the heliostat field area (m²) raises, the payback period is reducing .At the same time the Net Present Value is increasing. The desirable for the investment to be viable is the NPV to be positive. When the marginal price cost raises to 0,288€/KWh it can be monitored a drop in the payback period years.

What's more the NPV is increased with best match to be for 0,248€/KWh A6-V2 and for 0,288€/KWh also A6-V2.For the payback period in years the best combination for the investment is A6-V2 for both marginal price costs.

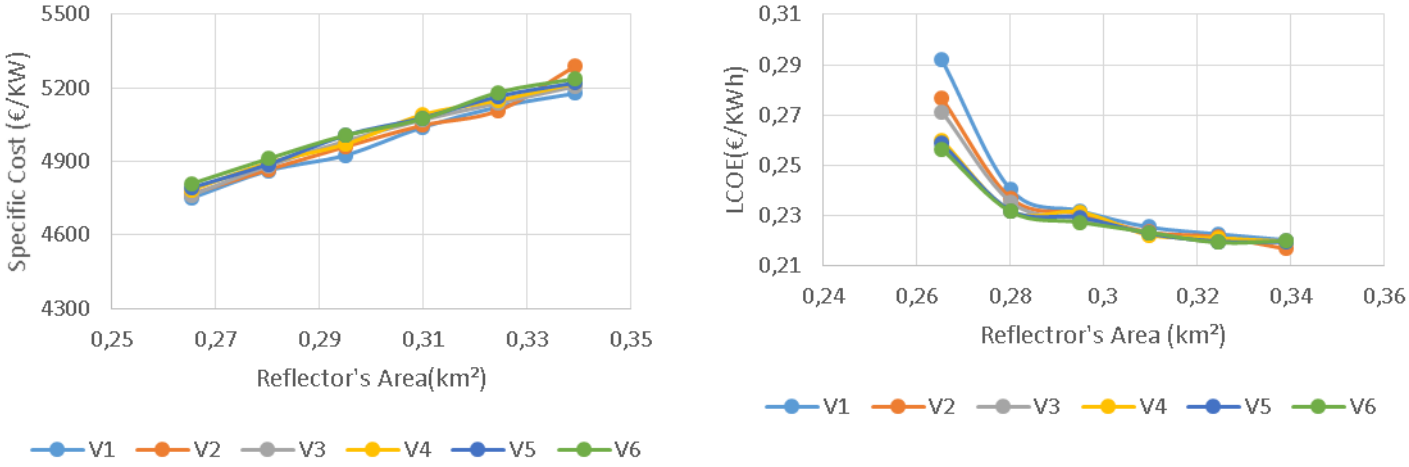

Figure 4-22. On the left side of the matrix is depicted the specific cost as a function of Reflector's Area and storage tank volume and on the right side the LCOE as a function of the same parameters in Athens.

In Figure 4-15 can be monitored the specific cost which increases due to the increase in the Reflector's Area (km²) and can be seen that its highest value is beyond 0,33km² for V2 storage tank. It can be seen that the LCOE for a constant Heliostat Field Area drops its value with the increase in the storage tank. This drop is negligible as the heliostat field area raises. The desirable LCOE is the smallest one which is achieved at the 0,34km² reflector surface and at the value of 0,22.

4.5.2 Chania

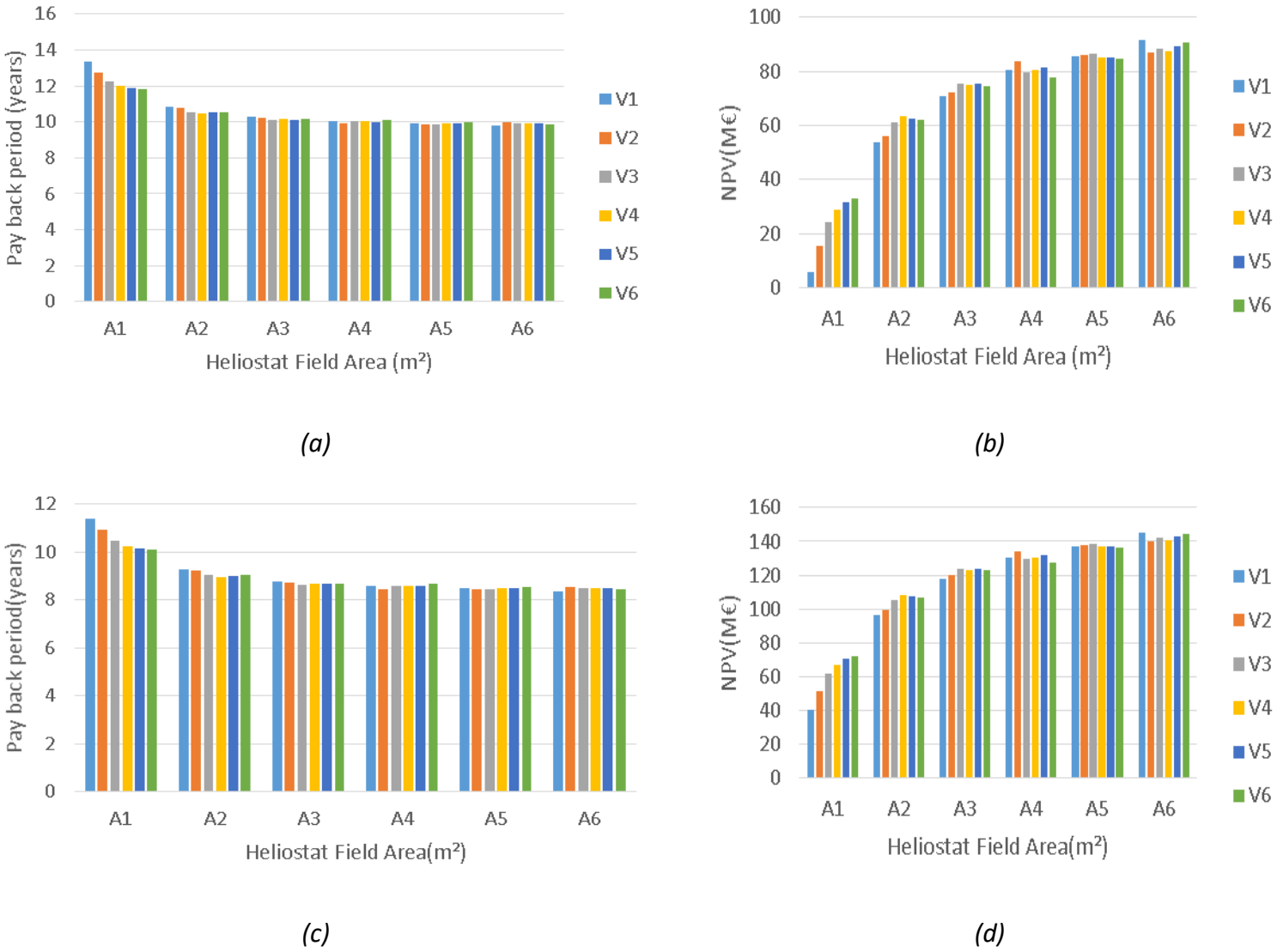

Figure 4-23. On the (a) and (b) can be depicted the PBP and NPV for 0,248€/KWh marginal price cost of the system and on (c) and (d) PBP and NPV for 0,288 €/KWh in Chania.

From the Figure 4-16 above it can be observed that as in Athens, while the reflecting surface area is scaling up the payback period is lowered .The NPV on the other hand is increasing with the best combination to be A6-V1 for all the marginal price costs. What's more for the payback period also A6-V1 is the best combination of the heliostat field area and the storage tank volume. It is concluded that in Chania comparing to Athens better results can occur in NPV but also payback period for smaller tank volume but the same heliostat field area. The payback period and Net Present Value are lower than that of Athens due to the biggest annual power output of Chania investment.

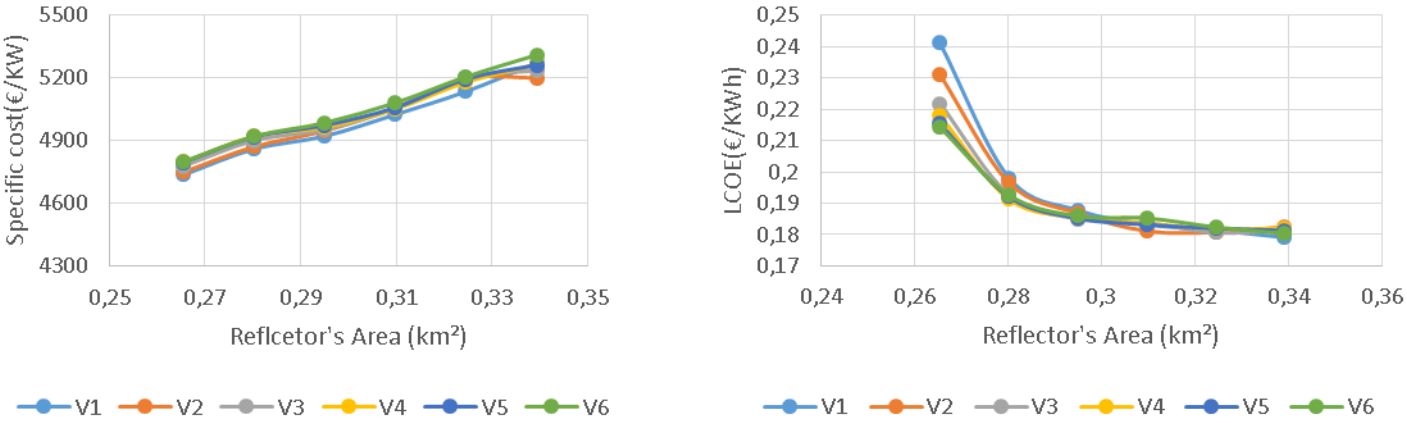

Figure 4-24. **On the left side of the matrix is depicted the specific cost as a function of Reflector's Area and storage tank volume and on the right side the LCOE as a function of the same parameters in Chania.**

From Figure 4-17 can be spotted that the specific cost is rising with the increase in heliostat field area with its biggest value to be above 5200€/KW for a heliostat field area of A6 and volume storage tank of V6.LCOE index in Chania is lower than that of Athens and fixes its value beyond A3 heliostat field area at 0,18€/KWh .It is obvious that LCOE of Athens drops steeper than that of Chania which from the A3 heliostat field area almost reaches its value.

4.5.3 Thessaloniki

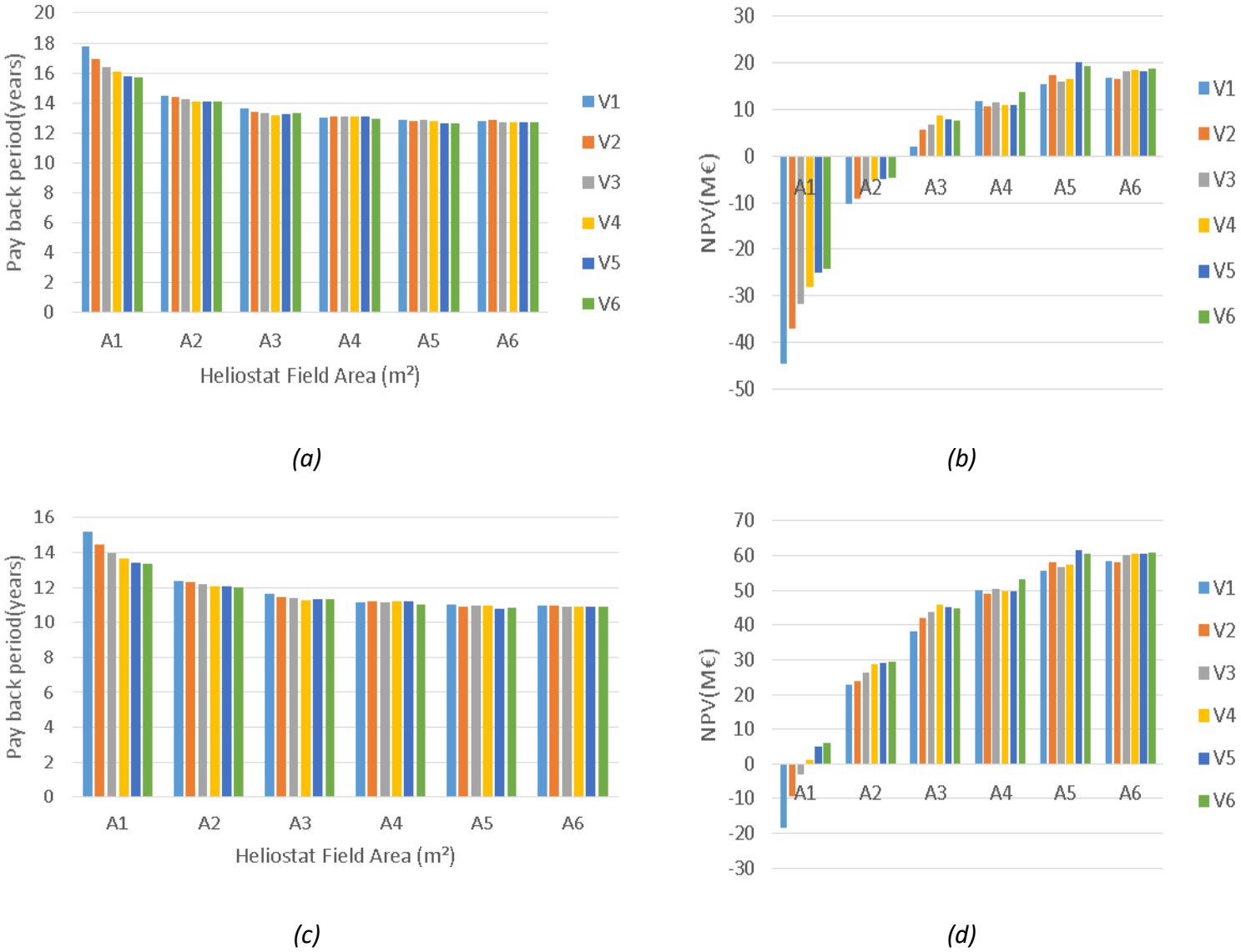

Figure 4-25. On the (a) and (b) can be depicted the PBP and NPV for 0,248€/KWh marginal price cost of the system and on (c) and (d) PBP and NPV for 0,288 €/KWh in Thessaloniki.

From the above Figure 4-18 for a marginal price cost of 0,248€/KWh the results of the payback period are worse than that of Athens. The comparison is being made with Athens because it has no sense to compare with Chania investment due to far better results. Again, it is observed that with the raise in heliostat field area the payback period is reduced with the better result to be the combination of A5-V5 for all marginal prices. It can be understood that the heliostat field area is lower than that of Athens due to the bigger cost but storage tank volume is higher due to the less sunny hours throughout the year in Thessaloniki and the need to store more energy.

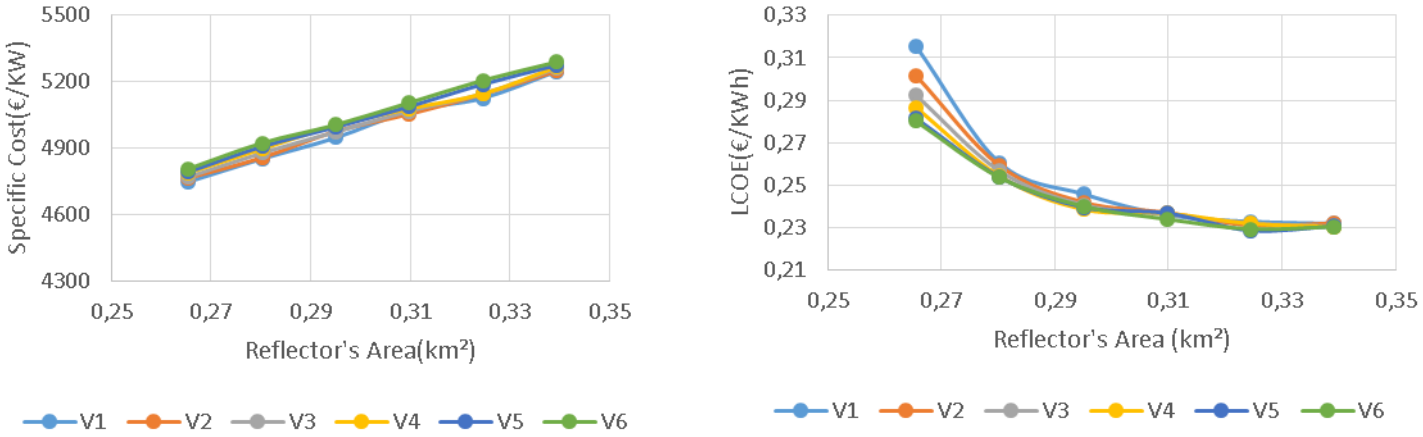

Figure 4-26 **On the left side of the matrix is depicted the specific cost as a function of Reflector's Area and storage tank volume and on the right side the LCOE as a function of the same parameters in Thessaloniki.**

The specific cost on the matrix above is rising with the increase in the reflector's area with the highest value to be for storage V6 the heliostat field area A6. The LCOE in Thessaloniki drops smoothly and need more time to reach its steady value. Also the value of 0,23 €/KWh is bigger than that of Athens and in Thessaloniki reaches its steady value at A4 while in Athens has a tendency beyond A6 to drop more its value.

4.5.4 Kozani

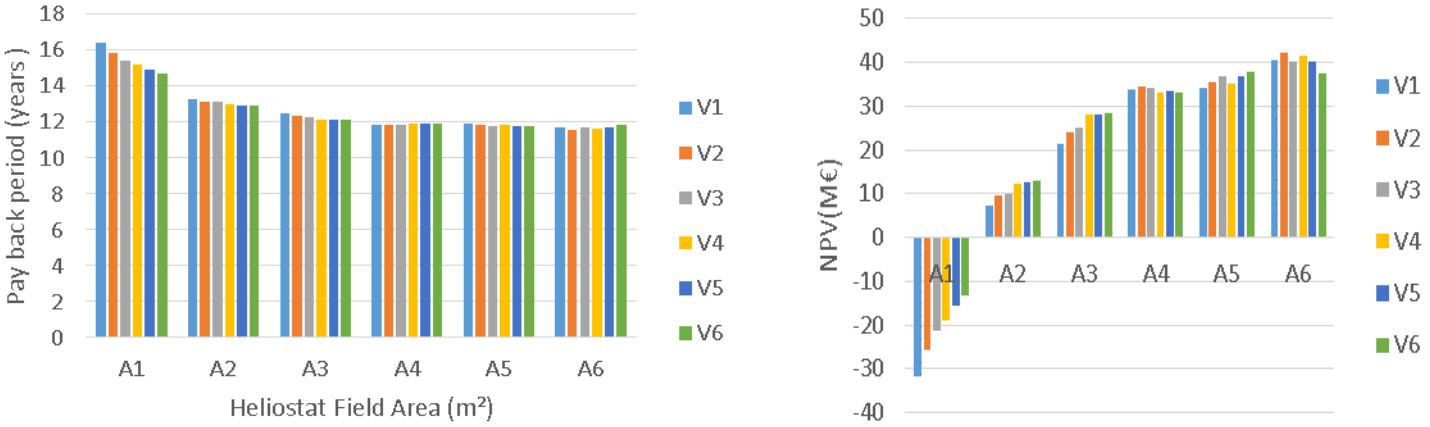

(a) *(b)*

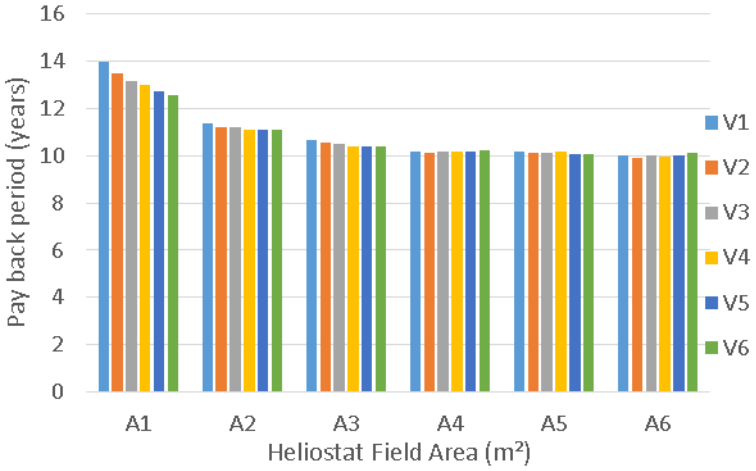

(c)

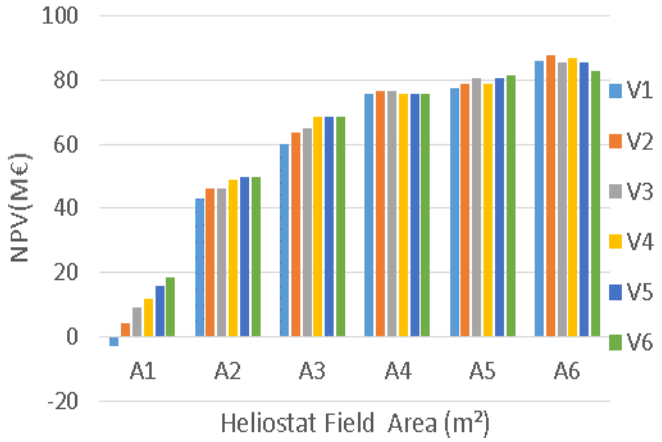

(d)

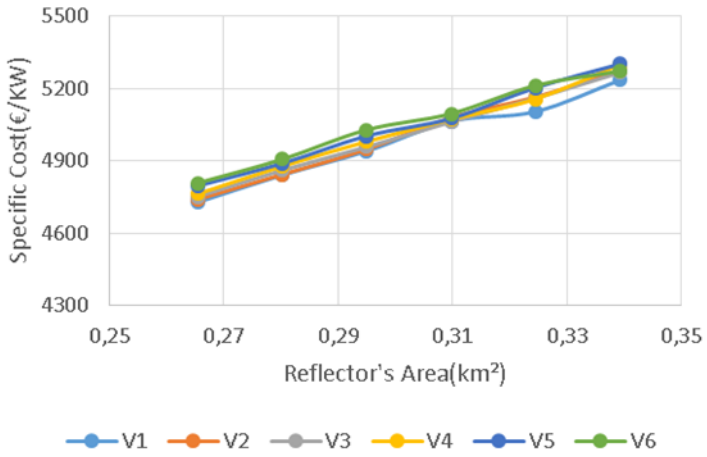

(e)

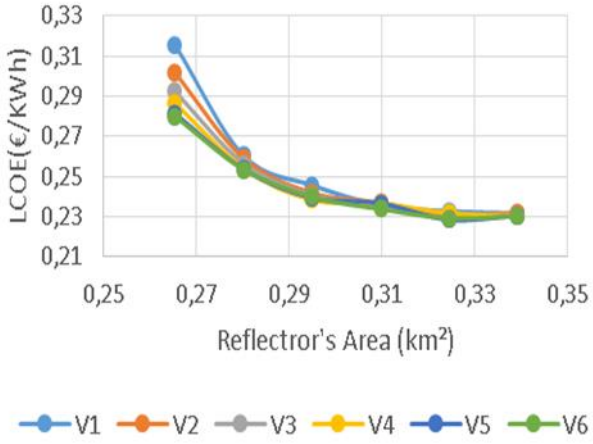

(f)

Figure 4-27. On the (a) and (b) can be depicted the PBP and NPV for 0,248€/KWh marginal price cost of the system and on (c) and (d) PBP and NPV for 0,288 €/KWh in Kozani, on the (e) the specific cost and on the (f) the LCOE in Kozani.

Comparing Thessaloniki and Kozani it can be monitored that Kozani has lower payback period and higher Net present value than that of Thessaloniki. This happens due to better total DNI that is received by the heliostat field area of Kozani. It was calculated that Thessaloniki had the worst results of total DNI received for the period of one year despite being the 3d Climate Zone in Greece with better temperatures than Kozani. Best combination for all marginal prices was found to be A6-V2 which is the same result as Athens. This is logical due to the convergence in their results. There is a difference in the LCOE, though, because Kozani has a steeper curve that

means that it reaches the lowest value of LCOE with the slightest increase in heliostat field area whereas the LCOE of Thessaloniki needs biggest changes in the field area in order to drop its value.

As can be observed on the below tables the summary analysis results occurred:

Table 4-6.Economic results for a marginal price cost of 0,248€/KWh in different cities

Cities	PBP	NPV	Combination	LCOE
Chania	9.78	91695651,21€	A6-V1	0,1791 €/KWh
Athens	11.93	34958218,27€	A6-V2	0,2166 €/KWh
Thessaloniki	12.63	20115756,76€	A5-V5	0,2285 €/KWh
Kozani	11.60	42319382,67€	A6-V2	0,2107 €/KWh

Table 4-7.Economic results for a marginal price cost of 0,288€/KWh in different cities

Cities	PBP	NPV	Combination	LCOE
Chania	8.38	144936461,2€	A6-V1	0,1791 €/KWh
Athens	10.21	79514976,71€	A6-V2	0,2166 €/KWh
Thessaloniki	10.79	61447163,76€	A5-V5	0,2285 €/KWh
Kozani	9.92	87690133,23€	A6-V2	0,2107 €/KWh

As it can be seen from the above analysis, Chania have the minimum LCOE value and Thessaloniki with Kozani the maximum, as the net electric production is the highest and lowest in these cities, respectively. It is concluded that while the reflector's area is increased , after a particular size, it is obvious that the storage tank volume have to be increased far too much in order to take advantage of the surplus of energy. However ,this increase never happens due to the cost that's why the effect of the storage tank volume is negligible from a design point and beyond.

4.6 Sensitivity Analysis-Feed-in Tariff & Total Capital Cost

The evaluation that was accomplished before is affected by possible changes of some basic parameters of the problem. These parameters for example are the total capital cost, the inflation rate, the total power produced by the plant and many others that affect the lifetime of the investment and its efficiency.

The strategy that will be followed in this step is to change the value of feed-in tariff with a lower bound of 0,248€/KWh and an upper bound of 0,288€/KWh and also change the total capital investment cost and monitor the changes in other aspects of the project such as the payback period and net present value. The capital cost is initially reduced by 5% and the results are as followed.

4.6.1 Athens

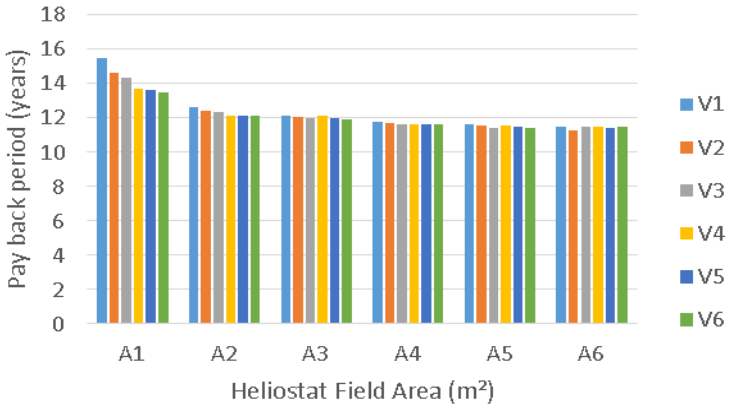

(a)

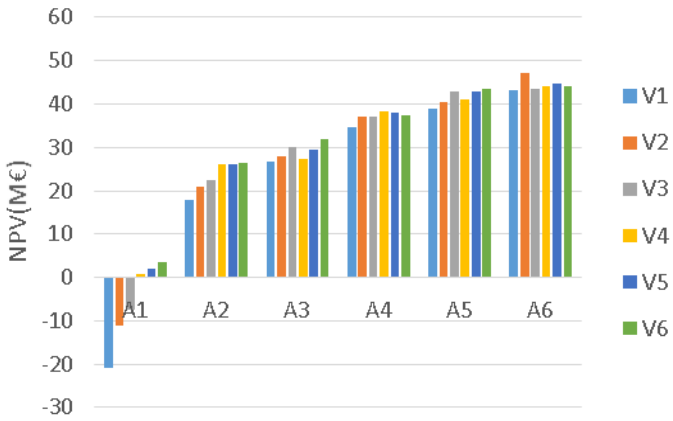

(b)

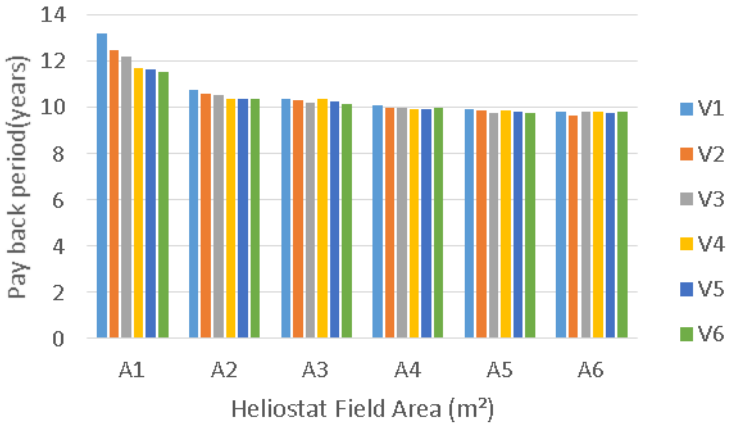

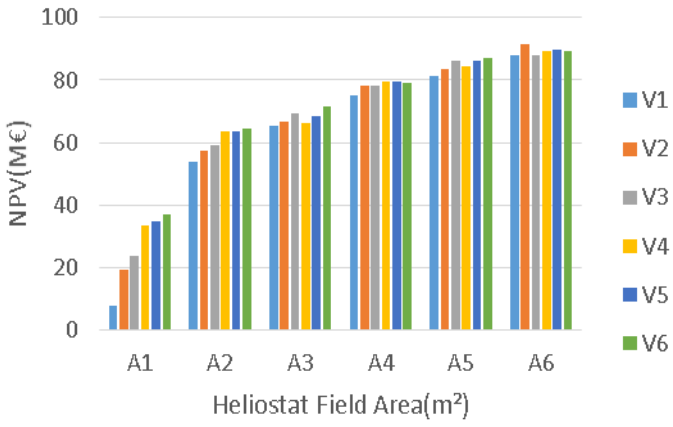

(c)

(d)

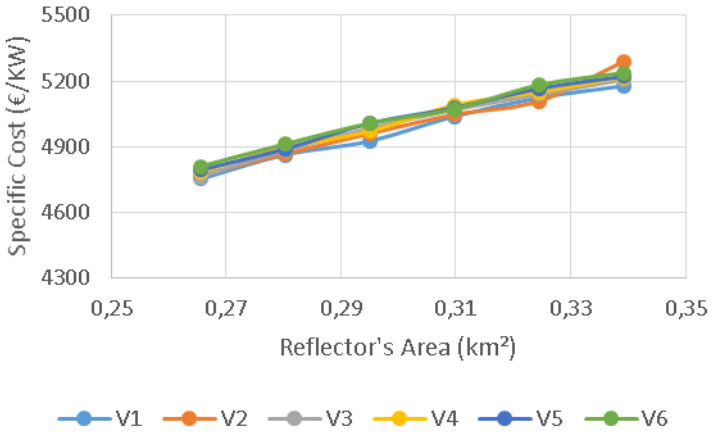

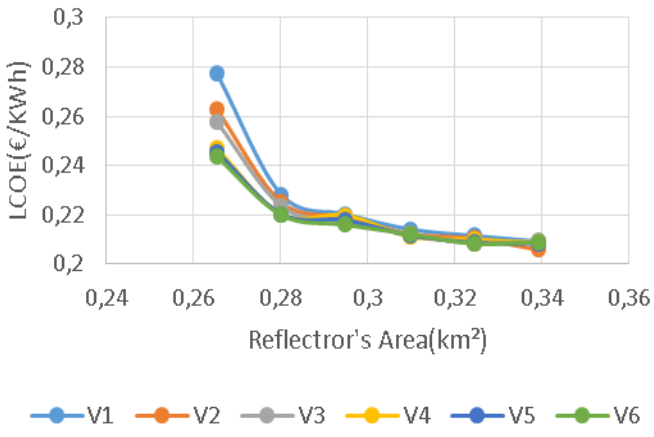

(e)

(f)

Figure 4-28. On the (a) and (b) can be depicted the PBP and NPV for 0,248€/KWh marginal price cost of the system and on (c) and (d) PBP and NPV for 0,288 €/KWh in Kozani, on the (e) the specific cost and on the (f) the LCOE in Athens.

Comparing the results of Athens after the implementation of sensitivity analysis on capital cost and the previous economic results, the LCOE was reduced as it was reduced the specific cost. This was as expected due to the dependence of LCOE from the total capital cost. Apart from that both NPV and PBP were reduced due to the lower investment cost and as a result the better depreciation of the project. The best combination of the heliostat field area but also the storage tank volume was as in the previous analysis A6-V2.The LCOE dropped nearly by 0,01€/KWh.

4.6.2 Chania

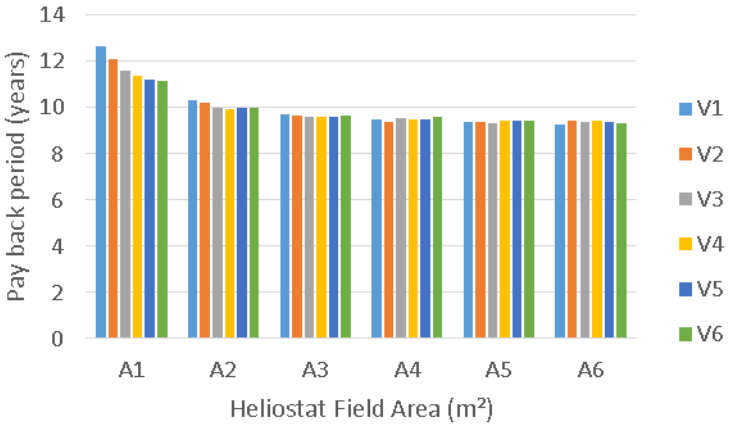

(a)

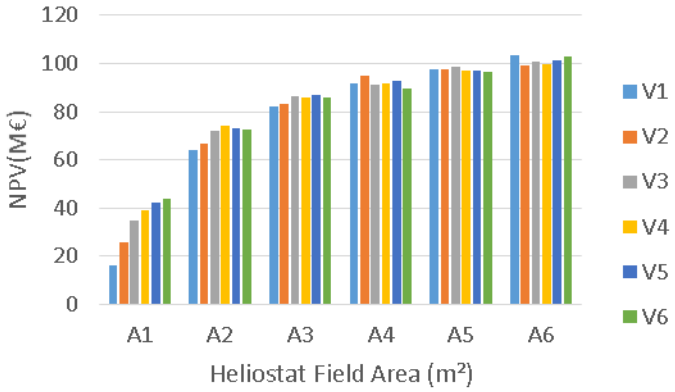

(b)

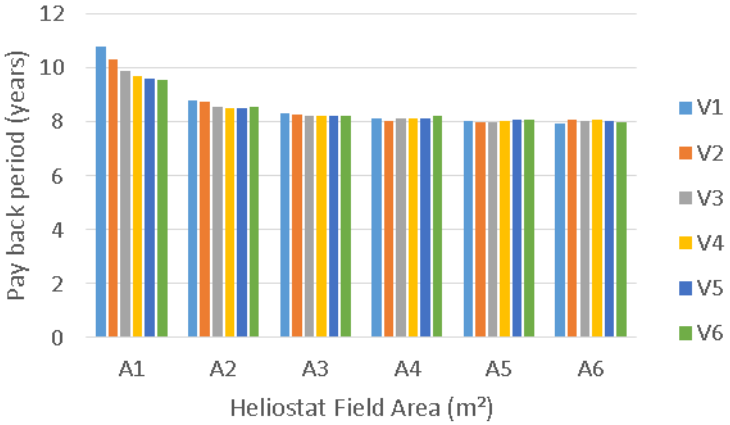

(c)

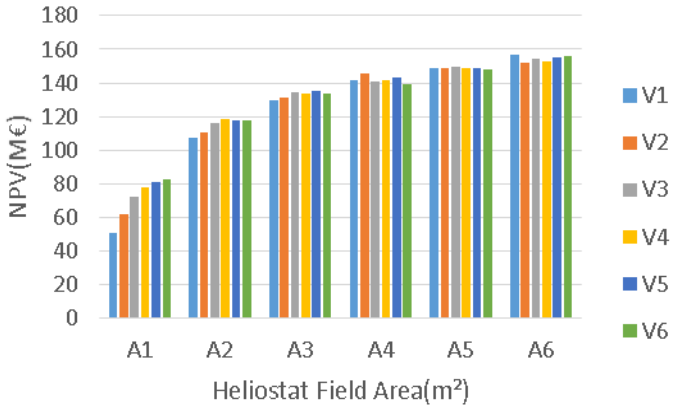

(d)

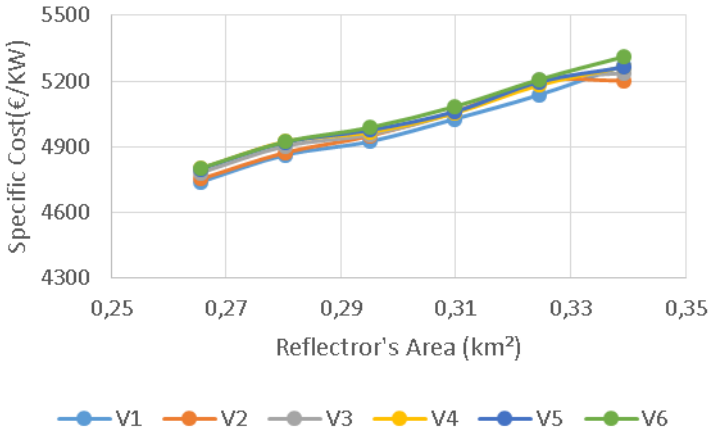

(e)

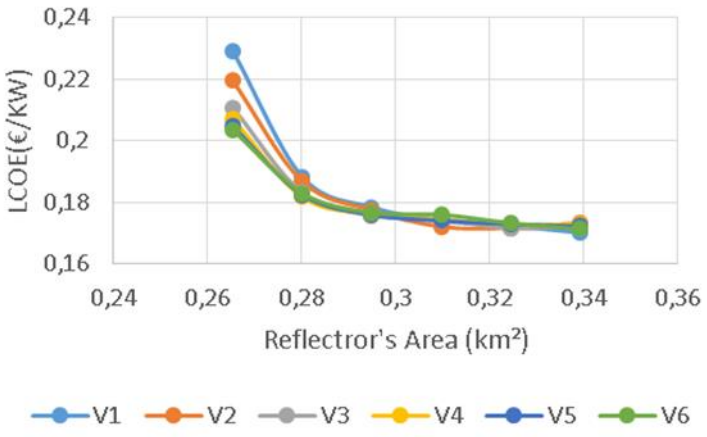

(f)

Figure 4-29 On the (a) and (b) can be depicted the PBP and NPV for 0,248€/KWh marginal price cost of the system and on (c) and (d) PBP and NPV for 0,288 €/KWh in Kozani, on the (e) the specific cost and on the (f) the LCOE in Athens.

Comparing Chania with Athens but also with previous results before the sensitivity analysis it is obvious that one more time Chania have better results in PBP and NPV than in Athens but also better results from their previous analysis without the reduction at total capital cost. The best combination of heliostat field area but also storage tank volume was found to be again A6-V1. The LCOE was lowered and reached 0,165 €/KWh from 0,18€/KWh without the sensitivity analysis.

4.6.3 Thessaloniki

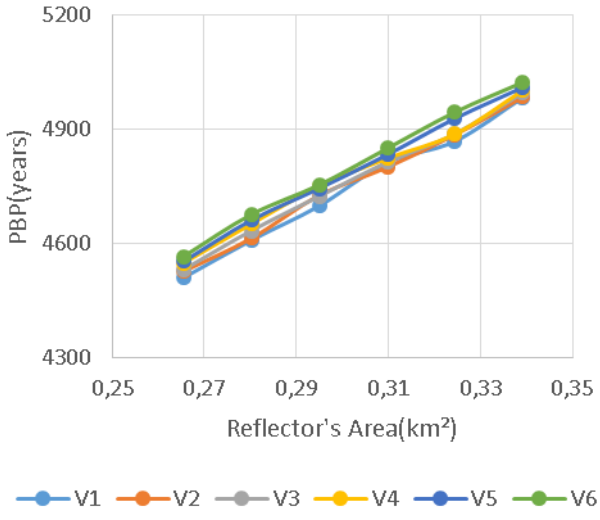

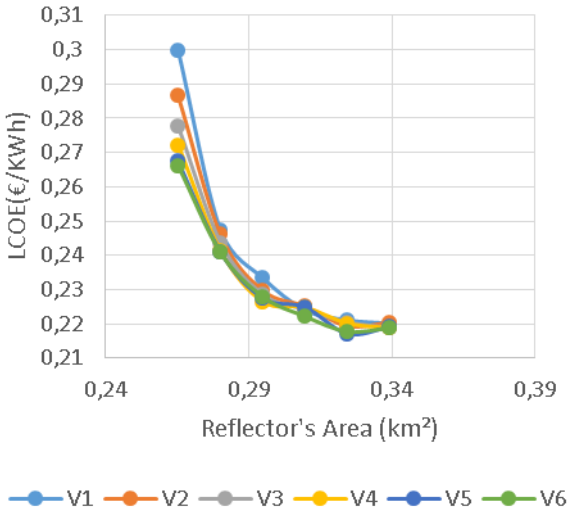

Figure 4-30 On the left side of the matrix is depicted the specific cost as a function of Reflector's Area and storage tank volume and on the right side the LCOE as a function of the same parameters in Thessaloniki.

From the above Figure 4-23 it can be observed that LCOE dropped from 0, 23€/KWh to 0,22€/KWh with the sensitivity analysis. The curve is steeper than previously .The specific cost of course dropped due to the drop in capital cost.

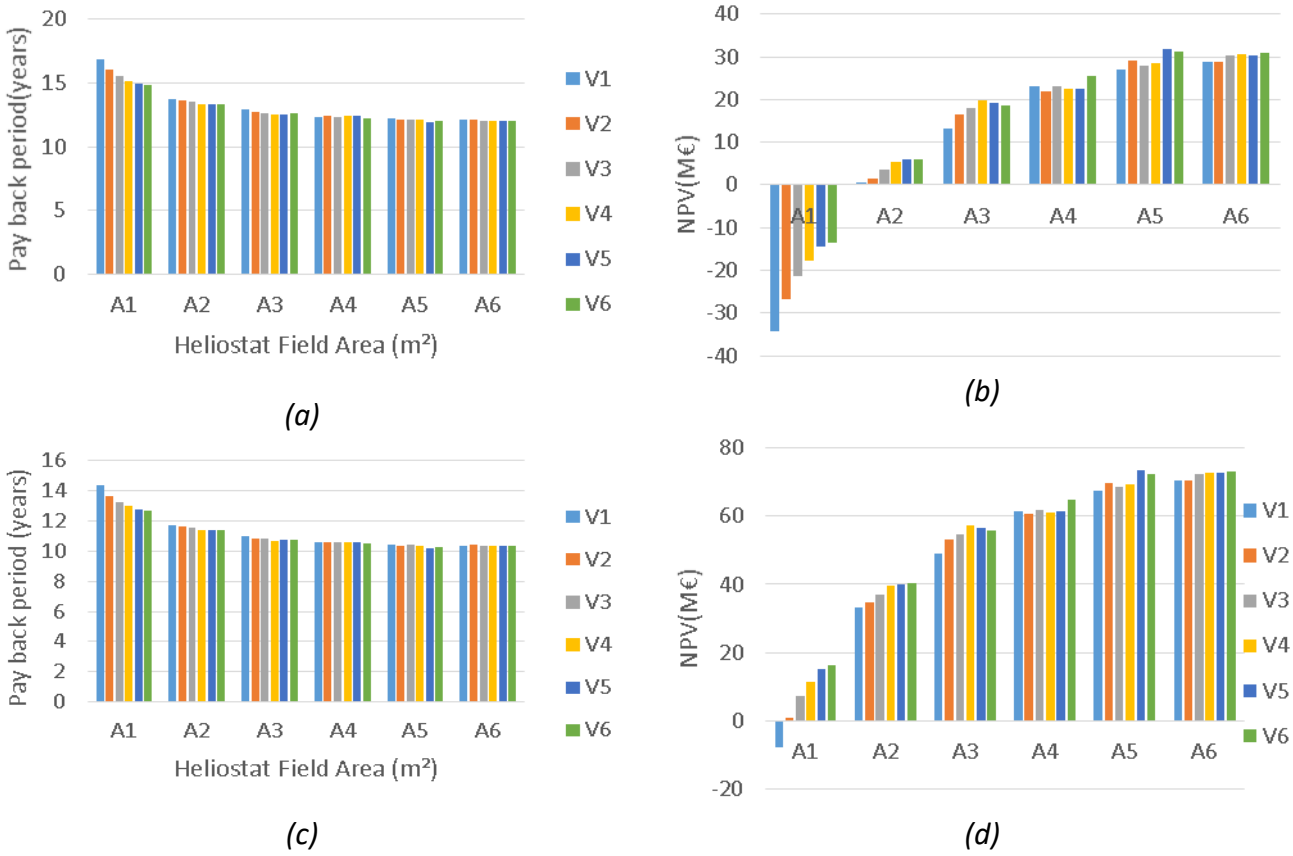

Figure 4-31. On the (a) and (b) can be depicted the PBP and NPV for 0,248€/KWh marginal price cost of the system and on (c) and (d) PBP and NPV for 0,288€/KWh in Thessaloniki.

From the Figure 4-24 above it can be observed that the payback period dropped while the NPV also dropped from the previous chapter analysis on Thessaloniki. What's more it remained higher than the respective values of Athens. The LCOE of the Athens is lower than that of Thessaloniki also in this chapter.

4.6.4 Kozani

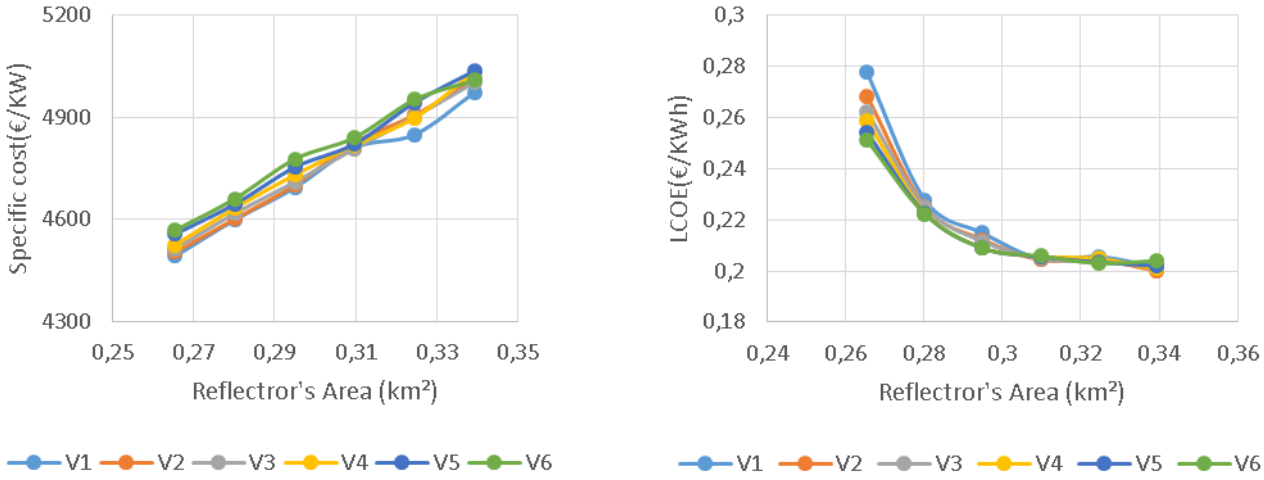

Figure 4-32. **On the left side of the matrix is depicted the specific cost as a function of Reflector's Area and storage tank volume and on the right side the LCOE as a function of the same parameters in Kozani.**

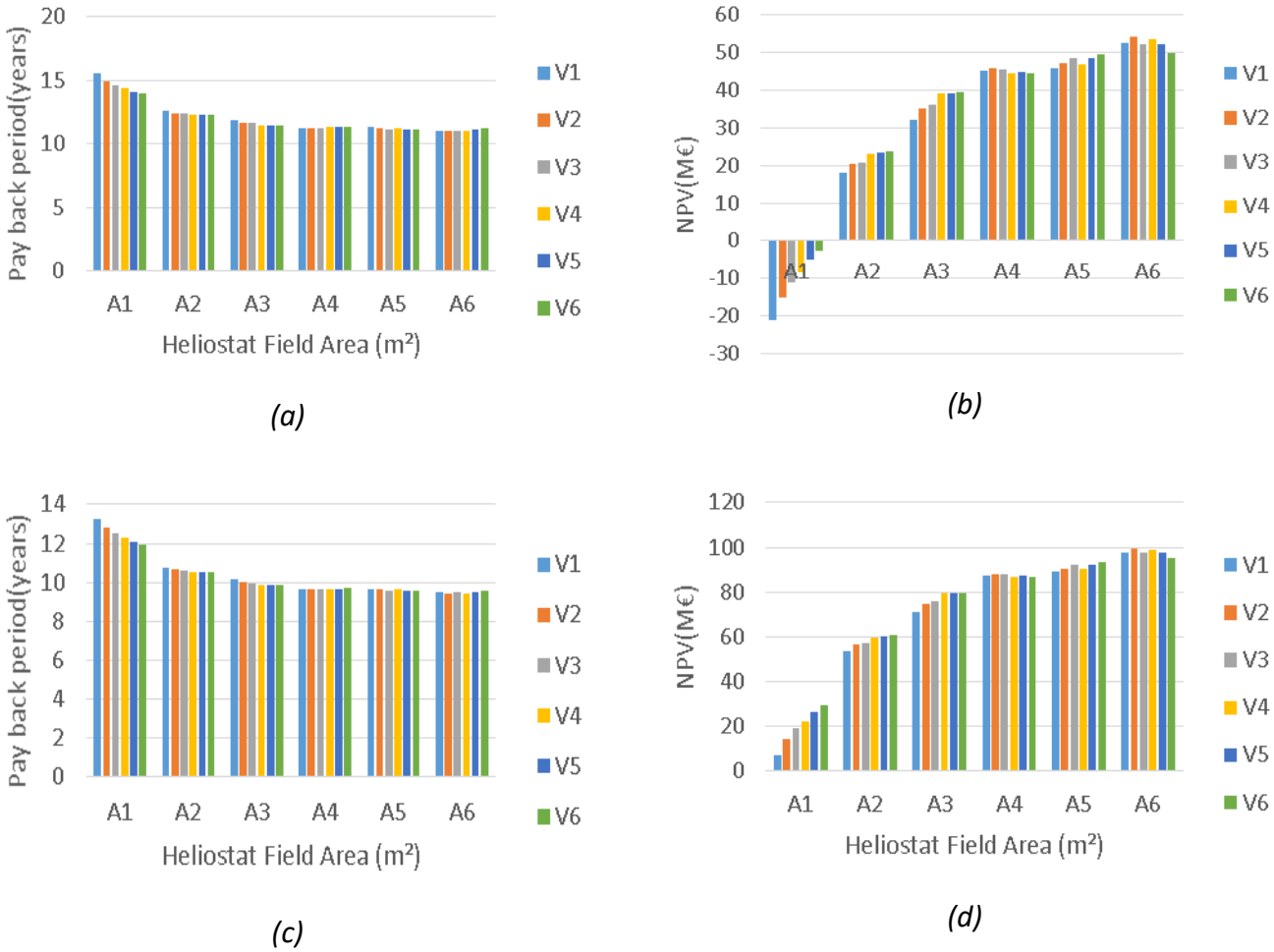

Figure 4-33 On the (a) and (b) can be depicted the PBP and NPV for 0,248€/KWh marginal price cost of the system and on (c) and (d) PBP and NPV for 0,288 €/KWh in Kozani.

From the Figure 4-25 it can be observed that LCOE dropped enough and from the value of 0, 23€/KWh it reaches 0,205€/KWh. The Payback period and NPV reduced and raised respectively from the previous chapter analysis on Kozani but the best combination remained A6-V2 as previously. Last but not least, the results of Kozani for the 5% reduce in total capital cost were better as that of Athens for 5% and obviously better than that of Thessaloniki.

To summarize the results of 5%reduce of total capital cost can be depicted below:

Table 4-8. Economic results for a marginal price cost of 0,248€/KWh in different cities.

Cities	PBP	NPV	Combination	LCOE
Chania	9.27	103615519,7 €	A6-V1	0,1702 €/KWh
Athens	11.31	47022902,48 €	A6-V2	0,2058 €/KWh
Thessaloniki	11.96	31922705,09 €	A5-V5	0,2171 €/KWh
Kozani	10.96	54268346,21 €	A6-V2	0,2002 €/KWh

Table 4-9. Economic results for a marginal price cost of 0,288€/KWh in different cities.

Cities	PBP	NPV	Combination	LCOE
Chania	7.94	156856329,7 €	A6-V1	0,1702 €/KWh
Athens	9.67	91579660,91 €	A6-V2	0,2058 €/KWh
Thessaloniki	10.23	73254112,09 €	A5-V5	0,2171 €/KWh
Kozani	9.40	99639096,77 €	A6-V2	0,2002 €/KWh

To conclude this chapter all the PBP values were reduced with the reduction of 5% in the total capital cost and all the NPV values were increased in all the cities, respectively. Chania still remained the best option with the lowest PBP of 9.67 years and 91579660,91 € net present value which is the highest NPV.Also,the LCOE was reduced with 0,1702 €/KWh of Chania being the lowest.

4.7 Sensitivity Analysis-Feed-in Tariff & Annual Power Production

At this strategy also the feed-in Tariff changes by raising the annual power production by 6%. Apart from the reduce of 5% in the total capital cost another strategy that will be followed is to keep constant the total investment cost and raise by 6% the total power output. At the same time feed-in tariff changes and takes a lower 0,248 €/KWh and an upper value of 0,288 €/KWh. As a result the LCOE, the Payback period and the Net Present Value is going to change. Below are going to be presented the results of that change for the 4 different cities of Greece.

4.7.1 Athens

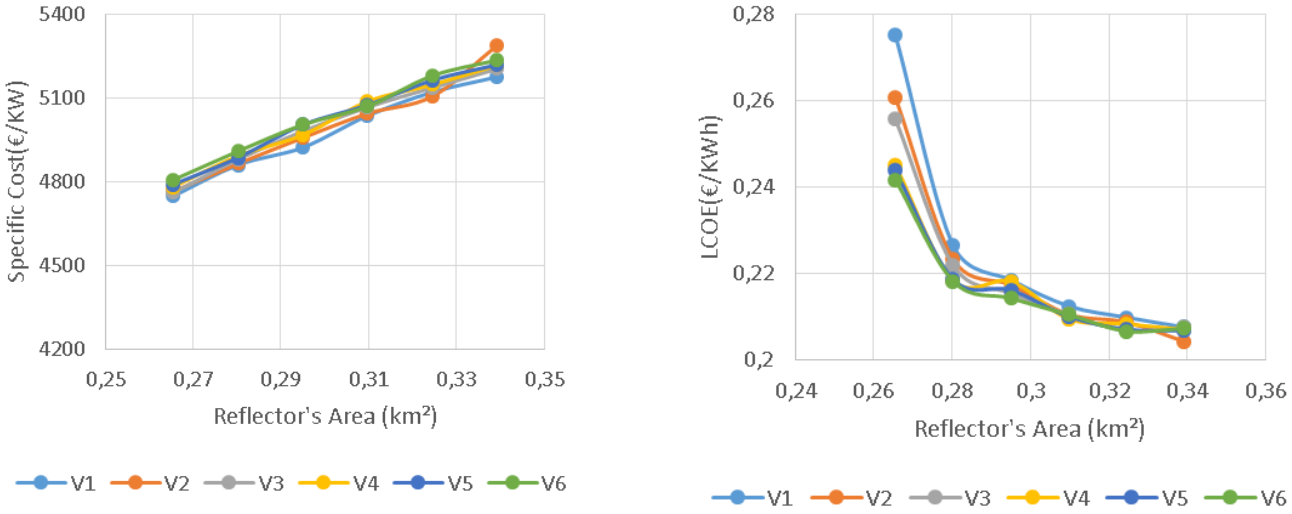

Figure 4-34. On the left side of the matrix is depicted the specific cost as a function of Reflector's Area and storage tank volume and on the right side the LCOE as a function of the same parameters in Athens.

According to Figure 4-27 it can be observed that the specific cost for the city of Athens remained the same as only the total power output changed. The LCOE was reduced but kept its shape and from 0,215€/KWh dropped to 0,2057€/KWh.

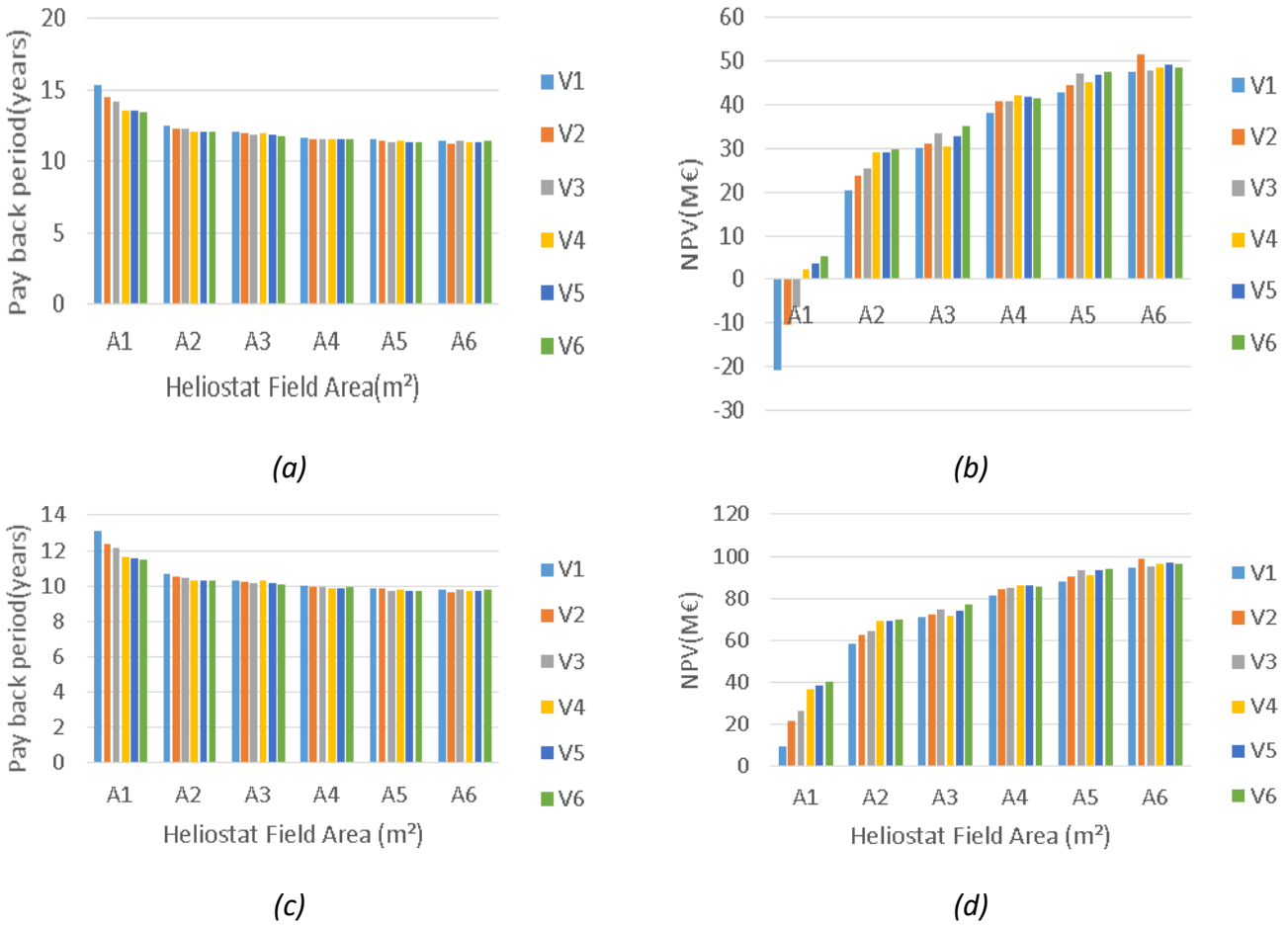

Figure 4-35. On the (a) and (b) can be depicted the PBP and NPV for 0,248€/KWh marginal price cost of the system and on (c) and (d) PBP and NPV for 0,288 €/KWh in Athens.

According to the Figure 4-28 above the best combination also in this chapter for Athens is A6-V2 .Comparing Athens of this chapter with the analysis that was made in the chapter 4.3 it is obvious that the payback period is lower and the net present value is higher too.The best combination remained the same in the two different analysis .The LCOE as is the previous sensitivity analysis reached almost the same value. That depicts how effective both strategies are in order the capital investment cost to be reduced.

4.7.2 Chania

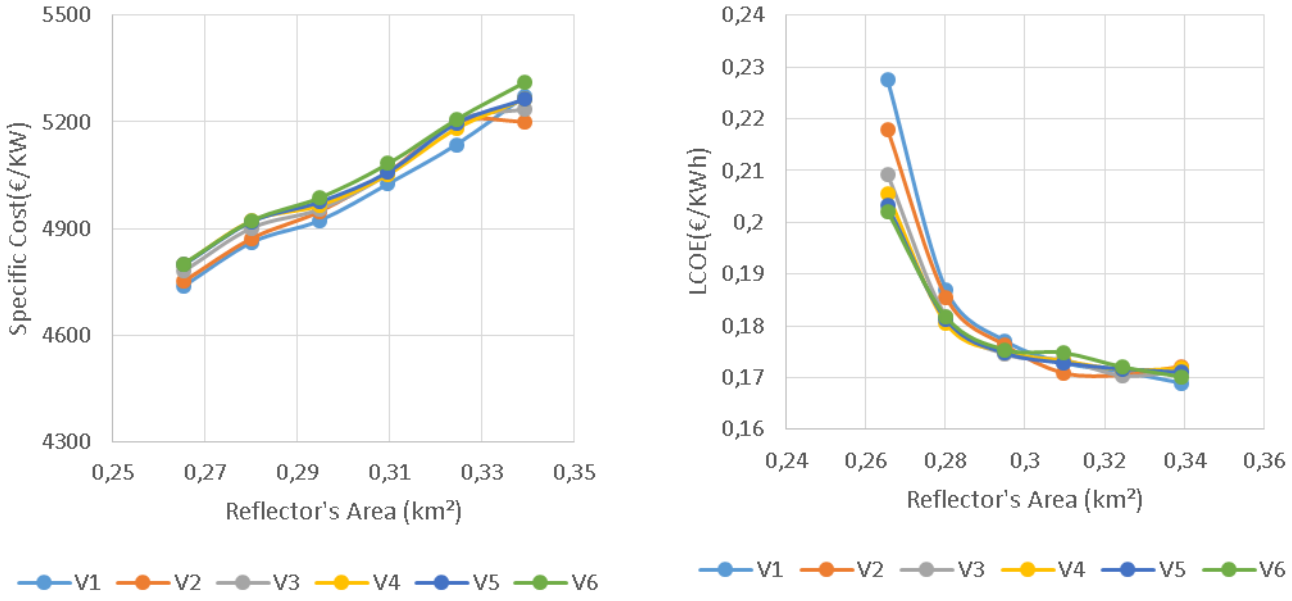

Figure 4-36. On the left side of the matrix is depicted the specific cost as a function of Reflector's Area and storage tank volume and on the right side the LCOE as a function of the same parameters in Chania.

According to the above Figure 4-29 LCOE in Chania comparing to the sensitivity-capital cost analysis took higher values and from 0,165€/KWh converted to 0,17€/KWh. The specific cost remained the same.

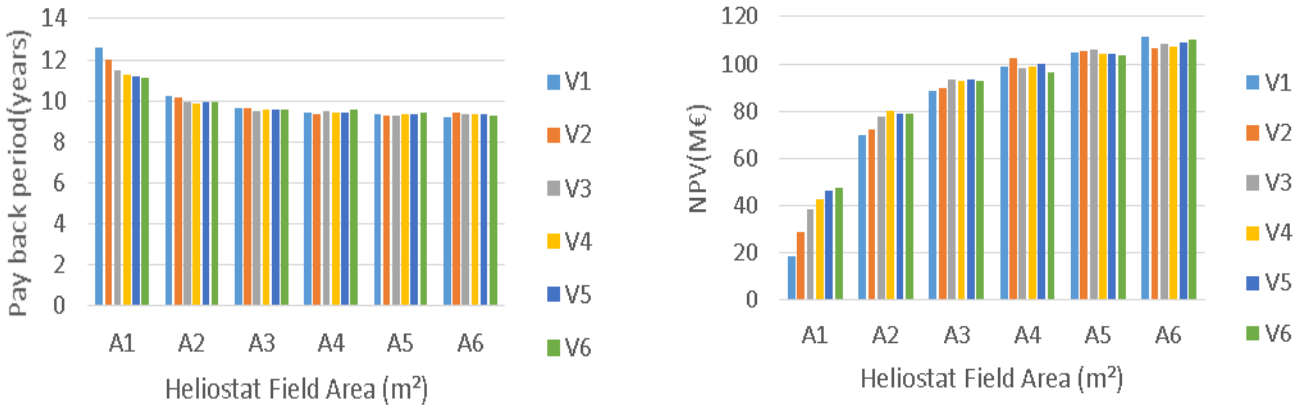

(a) *(b)*

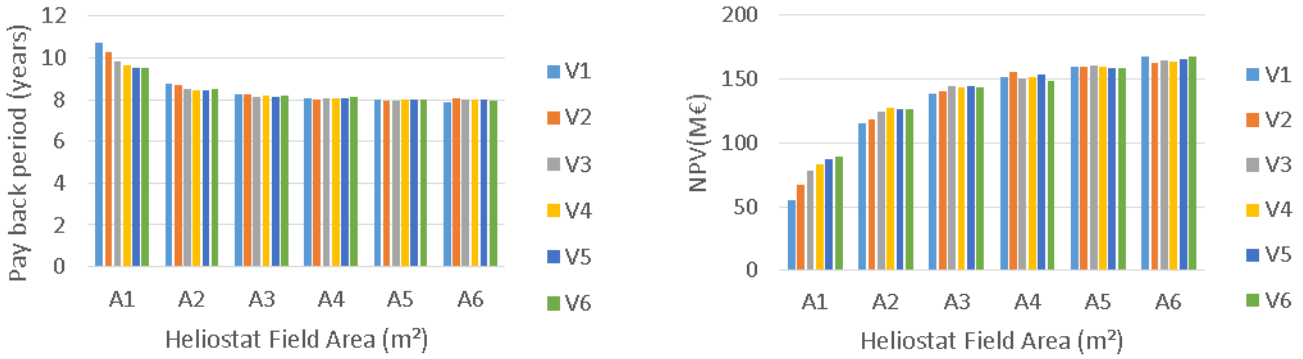

(c) *(d)*

Figure 4-37. On the (a) and (b) can be depicted the PBP and NPV for 0,248€/KWh marginal price cost of the system and on (c) and (d) PBP and NPV for 0,288 €/KWh in Chania.

According to the figure above it can be seen that the Payback period and Net Present Value were calculated to be lower and higher respectively as were in the previous chapter 4.3.The best combination for better results was also A6-V1.

4.7.3 Thessaloniki

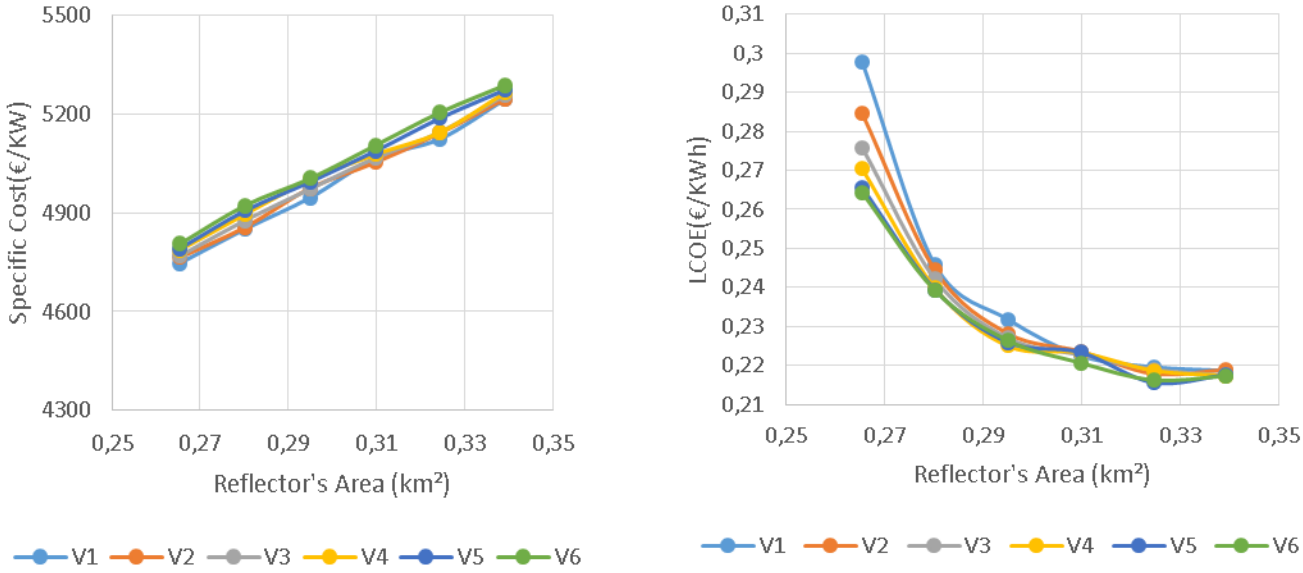

Figure 4-38. On the left side of the matrix is depicted the specific cost as a function of Reflector's Area and storage tank volume and on the right side the LCOE as a function of the same parameters in Thessaloniki.

According to Figure 4-31 LCOE of Thessaloniki dropped below the LCOE that was calculated at the Sensitivity of Capital Cost .The specific cost as aforementioned remained the same.

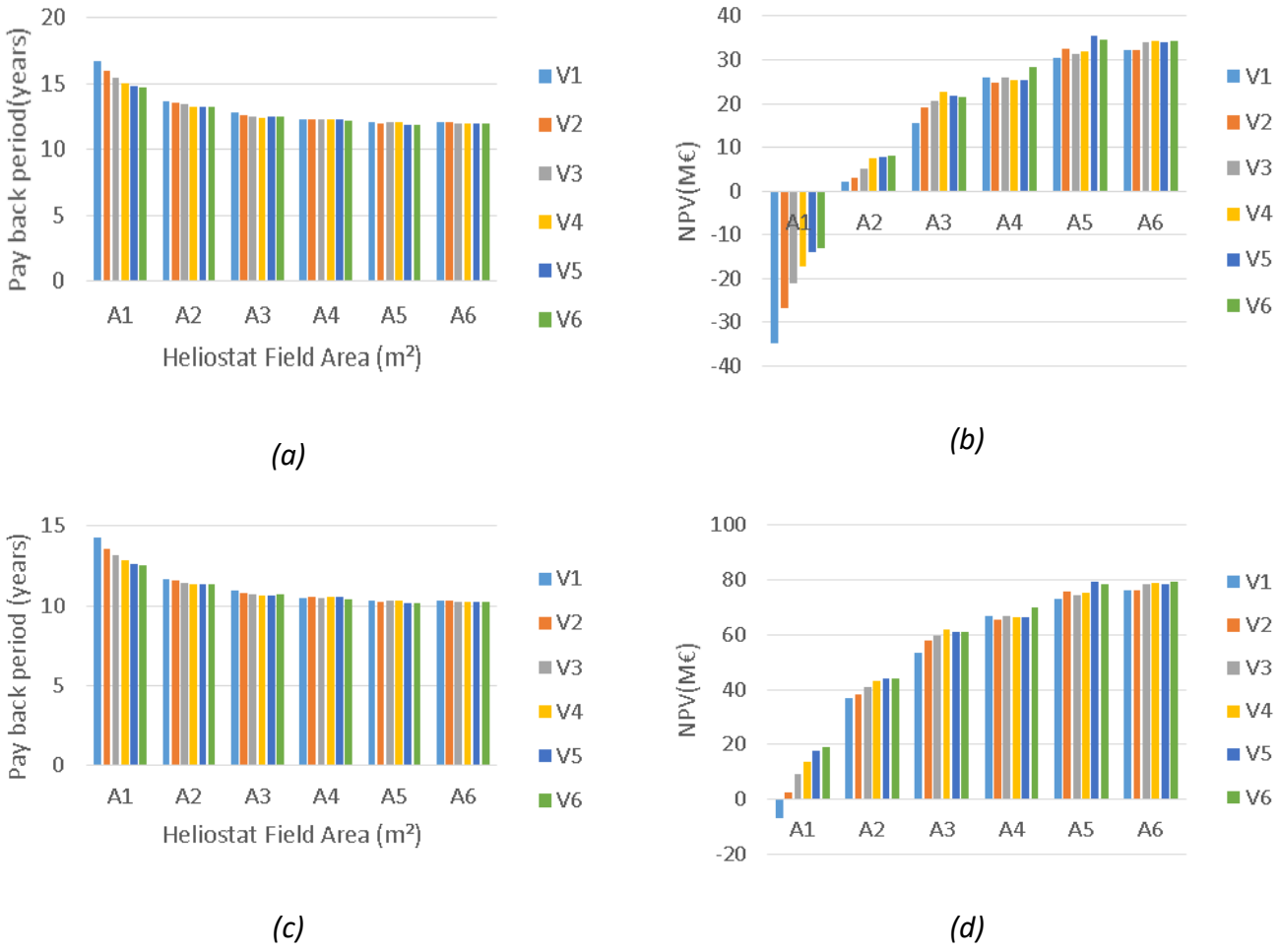

Figure 4-39. On (a) and (b) sides can be depicted the PBP and NPV for 0,248€/KWh marginal price cost of the system and on (c) and (d) the PBP and NPV for 0,288€/KWh in Thessaloniki.

The Payback period and Net Present Value of Thessaloniki for both marginal prices are better in this kind of analysis. The best combination is also A5-V5 as was found in the previous chapters.

4.7.4 Kozani

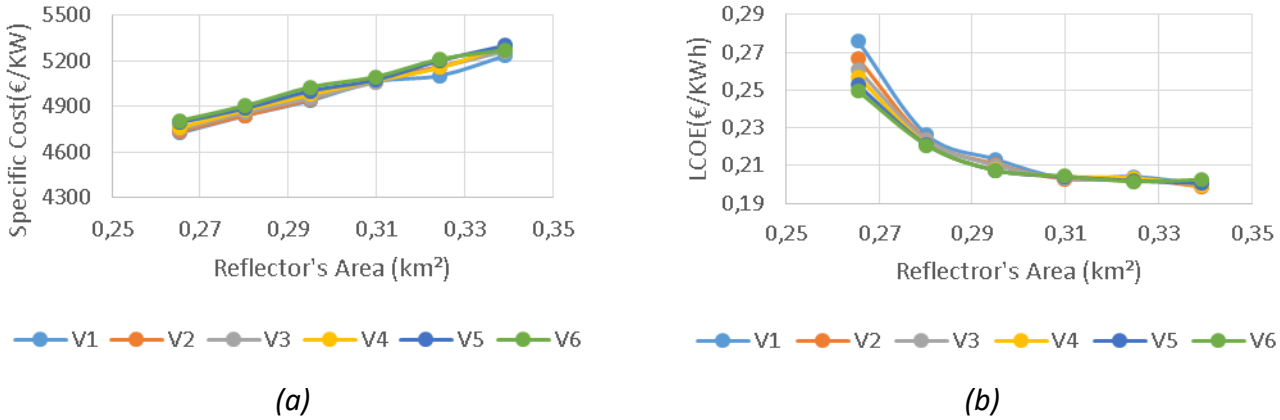

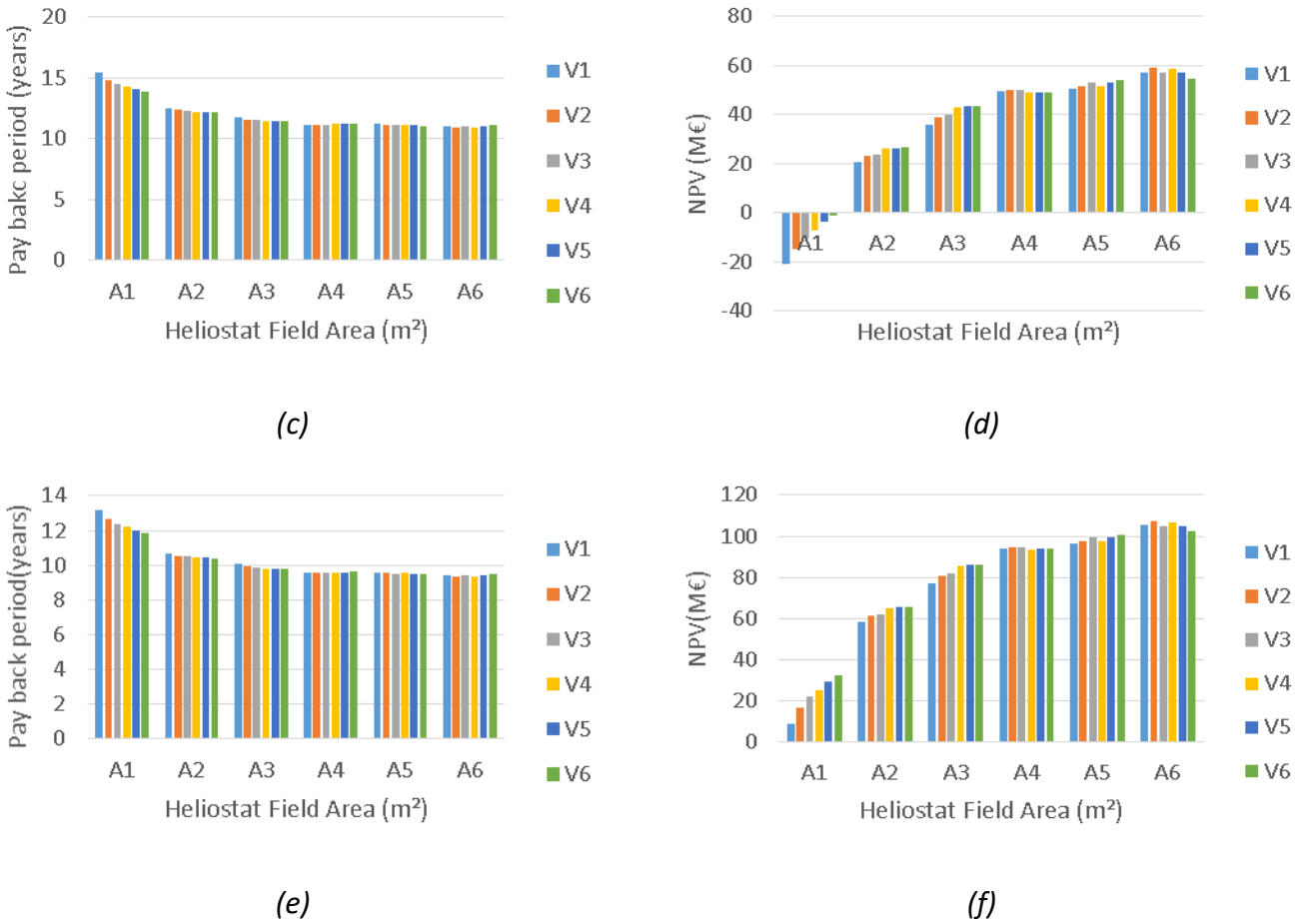

Figure 4-40. On the (a) side of the matrix is depicted the specific cost, on the (b) side the LCOE ,on the (c) and (d) can be depicted the PBP and NPV for 0,248€/KWh marginal price cost of the system and on (e) and (f) PBP and NPV for 0,288 €/KWh in Kozani.

As it can be seen from the LCOE chart on the (b) thesis the cost drops under 0, 2€/KWh which is good result .This must had happened because of the increase in annual production of power where in combination with the low temperatures and the high energetic and exergetic efficiency had as a result the drop in this value. Both sensitivity analysis gave the expected results .Better payback period, NPV and LCOE.

Table 4-10. Economic results for a marginal price cost of 0,248€/KWh in different cities.

Cities	PBP	NPV	Combination	LCOE
Chania	9.21	111501232,5 €	A6-V1	0,1690 €/KWh
Athens	11.23	51533332,41 €	A6-V2	0,2043 €/KWh
Thessaloniki	11.88	35491040,16 €	A5-V5	0,2156 €/KWh
Kozani	10.91	59197301,88 €	A6-V2	0,1988 €/KWh

Table 4-11. Economic results for a marginal price cost of 0,288€/KWh in different cities.

Cities	PBP	NPV	Combination	LCOE
Chania	7.89	167936491,1 €	A6-V1	0,1690 €/KWh
Athens	9.60	98763496,36 €	A6-V2	0,2043 €/KWh
Thessaloniki	10.16	79302331,58 €	A5-V5	0,2156 €/KWh
Kozani	9.33	107290297,5 €	A6-V2	0,1988 €/KWh

To sum up, according to the analysis that was made in these chapters Chania had the lowest payback period the highest Net Present Value and the lowest LCOE. The combinations of the best results in all strategies remained the same. The result was as expected as Chania had the biggest total annual DNI and the biggest total annual power output. This in combination with the similar specific cost ,as all four cities are in Greece, where the marginal price costs are the same, make Chania the best investment choice.

5. Conclusion-Future Research

According to the results of the Net Present Values and the Payback period of this project in the different cities of Greece, it can be concluded that this project is viable in the period of 30 years that was studied. In addition, the best case scenario was found to be in Chania which had the lowest payback period, the highest NPV and the lowest LCOE. The worst results occurred in Thessaloniki which had the lower total annual power output and low temperatures and sunny days throughout the year. Athens and Kozani had mediocre results and worse than that of Chania. The best case scenario was with the increase in annual power output by 6% of the nominal and occurred for Chania, 7.89 years of payback period ,167936491,1 € of Net Present Value for 30years and best LCOE of 0,1690€/KWh. Before the sensitivity analysis , the best results occurred again for the city of Chania with payback period to be 8.69 years, 131626258,7 the Net Present Value and 0,1791€/KWh LCOE. However, has to be highlighted that this study did not take into consideration the tons of CO_2 and other greenhouse gases that such a plant can avoid.

For example, for 1MWh of coal fired plan 850kg CO2 according to [51] are saved and can be reached easily to the conclusion that for a period of 30 years with a 6% of inflation rate this project can save a lot of income, assuming that the price per ton of CO_2 is 25 € according to the European Emissions Trading Scheme (EU ETS) [52] .Taking into consideration all of that information, these projects which are fossil-fuel-free have as a result the payback period to be lowered more and the Net Present value to be raised more, respectively. This price of CO_2 ,however, is going to rise in the EU and reach the value of 55€ per ton according to [53] until 2025, due to Europeans program of reducing greenhouse gas emissions and thus these projects are going to be more and more profitable as the years go by despite their big investment costs.

Another important aspect of this analysis is that, according to the Greek legislation that was officially published under the Greek name “ΦΕΚ 213/A/24-12-2019”[50],until 2028 all the brown coal plants in Greece must be deactivated and be replaced by renewable energy sources. This will have as a result the general marginal price costs of the system to rise up and as a result the accepted feed-in-tariff of 0,278 €/KWh by the Greek legislation to be increased.

Future Research:

- More locations can be examined in Greece in areas with high DNI such as Southeastern Crete and Rhodes Island but also in other countries with high DNI and higher electricity prices.
- Instead of a Solar Power Tower, Linear Fresnel Reflectors can be used and coupled with TES system and the existing power block.
- Instead of steam-water Rankine cycle, ORC cycle could be used if the temperatures were lower.

- A cost relative analysis between solar thermal power plants and plants with natural gas and geothermal plants could be done.
- Auxiliary heater could be placed before the evaporator and extra cost of fuel and construction could be examined.

6. List of Tables

7. List of Figures

8. References

[1] Breeze, P. (2016). Solar power generation. Academic Press.

[2] Κακαράς, Ε., & Καρέλλας, Σ. (2015). Αποκεντρωμένα Θερμικά Συστήματα. Εκδόσεις Τσότρας.

[3] Moya, E. Z. (2021). Parabolic-trough concentrating solar power systems. In concentrating solar power technology (pp. 219–266). Elsevier.

[4] Karellas, S., & Roumpedakis, T. (2019). Solar Thermal Power Plants. In Solar Hydrogen Production. Academic Press.

[5] http://www.solarreserve.com/en/global-projects/csp/crescent-dunes

[6] Bhatia, S. (2014). Advanced renewable energy systems,(Part 1 and 2). CRC Press.

[7] https://www.solarpaces.org/how-csp-works/

[8] Gouthamraj, K., Jamuna Rani, K., & Satyanarayana, K. (2013). Design and Analysis of Rooftop Linear Fresnel Reflector Solar Concentrator. IJEIT, 2(11).

[9]https://www.energy.gov/eere/solar/articles/dishengine-system-concentrating-solar-power-basics

[10] Pitz-Paal, R. (2007). High temperature solar concentrators.

[11] Zheng, Z.-J., Li, M.-J., & He, Y.-L. (2015). Optimization of Porous Insert Configuration in a Central Receiver Tube for Heat Transfer Enhancement. Energy Procedia, 75, 502–507. https://doi.org/10.1016/j.egypro.2015.07.439

[12] Tiryaki, G., & Camdali, U. (2017). TUBE DIAMETER OPTIMIZATION OF A CAVITY RECEIVER FOR A SOLAR POWER TOWER SYSTEM.

[13] Liu, W., Wei, G., Huang, P., Xu, C., & Du, X. (2018). Design and performance analysis of volumetric solar receiver based on porous foam ceramics. 2033(1), 040022.

[14] Patel, K., & Choksi, H. (2015). Grid Integration of Concentrating Solar Power Plant and Cost Analysis. IJIRSET, 4(12)

[15] https://en.wikipedia.org/wiki/Themis_(solar_power_plant)

[16] Py, X., Sadiki, N., Olives, R., Goetz, V., & Falcoz, Q. (2017). Thermal energy storage for CSP (Concentrating Solar Power). 148, 00014.

[17] Rivera, W., Sánchez-Sánchez, K., Hernández-Magallanes, J. A., Jiménez-García, J. C., & Pacheco, A. (2020). Modeling of Novel Thermodynamic Cycles to Produce Power and Cooling Simultaneously. Processes, 8(3), 320. https://doi.org/10.3390/pr8030320

[18] Cengel, Y., & Boles, M. (2008). Thermodynamics an Engineering Approach (7th edition). McGraw-Hill Companies.

[19] Quoilin, S. (n.d.). Sustainable Energy Conversion Through the Use of Organic Rankine Cycles for Waste Heat Recovery and Solar Applications. University of Liege.

[20] http://www.brightsourceenergy.com/ashalim-solar-project#.XqDPYsgzbIU

[21] https://solarpaces.nrel.gov/ivanpah-solar-electric-generating-system

[22] Siemens press release Siemens to supply 123 MW steam turbine-generator set for solar thermal power plant in California 2017-12-13 at the Wayback Machine

[23]"Energy efficiency. Rethinking the energy system here in the U.S." Usa.siemens.com

[24] Walsh, Bryan (24 June 2013). "Tower of Power". Time (paper). pp. Business 1-4

[25] "Concentrating Solar Power Projects - Ivanpah Solar Electric Generating System. Concentrating Solar Power. NREL". Nrel.gov. 2014-11-20

[26] Danelski, David (21 October 2015). "It's not easy being green: Ivanpah solar plant near Nevada burns much natural gas, making it a greenhouse gas emitter under state law". Orange County Register. Santa Ana, California. Archived from the original on 22 October 2015. Retrieved 23 October 2015.

[27] Boretti, A., Castelletto, S., & Al-Zubaidy, S. (2019). Concentrating solar power tower technology: Present status and outlook. Nonlinear Engineering, 8(1), 10–31.

[28]http://analysis.newenergyupdate.com/csp-today/markets/no-drama-solarreserve-commissions-worlds-largest-csp-tower-storage

[29] "Crescent Dunes Solar Energy, Monthly", Electricity Data Browser, EIA, Retrieved October 8 2019

[30] http://helioscsp.com/tag/ashalim

[31] Relloso, S., & Gutiérrez, Y. (2017). SENER molten salt tower technology. Ouarzazate NOOR III case. AIP Conference Proceedings, 1850(1), 030041. https://doi.org/10.1063/1.4984384

[32] Minis, N., Rosenbluth, E., Hayut, R., & Am-Shallem, M. (2019). Spatial DNI measurement for accurate solar flux control in Megalim 121MWe solar receiver power plant. AIP Conference Proceedings, 2126(1), 030037. https://doi.org/10.1063/1.5117549

[33] Ineichen, P., Guisan, O., & Perez, R. (1990). Ground-reflected radiation and albedo. Solar Energy, 44(4), 207–214.

[34] https://lemco.co.za/our-projects/steel-structures-khi-solar-one-plant-renewable-energy

[35] Falcoz, Q., Orozco, J. C., & Khoshbaf, A. M. J. (2018). Thermal energy storage in CSP technologies: From commercialized to innovative solutions.

[36] Mostafavi Tehrani, S. S., & Taylor, R. A. (2016). Off-design simulation and performance of molten salt cavity receivers in solar tower plants under realistic operational modes and control strategies. *Applied Energy*, *179*, 698–715. https://doi.org/10.1016/j.apenergy.2016.07.032

[37] Li, X., Kong, W., Wang, Z., Chang, C., & Bai, F. (2010). Thermal model and thermodynamic performance of molten salt cavity receiver. Renewable Energy, 35(5), 981–988.

[38] Benammar, S., Khellaf, A., & Mohammedi, K. (2014). Contribution to the modeling and simulation of solar power tower plants using energy analysis. Energy Conversion and Management, 78, 923–930.

[39] Winter, C.-J., Sizmann, R. L., & Vant-Hull, L. L. (2012). Solar power plants: Fundamentals, technology, systems, economics. Springer Science & Business Media.

[40] Siebers, D. L., & Kraabel, J. S. (1984). Estimating convective energy losses from solar central receivers. Sandia National Lab.(SNL-CA), Livermore, CA (United States).

[41] Xu, C., Wang, Z., Li, X., & Sun, F. (2011). Energy and exergy analysis of solar power tower plants. Applied Thermal Engineering, 31(17–18), 3904–3913.

[42] Le Roux, W. G., Bello-Ochende, T., & Meyer, J. P. (2012). Thermodynamic optimisation of the integrated design of a small-scale solar thermal Brayton cycle. International Journal of Energy Research, 36(11), 1088–1104.

[43] Burgaleta, J. I., Arias, S., & Ramirez, D. (2011). Gemasolar, the first tower thermosolar commercial plant with molten salt storage. Proceedings of the SolarPACES 2011 conference on concentrating solar power and chemical energy systems, Granada, Spain.

[44] Wakao, N., & Funazkri, T. (1978). Effect of fluid dispersion coefficients on particle-to-fluid mass transfer coefficients in packed beds: Correlation of Sherwood numbers. Chemical Engineering Science, 33(10), 1375–1384.

[45] https://www.irena.org/publications/2020/Jun/Renewable-Power-Costs-in-2019

[46] Yang, S., Zhu, X., & Guo, W. (2018). Cost-benefit analysis for the concentrated solar power in China. Journal of Electrical and Computer Engineering, 2018.

[47] https://eur-lex.europa.eu/legal content/EL/TXT/PDF/?uri=CELEX:C2013/361/03&from=EN

[48] https://www.chemengonline.com/site/plant-cost-index/

[49] https://fred.stlouisfed.org/series/PCU327211327211

[50] https://www.e-nomothesia.gr/kubernese/praxe-upourgikou-sumbouliou-tes-23-12-20192.html

[51] https://www.innovasjonnorge.no/globalassets/eea-grants/romania/ro-energy/energy-audit-call-for-proposals/er_6-conversion-guidelines-ghg_energy-audit_v0.2-14.03.2019.pdf

[52] https://ec.europa.eu/eurostat/documents/2995521/10820684/8-06052020-BP-EN.pdf/e1dd6cf1-09b5-d7ee-b769-ffe63e94561e

[53] https://www.ecb.europa.eu/pub/economic-bulletin/focus/2020/html/ecb.ebbox202002_04~a7d137cb35.en.html